Title
Soft X-ray Microscopy

Authors
Kirz, J.
Jacobsen, C.
Howells, M.

Publication Date
1994-11-01

LBL-36371
UC-410
Preprint

Lawrence Berkeley Laboratory
UNIVERSITY OF CALIFORNIA

Accelerator & Fusion Research Division

Invited by Quarterly Reviews of Biophysics

Soft X-ray Microscopes and Their Biological Applications

J. Kirz, C. Jacobsen, and M. Howells

November 1994

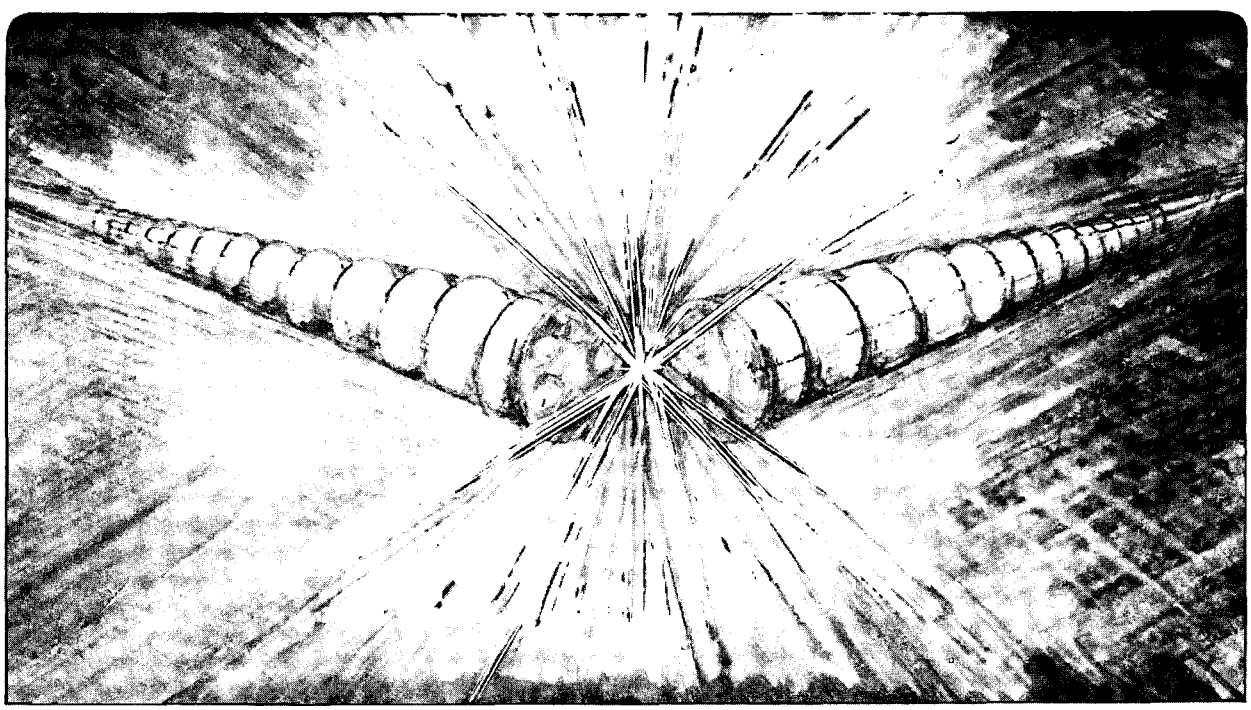

Prepared for the U.S. Department of Energy under Contract Number DE-AC03-76SF00098

DISCLAIMER

LBL-36371
LSBL-232
UC-410

Soft X-ray Microscopes and Their Biological Applications

Janos Kirz and Chris Jacobsen
Physics Department
State University of New York
Stony Brook, NY 11794-3800, USA

Malcolm Howells
Advanced Light Source
Lawrence Berkeley Laboratory
University of California
Berkeley, CA 94720, USA

Invited by *Quarterly Reviews of Biophysics*

November 1994

This work was supported by the National Science Foundation, under grants BIR-9316594 and BIR-9112062 (JK and CJ); by Presidential Faculty Fellow award RCD-9253618 (CJ); and by the Director, Office of Energy Research, Offices of Health and Environmental Research, under contract FG02-89ER60858 (all), and Basic Energy Sciences, Materials Sciences Division, under Contract No. DE-AC03-76SF00098 (MH), of the U.S. Department of Energy.

This paper is to appear in early 1995 in *Quarterly Review of Biophysics.*

Soft x-ray microscopes and their biological applications

Janos Kirz and Chris Jacobsen
Physics Department, State University of New York
Stony Brook, NY 11794-3800 USA

Malcolm Howells
Advanced Light Source
Lawrence Berkeley Laboratory, Berkeley CA 94720 USA

Contents

List of Figures

List of Tables

1 Introduction

1.1 Overview

In this review we propose to address the question: for the life-science researcher, what does x-ray microscopy have to offer that is not otherwise easily available?

We will see that the answer depends on a combination of resolution, penetrating power, analytical sensitivity, compatibility with wet specimens, and the ease of image interpretation. Ultimately all these depend on the physics of the interaction of soft x-rays with the sample, and we shall begin with that in Sec. 2. An important limitation in high resolution imaging is radiation damage to the specimen, and we discuss that in both absolute terms and for x-rays in comparison with electrons in Sec. 2.5.

The ultimate resolution of soft x-ray microscopes is limited in principle only by the wavelength

$$\lambda = \frac{hc}{E} = \frac{1239.8 \text{ eV} \cdot \text{nm}}{\text{photon energy (eV)}}, \tag{1}$$

which is typically a few nanometers. Instruments available today deliver about five times better resolution than visible light microscopes on a routine basis, and recent developments promise that the resolution will improve to maybe 20–30 nm in the near term. The resolution is intermediate between the visible light microscope on the one hand (see Figs. 1 and 2), and the electron microscope on the other.

The penetrating power of x-rays is illustrated in Fig. 3. Soft x-rays are more penetrating than electrons; furthermore, soft x-ray penetrating power varies much more strongly with photon energy and chemical composition. Both of these features have a significant effect on their imaging properties. Soft x-rays in the range of greatest interest have an absorption length in water that varies between 2 μm and 10 μm. This privileged spectral region is the "water window" which lies between the carbon (284 eV; 4.3 nm) and oxygen (540 eV; 2.3 nm) K absorption edges. Within this spectral region, water is nearly an order of magnitude more transparent than organics. As a consequence, x-ray microscopes can view many biological specimens wet and intact (without sectioning) and in atmospheric-pressure air (the penetration distance in atmospheric air is 0.4–4 mm within the "water window", and for helium it is 20–100 mm). Several labs are also developing the capability to view radiation-tough frozen-hydrated specimens in x-ray microscopes. In all these cases, objects of thickness up to several μm should be observable with no compromise of the resolution when within the microscope depth of focus.

Several other properties of x-ray images follow from the basic interactions described in Fig. 3. X-ray absorption edges (jumps in the absorption cross section curve which occur when the x-ray energy passes the threshold energy for removing an inner-shell electron) and near-edge resonances enable the microscopist to map both chemical elements and their chemical binding states as will be described in Sec. 3.4.1. Such an ability to recognize chemical differences helps significantly in image interpretation. In addition, one can add specific chemical labels to the specimen, as is done in visible and UV fluorescence microscopy. Using the scanning x-ray microscope, such selective, visible-light-emitting labels can then be imaged with the resolution of the x-ray microscope and the sensitivity of the labeling procedure. Both molecular labels and dye-labeled microspheres can be used (see Sec. 3.4.5) and there has been progress towards the use of immunogold labels. Further descriptions and literature citations are provided for all these schemes in the sections that follow.

1.2 Organization of this review

This review is biased towards soft x-ray microscopes which can deliver submicron resolution images of hydrated biological specimens. In Section 3, we provide descriptions of some working instruments and their operating principles. The ones with the most extensive biological applications to date are the Göttingen microscope at BESSY, treated in Sec. 3.2, and the scanning transmission microscope at Brookhaven, treated in Sec 3.4. Both of these use zone plates (Sec. 3.1) as focusing elements, and operate at major synchrotron radiation laboratories. These instruments exemplify the two main classes of x-ray microscope, but there are several other microscope types as well as other imaging methods based on holography and diffraction. These are all considered in Section 3. Our assessment of the relative merits of the various microscopes is presented in Sec. 3.8.

Applications, mostly from the Brookhaven and BESSY microscopes, are presented in Sec. 4. In Sec. 5 we attempt to look into the future, and indicate what we see as the expected development of the field.

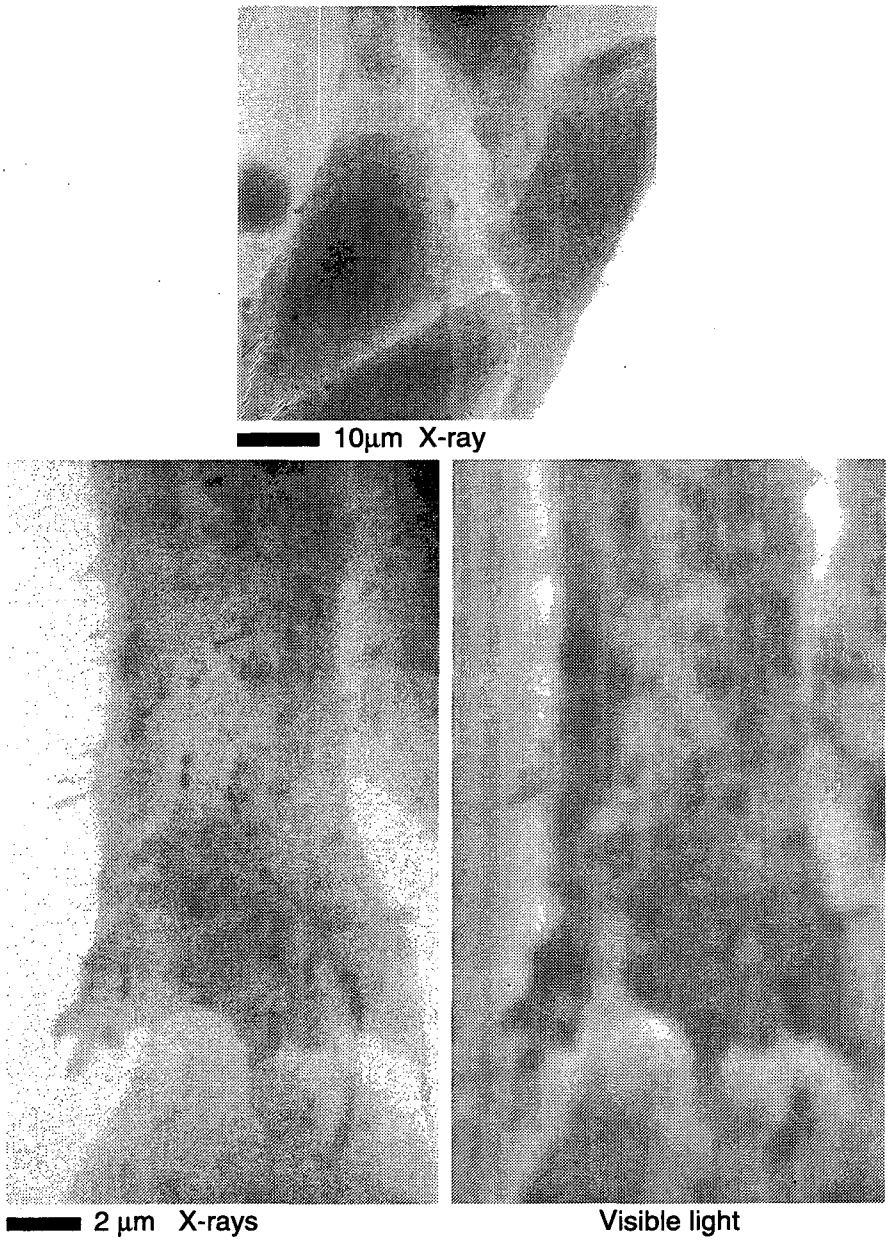

Figure 1: X-ray and optical micrographs of a whole, wet, cultured Chinese hamster ovarian fibroblast fixed in 1% glutaraldehyde. The area outlined near the top of the upper picture is shown at higher magnification in the two pictures below. The optical micrograph at right was taken first, using a Zeiss 63×, N.A.=1.4 oil immersion objective in phase contrast. The cell was then imaged using the X1A scanning transmission x-ray microscope with a 45 nm Fresnel zone plate (fabricated by E. Anderson, Lawrence Berkeley Laboratory). X-ray microscopy offers higher resolution and a more quantitative image. Figure courtesy J. Fu, A. Osanna, and C. Jacobsen (Stony Brook) and W. McGrath and W. Mangel (Brookhaven).

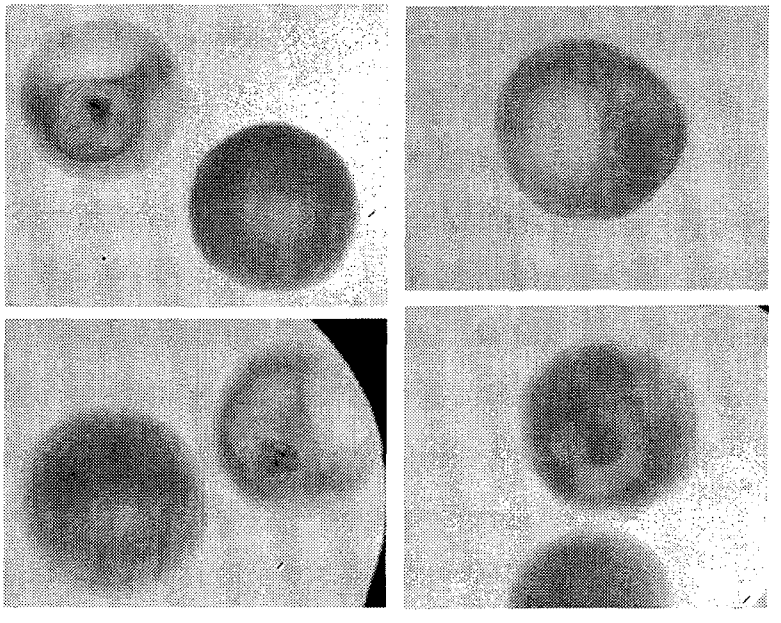

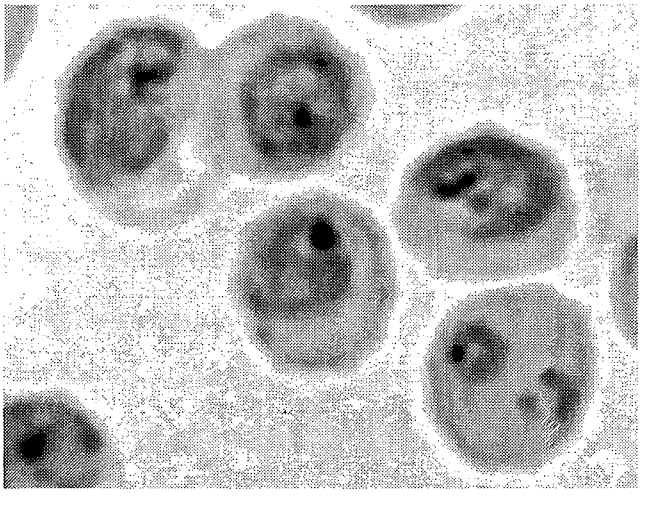

Figure 2: Human erythrocytes infected with *P. falciparum* trophozoites as viewed in x-ray and visible light microscopes. **A.** X-ray images of erythrocytes in an aqueous medium of 2% glutaraldehyde/150 mM phosphate buffered saline (pH 7.2). The images were taken using a $\delta_{r_N} = 35$ nm Ni zone plate (fabricated by E. Anderson, Lawrence Berkeley Laboratory) using the Göttingen x-ray microscope at BESSY. **B.** Visible light images (100×, N.A.=1.4 oil immersion objective and condenser) of air dried, methanol fixed, and Giemsa-stained thin blood smears. For further discussion, see Sec. 4.2. From C. Magowan, M. Moronne, and W. Meyer-Ilse (Lawrence Berkeley Laboratory) [Meyer-Ilse 1994b].

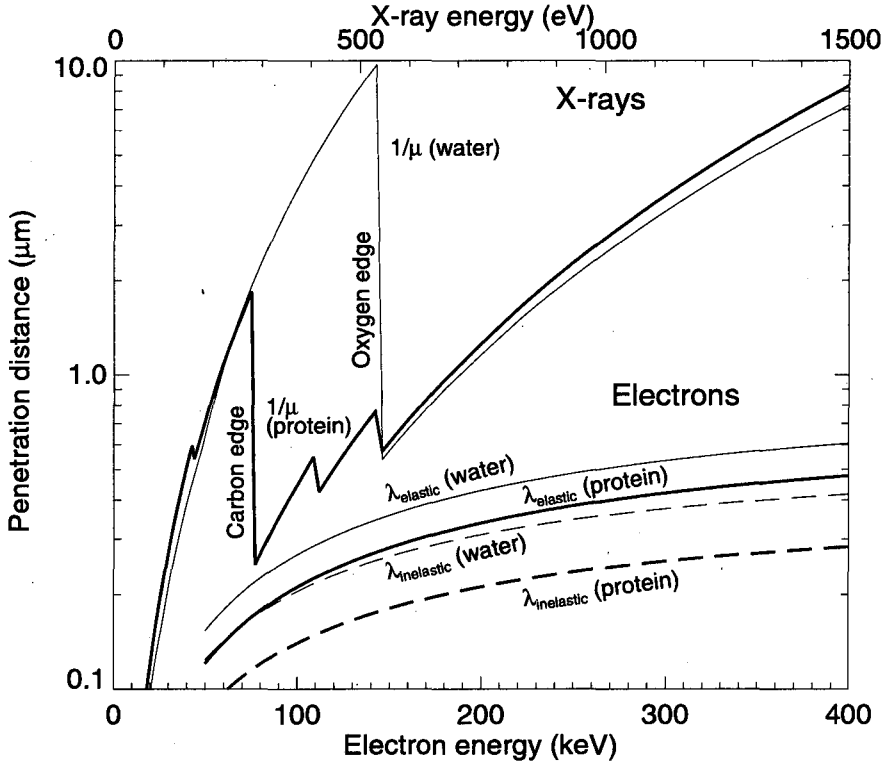

Figure 3: Penetration distances in water and protein for electrons and x-rays. For electrons, the mean free paths λ for elastic and inelastic scattering were obtained using the approximate expressions of Langmore and Smith [Langmore 1992]. For x-rays, the $1/e$ attenuation lengths $1/\mu$ were obtained using the data of Henke *et al.* [Henke 1993, Henke 1994].

1.3 Historical comments

Soon after Röntgen's discovery of x-rays [Röntgen 1895], investigators including Ranwez [Ranwez 1896] and especially Goby [Goby 1913] began enlarging x-ray radiographs for the study of structural details in biological samples in a technique Goby termed "microradiography". Beginning in the late 1940's, interest in x-ray microscopy grew considerably as several groups developed grazing incidence mirror optics [Kirkpatrick 1948, Wolter 1952]. These efforts led to semi-popular articles "announcing" the availability of x-ray microscopes [Kirkpatrick 1949]. In spite of this high level of interest, x-ray microscopy with reflection optics did not catch on at the time, due to long exposure times and, more importantly, insufficient image resolution in part due to the inability (then and now) to fabricate aspheric grazing incidence optics with sufficient control on figure and finish to deliver submicron resolution.

The next phase of x-ray microscopy (in the 1950s) was an outgrowth of earlier developments in electron microscopy. The projection x-ray microscope [Cosslett 1951] (see Sec. 3.6.3) enjoyed substantial popularity for a decade or so. In this period, there were several international conferences [Cosslett 1957, Engström 1960, Pattee 1963] and a monograph [Cosslett 1960], but then activity in the field declined. In the early 1970s, several groups began to recognize that opportunities were being created by new technological developments, and the modern era of x-ray microscopy began to unfold. At the IBM Research Center in Yorktown Heights, Eberhard Spiller and Ralph Feder developed x-ray lithography [Feder 1970] and, along with David Sayre, recognized that the photoresists employed would also function well as high resolution detectors for contact microradiography or, as they called it, contact microscopy [Spiller 1976, Feder 1976] (see Sec. 3.6.2). At the Universität Göttingen, Günter Schmahl and collaborators built upon their expertise in making holographic diffraction gratings and zone plates [Schmahl 1969, Niemann 1974] to demonstrate a zone plate transmission microscope in 1976 [Niemann 1976], as had been proposed by Myers [Myers 1951] and by Baez [Baez 1952, Baez 1961] some twenty years before. In 1977, two important theoretical developments emerged: Sayre *et al.* concluded that x-ray microscopes offer superior contrast and therefore reduced dose for biological objects in relatively thick water layers [Sayre 1977b, Sayre 1977a], and Kondratenko and Skrinsky recognized that synchrotron radiation sources produce high flux coherent x-ray beams [Kondratenko 1977]. By 1980, several groups had become active in the field, including the Stony Brook group. Developments since 1980 are described in several conference procedings [Schmahl 1984a, Cheng 1987b, Sayre 1988a, Shinohara 1990b, Michette 1992, Erko 1994], popular articles (see e.g., [Howells 1985b, Howells 1991]), and review articles (see e.g., [Schmahl 1980, Kirz 1980, Kirz 1985, Michette 1988a, Howells 1990a, Schmahl 1991, Sayre 1995]), and the early history is discussed further by Newberry [Newberry 1987a].

2 Interaction of soft x-rays with matter

To understand the capabilities of the x-ray microscope and to interpret the micrographs made with it one needs to understand the way x-rays interact with both the sample and the optical elements in the microscope. In the sections that follow we present some of the needed results mostly without proof. Further details are available elsewhere [James 1982, Lipson 1958, Henke 1981, Burge 1993].

2.1 Scattering by a single electron

Following conventional treatments of scattering processes, we suppose that the x-ray amplitude $\psi(r)$ must have an asymptotic form comprising a plane wave incident along the z axis and a spherical scattered wave with a dependence on the polar angle θ and azimuthal angle φ of

$$\psi(r) = \exp[-ik_0 z] + \frac{\exp[-ik_0 r]}{r} F(\theta, \varphi) \tag{2}$$

where $k_0 = 2\pi/\lambda$, λ is the wavelength in vacuum, and $F(\theta, \varphi)$ is related to the differential cross section $d\sigma/d\Omega$ by

$$\frac{d\sigma}{d\Omega} = |F(\theta, \varphi)|^2 . \tag{3}$$

When the scatterer is a single free electron at the origin, the process is simple Thomson scattering and, for radiation linearly polarized along $\varphi = 0$, we have [Jackson 1962]

$$F(\theta, \varphi) = -r_e \sqrt{1 - \sin^2\theta \cos^2\varphi}, \tag{4}$$

where $r_e = 2.818 \times 10^{-15}$ m is the classical radius of the electron. Integrating Eq. 3 over θ and φ leads to the Thomson total cross section for one electron

$$\sigma_{\text{Thom}} = \frac{8}{3}\pi r_e^2. \tag{5}$$

Averaging Eq. 3 over all incident polarizations [Jackson 1962] leads to a cross section for unpolarized radiation of

$$\frac{d\sigma}{d\Omega}\Big|_{\text{electron}} = r_e^2 \frac{1+\cos^2\theta}{2}. \tag{6}$$

2.2 Scattering by an atom

For an assembly of electrons, it can be shown [Lipson 1958] that, within the first Born approximation, the x-ray amplitude $G(\vec{K})$ diffracted in direction $\vec{k}$ by an electron density distribution $\rho(\vec{r})$ relative to a single free electron at the origin is given by

$$G(\vec{K}) = \int_{-\infty}^{+\infty} \rho(\vec{r}) \exp[i\vec{K}\cdot\vec{r}]d^3\vec{r} \tag{7}$$

Here, $\vec{k_0}$ and $\vec{k}$ represent incident and scattered wave vectors, and $\vec{K} = \vec{k_0} - \vec{k}$ so that $|\vec{K}| = K = 2k_0\sin(\theta/2)$. In the particular case that $\rho(\vec{r})$ represents an atom, $G(\vec{K})$ can be regarded as an atomic form factor $f_0(\vec{K})$. For the forward direction ($\theta = 0$), the integral of Eq. 7 shows that $f_0(0) = Z$. For a spherically symmetric atom, the integrals over the polar and azimuthal angles can be carried out so that the (in this case) real function $f_0(\vec{K})$ is given by

$$f_0(\vec{K}) = 4\pi \int_0^{\infty} \rho(r) \frac{\sin Kr}{Kr} r^2\, dr. \tag{8}$$

Values of $f_0(\vec{K})$ can be calculated for particular wave functions, and are tabulated [Lonsdale 1962].

This procedure accounts for the *spatial distribution* of the atomic electrons but not for the fact they are bound. That is, it applies for *normal* but not for *anomalous* dispersion. In order to represent the effects of anomalous dispersion, we replace $f_0(\vec{K})$ with a complex number $\tilde{f}$ representing the effective number of electrons per atom which is defined (in view of Eq. 4) by

$$F(\theta,\varphi)\Big|_{\text{atom}} = -\tilde{f}\, r_e \sqrt{1-\sin^2\theta\cos^2\varphi} \tag{9}$$

In the hard x-ray spectral region, it is conventional to write $\tilde{f}$ as

$$\tilde{f} = f_0(\vec{K}) + \Delta f' + i\Delta f'', \tag{10}$$

where $\Delta f'$ and $\Delta f''$ are small and, for light elements, are independent of θ and φ [Lonsdale 1962]. In the soft x-ray region, the standard notation is [Henke 1981]

$$\tilde{f} = f_1 + if_2 \tag{11}$$

where values of f_1 and f_2 have been tabulated by Henke *et al.* [Henke 1993, Henke 1994] for all the elements (see Fig. 4). When the atom is much smaller than the x-ray wavelength, as it is in the soft x-ray region, the amplitudes scattered by the individual electrons add coherently for all values of the polar angle. On the other hand, for shorter wavelengths, the coherent superposition is applicable only near the forward direction. Thus the f_1 and f_2 tables apply for all $\vec{K}$ vectors in the soft x-ray range, but only for $\vec{K} \to 0$ in the hard x-ray region.

The expression for $F(\theta,\varphi)$ given in Eq. 9 allows us to apply the Optical Theorem [Jackson 1975] to write the total atomic cross section σ_{T} as

$$\sigma_{\text{T}} = 2\lambda\,\text{Im}[F(\theta=0)] = 2\lambda r_e f_2, \tag{12}$$

where σ_{T} is equal to the sum of the cross sections for absorption and scattering. Because f_1 and f_2 do not depend on $\vec{K}$ in the soft x-ray range (as discussed above), the elastic scattering cross section can be found by integrating Eq. 9 over θ and φ (as was done to obtain Eq. 5 from Eq. 4), giving

$$\sigma_{\text{elastic}} = \frac{8}{3}\pi r_e^2 |\tilde{f}|^2 \tag{13}$$

which holds roughly for $\lambda \gtrsim 1$ nm.

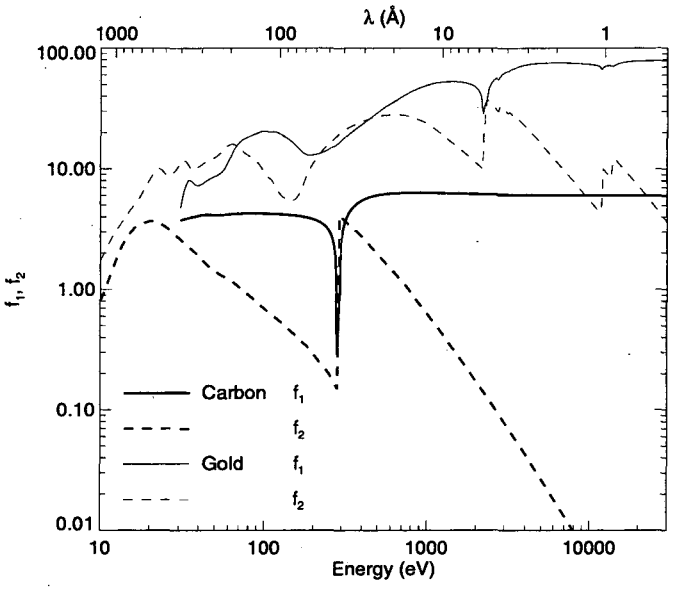

Figure 4: Complex number of electrons ($f_1 + if_2$) for carbon and gold *atoms* as a function of x-ray energy, as tabulated by Henke *et al.*[Henke 1993]. In the regions near x-ray absorption edges, this tabulation is generally not valid due to molecular and condensed matter effects. Note that $f_1 \to Z$ at high energies.

The fact that $F(\theta, \varphi)$ is real in Eqs. 4 and 9 might suggest that the optical theorem will require that $\sigma_T = 0$ for a single free electron. This surely cannot be true; the explanation is that while the optical theorem is exact, Eqs. Eqs. 6 and 9 are approximations which neglect the effect of the energy radiated on the motion of the driven electron. When this is taken into account [Heitler 1954], $F(\theta, \varphi)$ acquires an extra factor $[1 - i4\pi r_e/(3\lambda)]$. The value of the imaginary part of this factor is too small to be important for most purposes (although it was apparently known to Thomson) but it is exactly the factor needed to reproduce the correct Thomson total cross section $\sigma_{\text{Thom}} = (8/3)\pi r_e^2$ by application of the optical theorem.

Examination of Eqs. 12 and 13 allows some conclusions concerning the magnitudes of σ_{T} and σ_{elastic}. The latter is much smaller by a factor of 10^3–10^4 because $r_e \ll \lambda$ in cases of interest to us. This is reflected in Fig. 5, which shows the absorption, elastic, and inelastic cross sections for carbon as a function of x-ray energy. One can see that, for free atoms, the dominant effect is photoelectric absorption, while the inelastic (Compton) cross section is neglible in the soft x-ray range. However, in spite of the relatively small size of the atomic elastic cross section, it would be wrong to conclude that elastic scattering is unimportant in soft x-ray optical systems. If the amplitudes scattered by the atoms in an element of matter are added coherently, the total scattered intensity scales with the square of the volume of the element while the total absorbed intensity scales linearly with volume. Therefore, as the element becomes larger, scattering is increasingly favored over absorption so long as the superposition continues to be coherent. This property is exploited in e.g., gratings and zone plates, and is considered further below. (Similar coherence arguments apply to other radiation, such as electrons, neutrons, or hard x-rays).

2.3 X-ray interactions with uniform matter

The influence of matter on an electromagnetic wave is described (macroscopically) by Maxwell's equations as a change in the phase velocity v compared to its vacuum value c according to the relation

$$v = \frac{c}{\sqrt{\mu_{\text{m}}\epsilon}}. \tag{14}$$

The complex refractive index $\tilde{n} = c/v$ is thus equal to $\sqrt{\tilde{\epsilon}}$ for a non-magnetic material ($\mu_{\text{m}} = 1$). In such a medium, the x-ray wavelength is increased compared to vacuum if $\text{Re}(\tilde{n}) < 1$, and the vacuum propagation constant k_0 becomes $\tilde{n}k_0$.

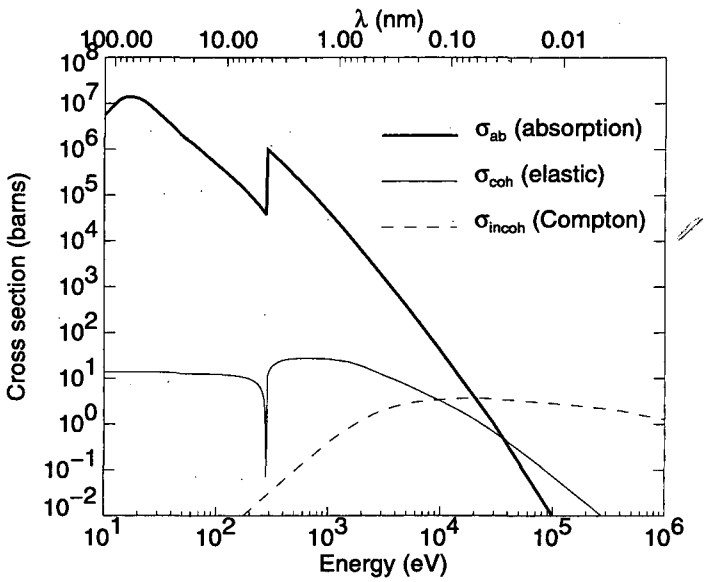

Figure 5: Photon cross sections in carbon as a fuction of energy, showing the contributions of different processes: photoelectric absorption $\sigma_{\rm ab}$, coherent scattering $\sigma_{\rm coh}$, and incoherent or Compton scattering $\sigma_{\rm incoh}$. Data from Henke [Henke 1993] and Hubbell [Hubbell 1980].

The complex dielectric function $\tilde{\epsilon}$ of a pure element with n_a atoms per unit volume can be calculated as a function of frequency ω as [Wooten 1972]

$$\tilde{\epsilon}(\omega) = 1 - \frac{n_a r_e \lambda^2}{\pi} \sum_j \frac{\omega^2 F_j}{(\omega^2 - \omega_j^2) + i\gamma_j \omega}, \tag{15}$$

where ω_j is the frequency, F_j the oscillator strength, and γ_j the damping constant of the $j^{\rm th}$ transition. This formalism is not limited to atomic transitions, but they are the ones of principal interest here. Each term of the summation is a complex scattering factor (expressed in electrons). The sum of such factors over the allowed atomic transitions is thus equal to the effective number of electrons per atom $\tilde{f} = f_1 + if_2$. The refractive index then becomes

$$\tilde{n} = \sqrt{\tilde{\epsilon}} = 1 - \frac{n_a r_e \lambda^2}{2\pi}(f_1 + if_2). \tag{16}$$

It is conventional [Henke 1981] to write $\tilde{n} = 1 - \delta - i\beta$ in the soft x-ray range, where

$$\delta = \frac{r_e \lambda^2}{2\pi} n_a f_1 \tag{17}$$

$$\beta = \frac{r_e \lambda^2}{2\pi} n_a f_2 \tag{18}$$

For $\lambda < 5$ nm, it is always true that $\delta, \beta \lesssim 10^{-3}$, implying that $\tilde{n} \simeq 1$ and justifying the binomial expansion which has been utilized in arriving at Eqs. 16–19. The quantity $n_a \tilde{f} = \rho(\vec{r})$ is the scattering factor of the material in electrons per unit volume. Its real and imaginary parts, $n_a f_1$ and $n_a f_2$, are to be replaced by $\sum_i n_{ai} f_{1i}$ and $\sum_i n_{ai} f_{2i}$ for compounds or mixtures. In view of Eq. 16, one can see that

$$4\pi r_e \rho(\vec{r}) = k_0^2(1 - \tilde{n}^2) = 2k_0^2(\delta + i\beta). \tag{19}$$

Equations 16–19 provide the link between the atomic composition of the material and its refractive index (which describes its macroscopic behavior in most x-ray optical experiments). For example, in the medium of index $\tilde{n}$, the plane wave $\exp[-ik_0 z]$ becomes $\exp[-i\tilde{n}k_0 z]$ and

$$\psi(z) = \psi_0 \exp[-ik_0 z] \exp[i\delta k_0 z] \exp[-\beta k_0 z]. \tag{20}$$

Since the intensity is $I = |\psi(z)|^2$, we have

$$I/I_0 = \exp[-2\beta k_0 z] = \exp[-\mu z] \tag{21}$$

so β represents removal of x-rays from the beam by absorption. The role of $1-\delta$ is the same as that of the conventional refractive index. The phase change in a distance z

$$\varphi(z) = \frac{2\pi}{\lambda}\delta z \tag{22}$$

can be exploited to enable phase-contrast x-ray microscopy (see Sec. 3.2.1). As an example, the *relative* phase change of protein versus water is shown in Fig. 6. The consequence of photoelectric absorption is the generation of Auger and photo-electrons. These energetic secondary electrons are responsible for radiation damage to the specimen, but they can also be used for sensitive surface microscopies with samples that are suitably vacuum compatible (see Sec. 3.4.4). From Eqs. 18 and 21, the absorption coefficient μ is given by

$$\mu = \frac{4\pi\beta}{\lambda} = 2\lambda r_e n_a f_2 = n_a \sigma_T, \tag{23}$$

which is consistent with Eq. 12 because, for *uniform* matter, the elastically scattered amplitudes add to zero in all directions except the forward. For observable scattering to take place there must therefore be some degree of nonuniformity, and this is the case we treat in the next section.

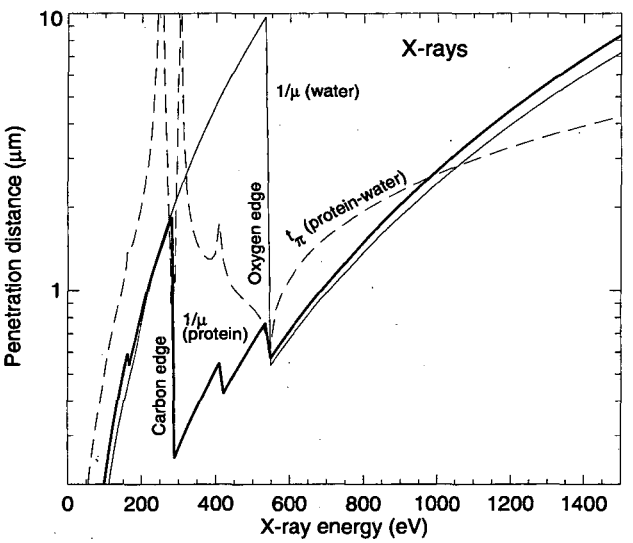

Figure 6: X-ray $1/e$ attenuation lengths (as in Fig. 3) along with the thickness $t_\pi = \lambda/(2|\delta_{\text{water}} - \delta_{\text{protein}}|)$ through which a π radian phase difference is accumulated in travel through water versus protein. C.f. Eq. 25.

2.4 X-ray interactions with non-uniform matter

For our purpose, the most interesting type of x-ray interaction is with the microscope sample which is an intrinsically non-uniform object that we initially suppose to be fully and coherently illuminated with x-rays. First we consider the forward problem of calculating the distribution of scattered x-rays when the three-dimensional sample is fully known. In its most general form, this problem is best approached numerically using, for example, the multislice method [Hare 1994] or the parabolic equation method [Popov 1994]. However, we consider here some special cases for which a useful analytical formula can be given.

2.4.1 Treatment within the first Born approximation

The clearest physical picture is provided by analysis within the Born approximation [Mott 1949] which, in view of Eqs. 2 through 7, leads to an intensity in the far field of

$$I(\vec{K}) = I_0 \frac{r_e^2}{r^2} \frac{1+\cos^2\theta}{2} \left| \int_{-\infty}^{+\infty} \rho(\vec{r}) \exp[i\vec{K}\cdot\vec{r}] d^3\vec{r} \right|^2 . \tag{24}$$

In other words, the intensity scattered in the direction $\vec{k}$ is proportional to the strength of the Fourier component of spatial frequency $\vec{K} = \vec{k} - \vec{k_0}$ of the sample. As a result, the scattered intensity is most simply related to the *frequency-space* representation of the sample and is determined by the distribution of material in the entire sample. In the event that $\rho(\vec{r})$ is embedded in a background material of index $1 - \delta_0 - i\beta_0$, then $\rho(\vec{r})$ in Eq. 24 would be replaced by a density $\rho_r(\vec{r})$ expressed relative to the background. That is, Eq. 19 would become

$$2\pi r_e \rho_r(\vec{r}) = k_0^2 [(\delta - \delta_0) + i(\beta - \beta_0)] . \tag{25}$$

For the use of the Born approximation to be justified, the amplitude illuminating each element of $\rho_r(\vec{r})$ would have to be well-approximated by the incident amplitude; for experiments which seek to push the penetration advantage of soft x-rays as far as possible, one expects fairly strong absorption which would tend to limit the accuracy of this type of calculation [Jochum 1992]. However, for conventional microscopy, precise theoretical modeling is often not necessary and the insight provided by the Born approximation is very helpful.

An accurate theory is much more important for addressing the inverse problem of finding $\rho_r(\vec{r})$ from multiview diffraction data. This is known as the diffraction-tomography problem [Wolf 1969, Devaney 1986] and we discuss it briefly later. At this stage we only point out that there is another approximation due to Rytov [Devaney 1986, Goodman 1985] which can be used in soft x-ray tomography experiments even when the validity conditions for the Born approximation are not satisfied [Howells 1990b].

2.4.2 Treatment when the sample can be represented as a two-dimensional transparency function

If the participating sample features are much larger than $\sqrt{\lambda s}$ where s is the thickness of the sample, then the sample can be treated as a two-dimensional transparency function $T(\vec{r})$. (This same condition, with s also allowing for the sample-resist spacing and x-ray penetration in the resist, also guarantees that a contact microscopy recording will be a faithful projection of the sample–see Sec. 3.6.2). The scattered intensity at position $\vec{r}$ in the receiving plane is then given (using the Fresnel approximation and neglecting obliquity factors) by the Rayleigh-Sommerfeld diffraction formula [Goodman 1968]

$$I(\vec{r}) = I_0 \frac{1}{\lambda^2 z^2} \left| \int_S T(\vec{r'}) \exp\left[\frac{-i\pi|\vec{r}-\vec{r'}|^2}{\lambda z}\right] d^2\vec{r'} \right|^2 , \tag{26}$$

where S represents the area of the sample and $\vec{r}$ and $\vec{r'}$ are now two-dimensional vectors in the two planes separated by a distance z. This is a convolution of $T(\vec{r})$ with the propagator function which follows it; this expression is commonly used to model the behavior of optical elements like zone plates as well as suitably thin samples.

2.4.3 Scattering by a single resolution element

The expression of Eq. 24 tells us that, at least in the Born approximation, the intensity at any receiving point is formed by a superposition of wavelets of strength $\rho(\vec{r})d^3\vec{r}$ and phase $\vec{K}\cdot\vec{r}$. Therefore, if the object represented by $\rho(\vec{r})$ is sufficiently small, $\vec{K}\cdot\vec{r}$ will always be close enough to constant so that all the wavelets add in phase. For example, when θ is small and $\vec{r}$ is along the transverse ($\hat{x}$) axis, $\vec{K}\cdot\vec{r} < \pi$ when $|x| < \lambda/2\theta$. When $\vec{r}$ is along the incident ($\hat{z}$) axis, $\vec{K}\cdot\vec{r} < \pi$ when $|z| < \lambda/\theta^2$. In fact, these two limiting distances are simply the transverse and longitudinal resolution elements of an optical system with numerical aperture θ at wavelength λ. The conclusion is that the scattered waves from points inside a single resolution element add approximately coherently at any point inside the aperture defined by θ. When $\vec{K}\cdot\vec{r}$ is constant, the Born approximation expression of Eq. 24 becomes

$$I(\vec{K}) = I_0 \frac{r_e^2}{r^2} \frac{1+\cos^2\theta}{2} N^2, \tag{27}$$

where N is the total number of effective electrons in the element. Consequently, for scattering by small isolated particles of width $2x$, there is always a region of angular half width about $\lambda/2x$ over which there is coherent enhancement of the signal. (As an example, this describes the central peak in a small-angle scattering experiment).

2.4.4 Scattering by spherical particles

Spherical particles are sometimes used as labels in microscopy. A quantitative analysis of scattering from uniform spheres is given by Henke [Henke 1955]. He concludes that the angular distribution of scattered x-rays is given by

$$\frac{d\sigma}{d\Omega} = (\frac{d\sigma}{d\Omega})_1 8\pi^3 R^6 n_a^2 J_{3/2}^2(u)/u^3, \tag{28}$$

where $u = 4\pi R \sin(\theta/2)/\lambda$, J is a Bessel function of the first kind, R is the radius of the sphere, and $(d\sigma/d\Omega)_1$ is the differential cross section of a single atom. For the case where $\lambda \ll R$, Henke gives the approximate expression

$$\frac{d\sigma}{d\Omega} = (\frac{d\sigma}{d\Omega})_1 \left[(4\pi/3)R^3 n_a\right]^2 \exp[-u^2/5]. \tag{29}$$

This is small angle scattering with a Gaussian angular distribution. In the forward direction, where $u = 0$, we get a factor that is precisely the square of the number of atoms. The angular width $\sqrt{5/(8\pi^2)}(\lambda/R)$ is proportional to λ, so the solid angle is proportional to λ^2. Therefore the solid angle over which the enhancement factor is proportional to the square of the number of atoms scales as λ^2.

Henke integrates this expression to get a total elastic scattering cross section

$$\sigma_{\text{el,sphere}} = 2\pi r_e^2 \lambda^2 R^4 |n_a(f_1 + if_2)|^2. \tag{30}$$

If we compare this to Eq. 13, which gives the cross section for the single atom, we get an enhancement factor of $[3/4]\lambda^2 R^4 n_a^2$. Of this, $(4\pi/3)R^3 n_a$ is the number of atoms, and that leaves $[9/(16\pi)]\lambda^2 R n_a$ as the factor by which the sphere scatters more than the incoherent sum of its individual atoms.

2.4.5 Treatment in special illumination conditions in microscopes

So far we have mostly been considering the diffraction of an x-ray beam by the sample; this is the effect which is exploited in holography, diffraction and the dark field microscopies. We have mentioned contact microscopy, but there are several illumination conditions that we have not considered which we defer until the treatment of particular microscopes. We began by assuming a coherent illumination of the sample, but in real microscopes both the sample and the optical elements may be illuminated by partially coherent light. The application of coherence theory [Born 1980] to the operation of x-ray microscopes under such conditions has been discussed by Diehl [Diehl 1994] and by Jochum and Meyer-Ilse [Jochum 1994].

2.5 Contrast, dose, and radiation damage

2.5.1 Estimating contrast and dose

Amplitude contrast between water and organic matter in the "water window" (Sec. 1.1) is due to the dramatic difference in the f_2 values of these two types of materials in the wavelength range between the carbon and oxygen absorption edges. This can be seen in Fig. 3. The importance of this contrast mechanism was realized a long time ago [Wolter 1952]. More recently, Schmahl and Rudolph called attention [Schmahl 1987, Rudolph 1990] to the fact that if Zernike phase contrast can be implemented, the contrast for wet specimens can be further improved inside the water window, and excellent phase contrast can be obtained at shorter wavelengths provided there is a spatial variation in the $n_a f_1$ values in the sample.

Good contrast is particularly important when dealing with microscopies involving ionizing radiation, for contrast is directly related to the radiation dose that must be given to the specimen to record the image at a given resolution. The relationship between contrast and minimum exposure was established by Rose [Rose 1948]. His studies of image formation resulted in the following criterion: to render an arbitrarily shaped object visible in a noisy image, the signal to noise ratio must be larger than 5.

The Rose criterion was first applied to electron microscopy by Glaeser [Glaeser 1971], and to x-ray microscopy by Sayre *et al.* [Sayre 1977a, Sayre 1977b]. Much additional work has been done since in both electron [Glaeser 1975,

Isaacson 1976, Glaeser 1978] and x-ray [London 1989, Morrison 1989, Gölz 1992, London 1992b, Jacobsen 1994b] microscopy.

We shall adopt an approach similar to that of Sayre *et al.*, who subdivide the specimen into area elements (pixels) of size d^2, and illuminate it with n photons per area element. The signal by which one will recognize two area elements as different is the difference in detected events, or $n(p_1 - p_2)$, where p_1 and p_2 are the probabilities that an incident photon creates a detected event in the feature-present and feature-absent cases, respectively. The noise is the root-mean-squared variation in the feature-absent case, or $\sqrt{np_2}$. The Rose criterion is then simply stated as

$$\frac{n(p_1 - p_2)^2}{p_2} > 25. \tag{31}$$

This expression leads to a minimum exposure requirement of

$$np_2 > \frac{25}{C^2} \tag{32}$$

where

$$C = \frac{p_1 - p_2}{p_2} \tag{33}$$

is the contrast. The radiation dose, D, is then found as the energy deposited per unit mass, or

$$D = \frac{hc}{\lambda}\frac{n\mu}{d^2\rho}, \tag{34}$$

where ρ is the density, μ is the linear absorption coefficient defined in Eq. 23, and (hc/λ) is the energy carried by each photon (assumed to be deposited in the specimen).

Neglecting instrumental losses and inefficiencies, for bright field amplitude contrast microscopy p_1 and p_2 are the appropriate transmission probabilities I/I_0 as given by Eqs. 21 and 23. Sayre *et al.* used this formalism to perform dose and exposure calculations on model specimens consisting of a volume element of protein, nucleic acid or lipid embedded in water. Figure 7 illustrates the type of results obtained. A dose of about 10^5 Gray is required to identify a 50 nm cube of protein in a 10 μm thick water layer, while if the cube is only 10 nm in size, the dose grows to over 10^8 Gray. The dose increases sharply with decreasing feature size primarily because there are fewer atoms in the smaller feature to generate the signal. Note that in this case the absorption event that determines the transmission rate and the absorption event responsible for the dose are one and the same.

Although Sayre *et al.* performed similar calculations for electron microscopy as well, they did not consider phase contrast, which is the standard imaging mode for electron microscopy of frozen hydrated specimens. (Phase contrast has been recently demonstrated in x-ray microscopy by Schmahl and collaborators [Schmahl 1994a], as will be discussed in Sec. 3.2.1). Jacobsen and Williams [Jacobsen 1994b] extended the work of Sayre *et al.* to include phase contrast in frozen hydrated specimens both in conventional and energy-filtered electron microscopy and in x-ray microscopy (the x-ray microscopy case had been treated separately before [Schmahl 1987, Rudolph 1990, Gölz 1992, Schneider 1992a]). Their calculated exposure requirement for observing organic material in 60 nm of ice at 2 nm resolution using 100 keV electrons and an energy filter is 600 e^-/nm^2, which is consistent with experimental results of 600–700 e^-/nm^2 [Schröder 1990, Langmore 1992]. While an exact comparison between electron and x-ray microscopy is ultimately highly sample-dependent, Jacobsen and Williams' results (shown in Fig. 8) indicate that the relative suitability of x-ray or electron microscopes varies dramatically according to the ice or water thickness surrounding the sample. Electron microscopy is far superior for the imaging of macromolecules or viruses in thin (up to a few tenths of a micrometer) water/ice layers, but in thicker specimens inelastic and multiple scattering increase to the point where they dominate over single scattering and phase contrast. X-ray microscopy is much better suited to the few-μm-thick water/ice layers within and around cells. Examination of Fig. 3 indicates that the ratio of inelastic to elastic cross sections changes by a relatively small amount as the electron energy is increased to 400 keV, so this general conclusion should still hold true for intermediate and high voltage electron microscopy as well.

Calculations for x-ray microscopies which involve detection of the scattered component only (dark field as discussed in Sec. 3.4.2, and diffraction as discussed in Sec. 3.7.2) have been carried out by Sayre *et al.* [Sayre 1980, Sayre 1984, Sayre 1988b, Sayre 1987]. The strength of the signal in this mode is proportional to the coherent cross section (i.e., the scattering factor per unit volume squared), and it benefits from the coherent superposition of amplitudes as

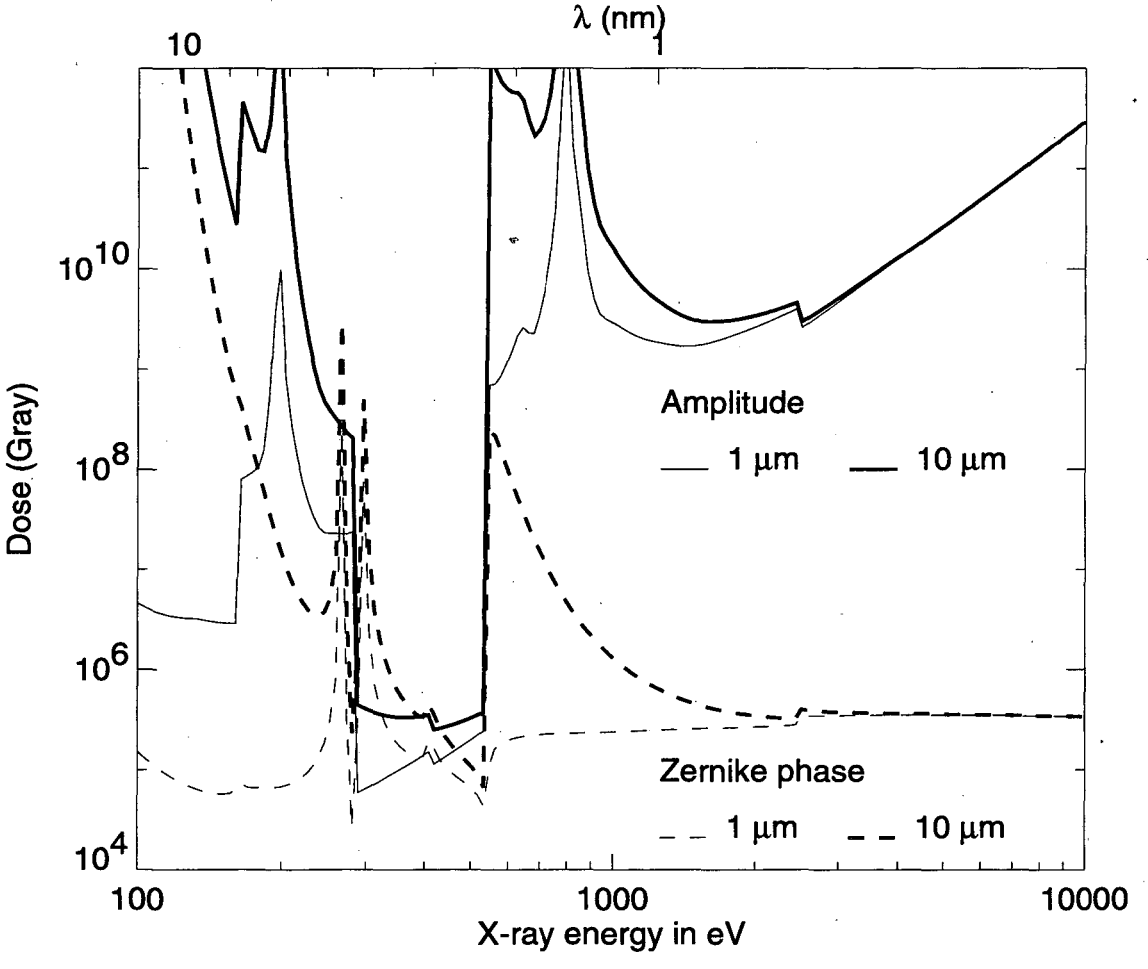

Figure 7: Radiation dose calculated for minimal exposure imaging (signal:noise=5:1) of 50 nm protein structures in 1 and 10 μm thick ice layers ($\rho = 0.92$). Both amplitude (solid lines) and Zernike phase contrast cases ($3\pi/2$ phase plate with no absorption) are shown.

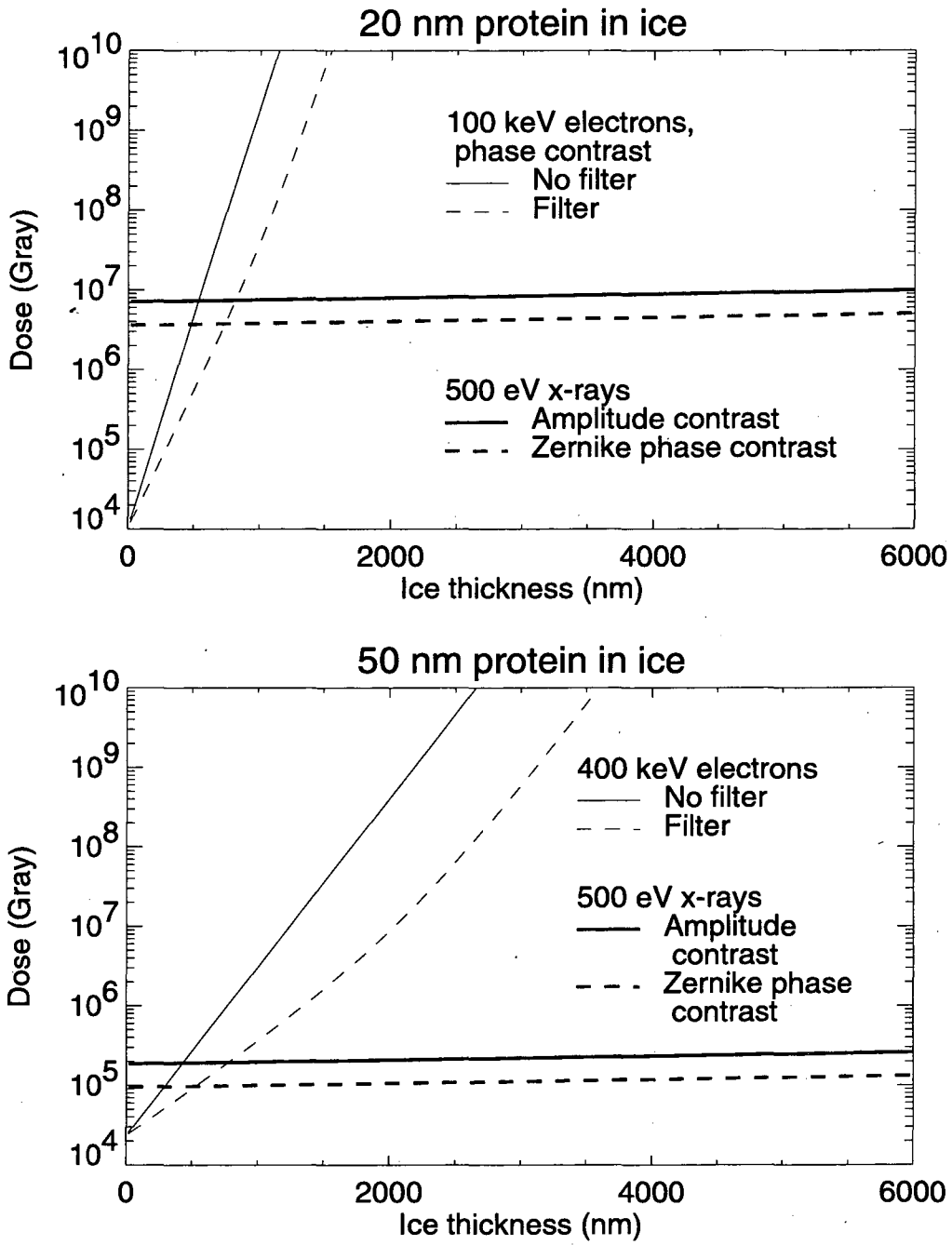

Figure 8: Radiation dose calculated for electron and x-ray minimal exposure imaging (signal:noise=5:1) of protein structures in varying ice thicknesses. The electron microscopy calculation are done both with and without the assumed use of an energy filter to select zero-inelastic-loss electrons [Jacobsen 1994b]. Top: dose calculated for imaging 20 nm structures with 100 keV electrons in phase contrast, and 500 eV x-rays. Bottom: dose calculated for imaging 50 nm structures with 400 keV electrons without phase contrast (since it is not available in thick specimens), and 500 eV x-rays. The relative suitability of x-ray or electron microscopes varies dramatically according to the ice or water thickness surrounding the sample.

discussed in the previous section. Sayre and Chapman [Sayre 1995] conclude that this coherent enhancement leads to an extremely steep d^{-8} dependence of dose on resolution.

In holography it is this same amplitude scattered by the specimen that interferes with the reference wave. Exposure and dose calculations based on the Rose criterion have been performed for holographic imaging using various assumptions by Solem and Baldwin [Solem 1982], Howells [Howells 1990a], Jacobsen *et al.* [Jacobsen 1990b], and London *et al.* [London 1989, London 1992b]. Although different assumptions lead to somewhat different results, the following conclusions emerge for all techniques that depend on scattering:

- Contrast is generated by *differences* in the complex scattering factor per unit volume $\rho(\vec{r})$ (Eqs. 19 and 25) within the sample.
- Radiation dose is due to the energy deposited in absorption events, which depends on f_2.
- Because f_1 has large variations near absorption edges, these special wavelengths offer dose advantages, as suggested by London *et al.* [London 1989].

As one goes to shorter x-ray wavelengths, it was noted earlier that the atomic scattering factor f_1 approaches a constant (equal to the atomic number Z), while f_2 falls sharply ($f_2 \sim \lambda^{5/2}$). It is then tempting to conclude that the dose is minimized by operating at the highest possible energy. This argument leaves out some compensating factors, however. First, in the f_1 = constant approximation, the scattered amplitude is energy independent, yet at shorter wavelengths the information on structure at a fixed resolution is shrunk into a narrower angular range. As a result, the useable signal (which scales with the solid angle) drops roughly as λ^2. Second, it is not f_1 that is responsible for the signal, but differences in $(f_1 + if_2)$ from the average.

2.5.2 Dose and damage

The radiobiology of soft x-rays has received considerable attention, especially during the past twenty years [Raju 1987, Folkard 1992]. The relationship between radiation dose and radiation damage is what determines whether the image recorded resembles the true biological structure, or the result of changes brought about by the exposure. The question of radiation damage in x-ray microscopy has been the subject of several studies (see e.g., [Shinohara 1991, London 1992b, Schneider 1992a]). We consider here the relationship between dose and damage in four cases: wet and living, wet and chemically fixed at room temperature, frozen hydrated, and dry.

2.5.2.1 Samples which are wet and living

For wet and living samples, classical radiation biology indicates that about half the cells in a colony exposed to a radiation dose of typically 3 Gray (1 Gray=100 rad) will die (see e.g., [Okada 1970]). For microscopy experiments, it is more relevant to ask about when the observation of a cell will give erroneous results because of radiation-damage-induced changes to the cell (e.g., morphological changes or structural deterioration). There is some data available in the case of electron microscopy [Joy 1973, Parsons 1974], and the question has been addressed in more recent soft x-ray experiments. Ford *et al.* [Ford 1992] used electron microscopy to show that doses of 1.5×10^3 Gray caused significant disturbances to the ultrastructural organization of the algæ *Chlorella*. Bennett *et al.* [Bennett 1993, Foster 1994] have shown that a dose of about 10^4 Gray will stop the ability of rabbit muscle myofibrils to contract in the presence of ATP. Gilbert, Pine, and collaborators [Gilbert 1992c, Gilbert 1992a, Gilbert 1992b], and more recently Oehler *et al.* [Oehler 1994], have shown that cultured fibroblasts begin to show immediate effects of irradiation at the 10^4–10^5 Gray level, while bacteria appear to be able to tolerate a dose somewhat above 10^5 Gray with no obvious immediate effect. An example of a more recent study on the effects of high radiation doses on fibroblasts is shown in Fig. 9.

2.5.2.2 Samples which are wet and chemically fixed

For wet and chemically fixed samples, x-ray microscopy studies on myofibrils [Bennett 1993, Foster 1994], cultured fibroblasts [Gilbert 1992a, Gilbert 1992b], and on chromosomes [Williams 1993] have shown that shrinking and especially mass loss become significant at radiation doses of about 10^6 Gray. Experience first with the Göttingen microscope at BESSY and later the Stony Brook microscope at Brookhaven has shown that a significant improvement (perhaps a factor of 2–10) in radiation damage resistance often can be obtained by using concentrated fixative (e.g., 2% glutaraldehyde), although ultrastructural changes associated with fixation may be significant [Stead 1992].

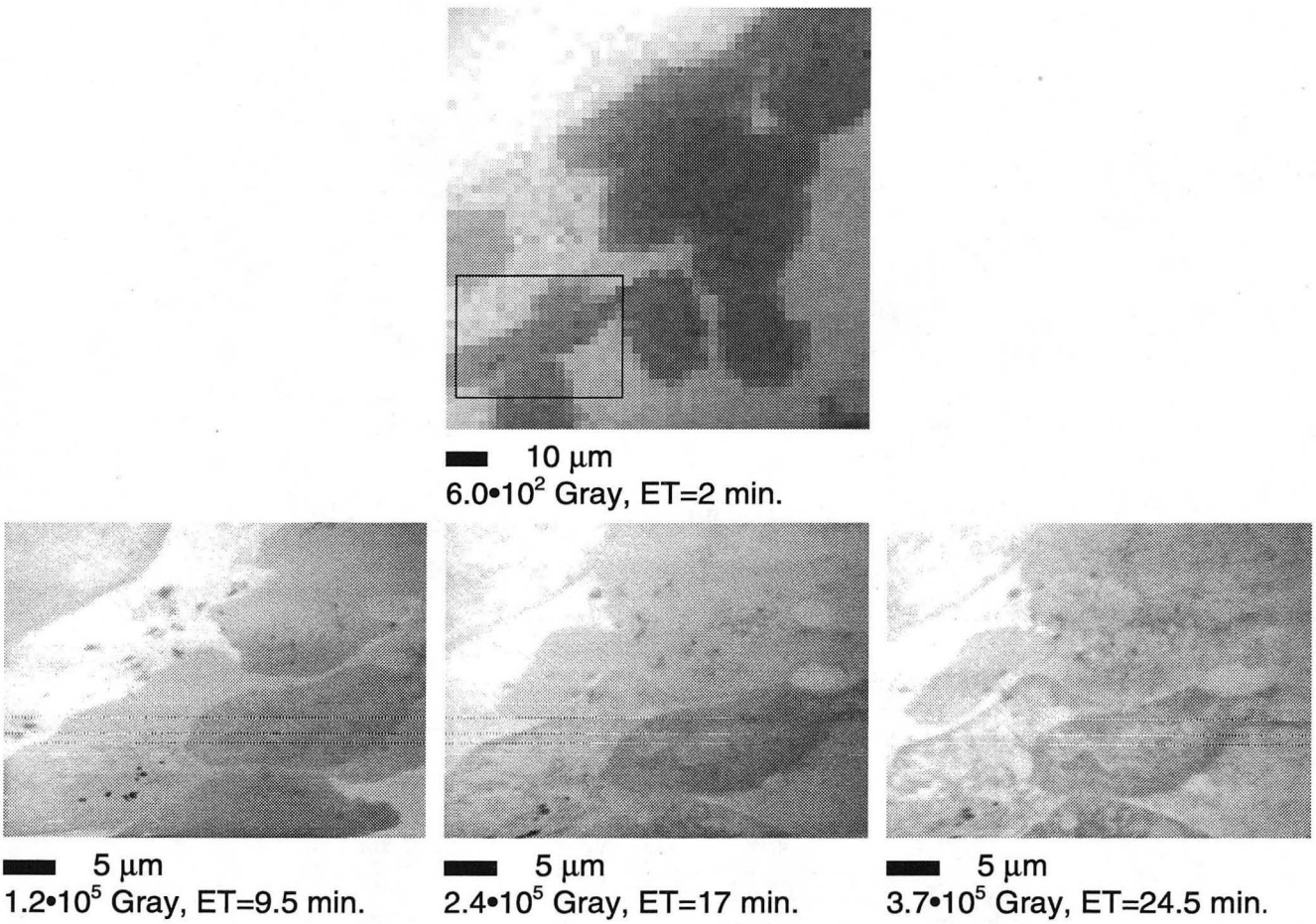

Figure 9: Initially living Chinese hamster ovarian (CHO) cells viewed using a scanning transmission x-ray microscope. Low-dose ($\lesssim 10^4$ Gray) images are compatible with at least 1–2 hours of cell survival as measured by viability dyes. Cells exposed to doses of 10^4–10^5 Gray lose membrane function and esterase metabolism functionality, and doses of about 10^5 Gray exhibit immediate morphological changes such as those shown here at various elapsed times ET in minutes. Cells outside the x-ray exposure field are unaffected as measured by morphology and viability dyes. Figure courtesy of V. Oehler *et al.* (Stony Brook) [Oehler 1994].

One additional insight has come from the work of Williams *et al.* (Fig. 10) in a study of lightly fixed (0.1% glutaraldehyde) *V. faba* metaphase chromosomes. They report that, in the *first* image of a previously unexposed metaphase chromosomes, measurements of two parameters (chromosome diameter and mass per unit length) give results which are independent of dose up to a first-image dose of about 2×10^6 Gray. On the other hand, *multiple* images of the same chromosome show radiation damage effects at doses above about 2×10^5 Gray. Williams *et al.* hypothesize from further evidence that radiation damage effects remain localized at the 50 nm level over timescales of 10 msec or longer, so that the information collected quickly in each pixel in a scanning microscope is accurately representative [Williams 1993].

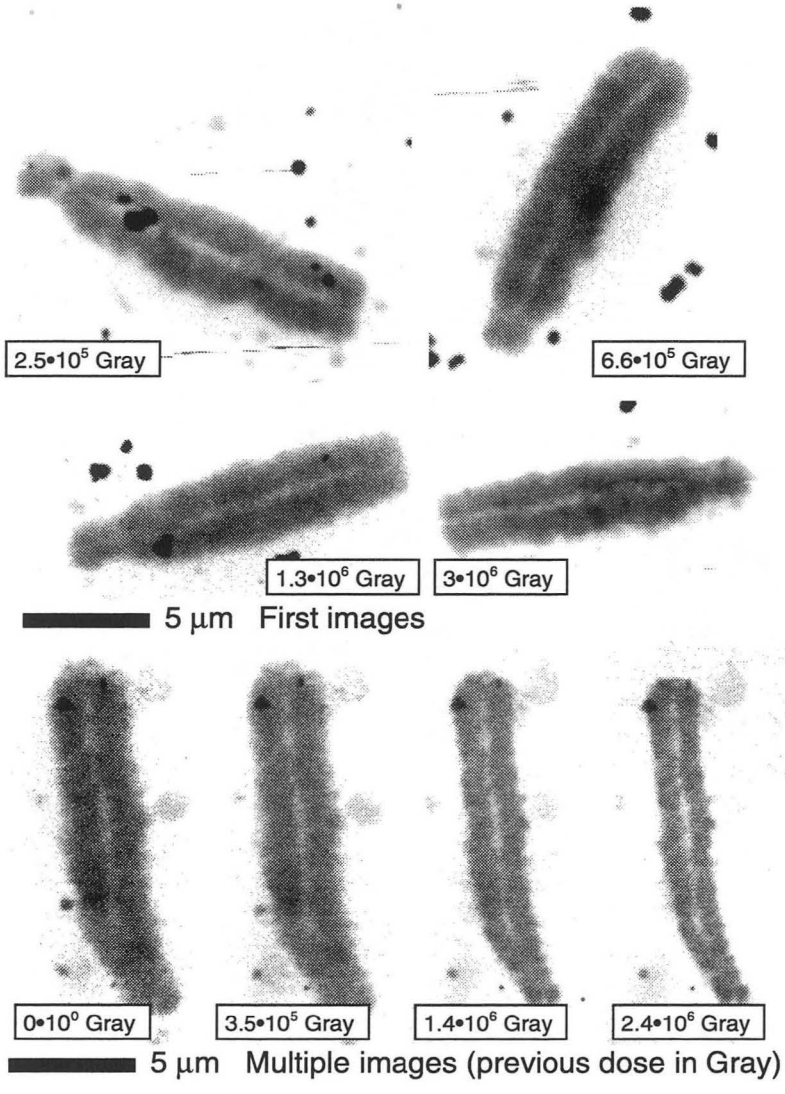

Figure 10: Wet *v. faba* chromosomes lightly fixed in 0.2% glutaraldehyde and viewed using the Stony Brook scanning transmission x-ray microscope at Brookhaven Laboratory. Multiple images of the same chromosome show degradation due to radiation damage; however, first images of previously unexposed chromosomes give accurate mass and diameter measurements up to $\sim 2 \times 10^6$ Gray. From Williams *et al.* [Williams 1993].

2.5.2.3 Samples which are frozen hydrated

For frozen hydrated specimens, there are considerable data on radiation damage limits from the cryo-electron microscopy community. While ultimate resolution limits can be inferred from the fading of electron diffraction spots [Glaeser 1978, Henderson 1992], mass loss [Lamvik 1991] and sample "bubbling" [Talmon 1987, Dubochet 1988] provide straightforward practical limits. In particular, "bubbling" is found to occur at doses of 10^3–10^4 e^-/nm^2 at 100 keV; using calculations of linear energy transfer [Berger 1964], this corresponds to doses of about 10^8–10^9 Gray. Since x-ray absorption leads to electron production, one would expect to find similar limits in soft x-ray microscopy (corresponding to about 100 high resolution images!). In fact, very recent work by Schneider and Niemann [Schneider 1994b] confirms that frozen hydrated algae are stable to doses in excess of 10^8 Gray in the Göttingen microscope at BESSY.

2.5.2.4 Samples which are dehydrated

Radiation damage of dehydrated specimens has been studied extensively by electron microscopy, where it is found that 75 keV electron exposures of 10^{-2} C/cm^2 or 600 e^-/nm^2 produce significant damage in room-temperature organic specimens as measured by mass loss [Reimer 1993]. We estimate that such exposures lead to a radiation dose of about 4×10^7 Gray. In x-ray microscopy, Williams *et al.* [Williams 1993] find no appreciable mass loss in chromosomes up to a maximum dose of 1×10^7 Gray, while Zhang *et al.* [Zhang 1994c] observe 50% mass loss in the resist polymethyl methacrylate (PMMA) at a dose of 1×10^7 Gray.

2.5.2.5 Comments

We summarize this body of work with the following general conclusions:

- Fixed but wet specimens show morphological change at 50 nm resolution at doses significantly in excess of 10^4 Gray. However, scanning microscopes can take meaningful single images up to doses of about 10^6 Gray, for the damage timescale reasons noted in Sec. 2.5.2.2.
- Dry specimens are stable up to doses of about 10^7 Gray.
- Frozen hydrated specimens preserve morphology to high resolution up to doses of about 10^8 Gray.

These statements are vast generalizations, of course, and there are many exceptions and variables not accounted for. They are nevertheless useful in designing imaging experiments.

Further evidence comes from a detailed model of what happens in the damage process developed by Schneider [Schneider 1994a]. He calculates the disruption of the molecules due to radiation, and the diffusion process of the molecular fragments that result. He finds that with very plausible choices of the parameters of the model (energy deposit per damaged molecule and diffusion coefficients), the results fit well the experimental observations. In this model it is easy to change the temperature, and it does predict that cryo x-ray microscopy will provide faithful images of biological specimens at the 10 nm level. It appears then that imaging of live cells, and even fixed wet specimens, should be limited to resolutions of about 100 nm and 50 nm respectively, even in the most efficient x-ray microscopes, with higher resolution to about 10 nm attainable for dry or frozen hydrated specimens.

In x-ray microscopy, considerations of the image collection time are also important, especially since several approaches are capable of operation with flash sources. How fast a flash is fast enough to capture the image before morphological changes corrupt its fidelity? At image timescales longer than about 0.1 sec for full-field illumination x-ray microscopes and pixel dwell times longer than about 0.01 milliseconds for scanning x-ray microscopes, thermal conductivity is sufficient to minimize specimen heating and therefore thermal distortions of the sample [Greinke 1992, Schneider 1992a, Jacobsen 1992e, Schneider 1994a]. The question of shorter exposures has been considered in some detail by Solem [Solem 1986] and also by London [London 1989, London 1992b] in the context of x-ray holography. Solem points out that if the exposure is fast but not fast enough, thermal conductivity cannot take care of the power dissipated in the specimen and a rapid hydrodynamic explosion results. The exposure time should be in the picosecond regime to capture a faithful holographic image at the 30 nm resolution regime. Such exposure times appear to be achievable with x-ray laser sources. Transmission and contact micrographs at this resolution level require a flash of a few nanoseconds or less.

One must conclude then that radiation damage processes in x-ray microscopy are physically similar to those in electron microscopy, and that they pose definite limitations to imaging. However, the reason that x-ray microscopy promises to provide progress in the imaging of radiation-sensitive samples is not that x-rays deliver any less dose per

particle, but rather that the lower background and improved contrast of x-ray images of thick specimens lead to a higher quality of information for whatever dose is permitted. Even so, while it may be possible to get a snapshot of an initially live specimen at high resolution either by flash exposure or flash freezing, it is contrary to all evidence to suggest that one should be able to make movies of, or otherwise follow normal physiological processes within a single specimen at resolution better than 100 nm by x-ray microscopy.

3 Soft X-ray Microscopes

Many types of x-ray microscope systems have been developed. Our purpose here is to concentrate on those which have been used for high resolution biological imaging. We note at the outset that x-ray contact microradiography and transmission x-ray microscopy (in analogy to transmission electron microscopy) can make use of spatially incoherent illumination, while scanning and holographic x-ray microscopes generally require coherent illumination (in analogy to scanning transmission electron microscopes) [Zeitler 1970, Jacobsen 1992b]. This has significant consequences, because the availability of high brightness soft x-ray sources for coherent illumination (as opposed to high flux soft x-ray sources for incoherent illumination) is a relatively recent development (see e.g., [Attwood 1985]).

3.1 Zone plates

Zone plates were invented about 120 years ago by Lord Rayleigh, and independently by Soret. These diffractive focusing elements are made up of concentric circular zones, with Fresnel half-period zone radii given by the approximate relationship

$$r_n^2 = mn\lambda f + m^2 n^2 \lambda^2/4, \tag{35}$$

where n is the zone number, f the focal length, λ is the wavelength, m denotes the diffractive order ($m = 1$ is the order usually used for imaging), and the $m^2n^2\lambda^2/4$ term is for correction of spherical aberration assuming a source or object at an infinite distance from the zone plate. They work like thin lenses, so they have a diffraction limit to their transverse resolution δ_t of

$$\delta_t = 0.61\frac{\lambda}{m\,\mathrm{N.A.}} \tag{36}$$

as calculated by Rayleigh for a lens with numerical aperture N.A. Two other especially useful relationships can be obtained from these expressions if the $m^2n^2\lambda^2/4$ spherical aberration correction term is neglected [Michette 1986]. One is a relationship between the width of the finest zone δ_{r_N} of a zone plate with N half-period zones and its Rayleigh resolution of

$$\delta_t = 1.22\delta_{r_N}/m. \tag{37}$$

Another is a relationship between the diameter $d = 2r_N$, outer zone width, focal length, diffractive order, and illumination wavelength of

$$d\delta_{r_N} = mf\lambda. \tag{38}$$

To deliver optimum performance [Thieme 1988], a zone plate should be illuminated with radiation with a monochromaticity equal to the total number of half-period zones multiplied by the diffractive order, or

$$\frac{\lambda}{\Delta\lambda} \gtrsim m\,N. \tag{39}$$

Furthermore, it is imperative to use the best microfabrication technology to form these rings, and place them with a precision that is about 1/3 of the desired resolution [Simpson 1983, Michette 1986]. The chromatically dispersive nature of zone plates can also be exploited to make a combined condenser/monochromator [Schmahl 1974, Niemann 1974, Spiller 1978, Niemann 1983, Kagoshima 1989].

Following a proposal by Schmahl and Rudolph in 1969 [Schmahl 1969], the first successful scheme for fabricating zone plates for x-ray microscopy using holography was developed by Rudolph *et al.* [Rudolph 1976]. They later succeeded in using this technique to make zone plates with outer zone widths as small as 55 nm [Schmahl 1984b]. Most transmission x-ray microscopes require condenser zone plates with large diameters and high zone numbers. These zone plates are being made exclusively by the holographic technique [Rudolph 1980, Schmahl 1984b].

In 1972, Sayre proposed that electron beam microfabrication would be a good technique for zone plate fabrication [Sayre 1972], and this approach has since been adopted by most of the groups active in the field [Ceglio 1983,

Kern 1984, Anderson 1992, Tennant 1991, David 1992, Charalambous 1992]. The best zone plates today have finest line widths in the 20–30 nm range [David 1994, Thieme 1994a, Attwood 1994, Charalambous 1994]. These zone plates are supported on thin membranes (typically $\sim$ 100 nm silicon or silicon nitride). These have proven to be both stable and adequately transparent throughout most of the wavelength range of interest. Silicon nitride is easier to fabricate, while silicon has superior transmission, especially for $\lambda < 3.1$ nm [Medenwaldt 1994a].

The efficiency of the zone plate denotes the fraction of the x-rays incident on this optical element that are diffracted into the desired order. For perfectly-made alternating opaque and transparent zones, the first order efficiency is about 10%. If the opaque zones are replaced by material that introduces phase shift of π, this efficiency can be as large as about 40%. Unfortunately, no material exists that affects the phase without absorbing part of the radiation in the soft x-ray region, and the efficiency falls in between [Kirz 1974, Ceglio 1983, Tatchyn 1984, David 1992]. To achieve optimal performance, the thickness of the rings must be controlled carefully, and for high resolution plates with narrow rings the thickness must be much larger than the ring width. Fabrication of such high aspect ratio structures is a particularly demanding task. Furthermore, as the aspect ratio becomes very large, the zones start acting as wave guides, and high efficiency can be obtained only by tilting the zones onto a conical shape according to the Bragg condition. Deviation from the Bragg condition results in a considerable drop in efficiency and in severe aberrations [Maser 1992, Maser 1994].

Much useful information regarding zone plates, including a treatment of aberrations, is found in the books by Michette [Michette 1986] and by Spiller [Spiller 1994].

3.2 The Göttingen transmission x-ray microscope

The Göttingen group has been operating transmission x-ray microscopes (TXM) of ever improving performance since 1974 [Niemann 1974]. The basic approach has been to use a zone plate as a microscope objective to create a magnified image of the object. While some of the earlier versions of their microscope are described in the literature [Niemann 1976, Niemann 1983, Rudolph 1984], we will concentrate on the current state of the instrument as it operates at the synchrotron radiation source BESSY in Berlin [Guttmann 1992b, Niemann 1994].

The layout of the BESSY microscope is shown in Fig. 11. X-rays from a synchrotron bending magnet source (critical wavelength $\lambda_c = 2$ nm) are incident on a condenser zone plate which, in combination with a 20 μm aperture, serves both as a condenser lens and as a monochromator. The condenser is made of germanium, and is fabricated holographically. It has 4.2×10^4 zones in a diameter of 9 mm, and a 4 mm diameter central stop. The condenser zone plate outer zone width is 53.7 nm, and its focal length is 201.4 mm for 2.4 nm x-rays. The specimen is located immediately downstream of a 20 μm illumination aperture, and the condenser zone plate is wobbled during the exposure to provide spatially uniform illumination. The micro zone plate forms a magnified real image of the object at roughly 1000$\times$ magnification; the magnified image is then recorded on a 1024 $\times$ 1024 pixel, backside-thinned CCD camera with 73% detective quantum efficiency [Meyer-Ilse 1993, Wilhein 1994]. A channelplate detector with a phosphor screen can also be used for alignment purposes.

The microscope has been redesigned to enable rapid changeover between two modes. First, a reflective DIC optical microscope is used for sample selection, alignment, and prefocusing. An electronically controlled and pneumatically driven system then raises and removes the optical microscope, and swings a snout carrying the condenser aperture into place. The sample is held on a polymer/silicon dioxide thin film at atmospheric pressure (vacuum windows are used on either side to keep the air path to $\sim$ 0.5 mm), and a sandwich of two additional films with syringe control of the water layer can be used for studies of wet specimens [Schneider 1992b, Niemann 1994]. Image exposure times range from under a second with dry specimens to a few seconds for wet specimens, depending on the zone plate used. The microscope operates routinely at 2.4 nm wavelength for maximum penetrating power in wet specimens. To image larger specimen areas beyond the 20 μm limit imposed by the aperture, step-and-repeat exposures may be performed under manual micrometer control. The optical performance of the microscope is illustrated in Fig. 12, which shows that 25 nm lines and spaces can be imaged.

3.2.1 Zernike phase contrast

In Zernike phase contrast, the complex (magnitude and phase) wavefield leaving the specimen is imaged in a way such that it is mixed with a phase-shifted unscattered wave. If the phase-shifted "reference" wave is reduced in amplitude by a factor of a, the image intensity is well approximated by [Born 1980, Eq. 8.7-74] $I = a^2 \pm 2a\varphi$, where $\varphi = 2\pi\delta t/\lambda$ for a sample of thickness t and refractive index $n = 1 - \delta$, and the $\pm$ sign indicates whether positive ($\pi/2$

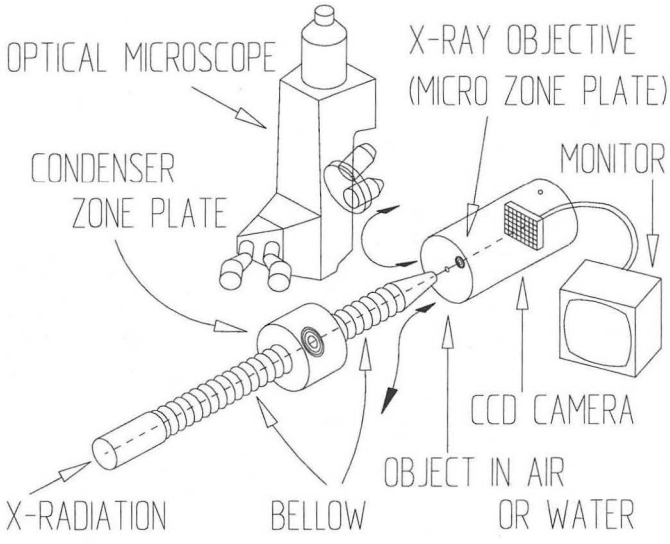

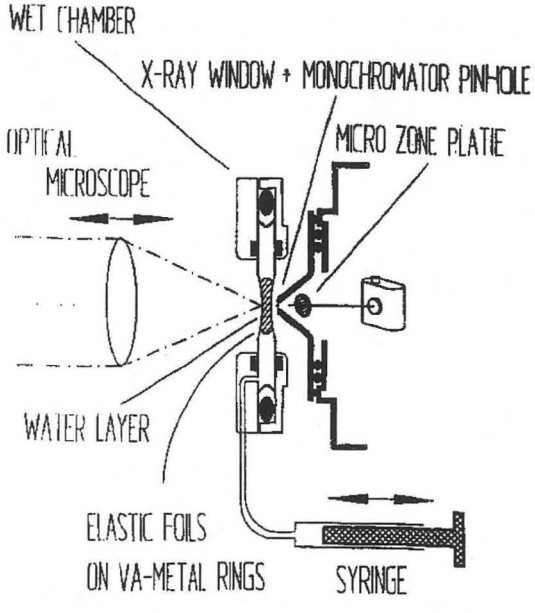

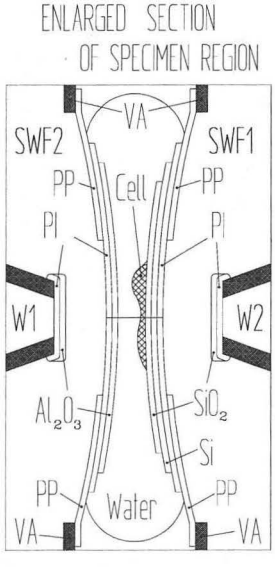

Figure 11: Schematic of the BESSY microscope. **Top**: x-rays come from the BESSY storage ring (at left in this figure), are monochromatized and concentrated onto the sample area using a condenser zone plate. The objective zone plate projects an enlarged image of the sample onto a soft x-ray CCD camera. The condenser zone plate can be swung down to allow for sample examination using a differential interference contrast optical microscope which swings down from above. **Bottom:** Wet samples are mounted in an atmospheric pressure environment using a combination of thin films of polypropylene (PP), polyimide (PI), aluminum oxide (Al_2O_3), and silicon oxide (SiO_2). The films are mounted on support rings (VA). From Niemann *et al.* [Niemann 1994].

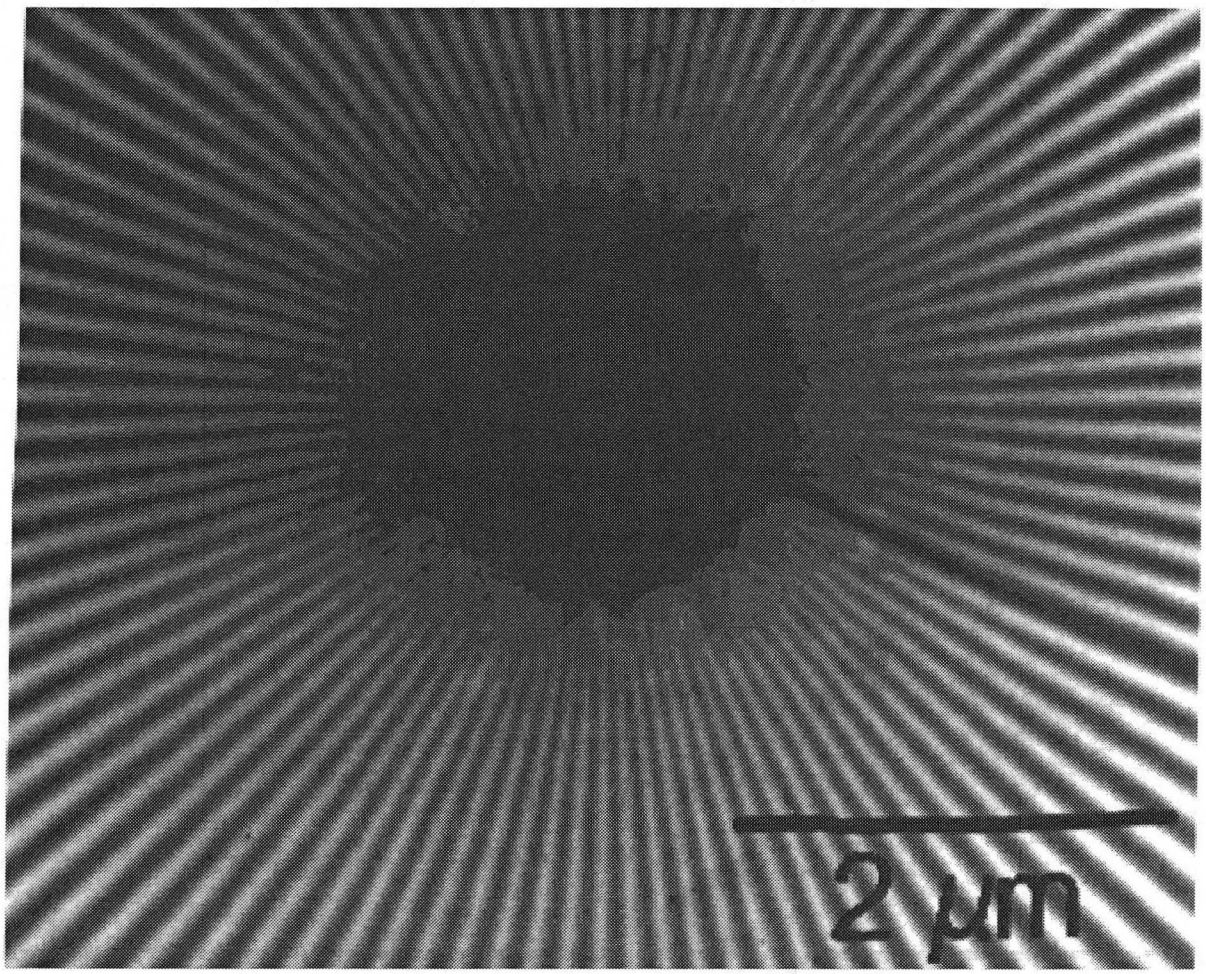

Figure 12: Test pattern imaged with the Göttingen transmission x-ray microscope at BESSY. A negative contrast image is shown. The test pattern was fabricated using the same electron beam lithography technology used for zone plate fabrication; lines and spaces as small as 25 nm can be observed using a δ_{r_N}=29 nm objective zone plate. From Aschoff [Aschoff 1994].

phase shift) or negative ($3\pi/2$ phase shift) is used. Since the wavefront scattered by the specimen is itself shifted in phase by $\pi/2$, the object and the phase-shifted reference waves are either fully in or fully out of phase; the contrast is thereby maximized.

Phase contrast x-ray microscopy has been beautifully demonstrated in the Göttingen transmission x-ray microscope (Fig. 14). By placing a removable ring aperture near the condenser, and a permanently-mounted phase-ring in the conjugate plane (see Fig. 13), the direct analog of Zernike phase contrast in visible light microscopy is realized. The advantages in improved contrast of such an arrangement were emphasized several years ago [Schmahl 1987, Rudolph 1990]. Schmahl *et al.* calculate [Schmahl 1994a] that, for 50 nm protein structures in a 10 μm thick water layer, optimized negative phase contrast ($3\pi/2$ phase shift) provides considerably better contrast than positive phase contrast ($\pi/2$ phase shift), which in turn is considerably better than pure amplitude contrast throughout almost the entire wavelength region from 0.2 to 5 nm. The improved contrast should allow for reduced illumination and therefore reduced radiation dose to the specimen.

The specific arrangements are as follows: The removable ring aperture leaves a 1 mm wide outer ring of the 9 mm diameter condenser unobstructed. The phase ring is 460 nm thick copper, and is permanently attached to the objective. It is designed for a wavelength of 2.4 nm, where it provides $3\pi/2$ phase shift (negative phase contrast) and transmits 7% of the incident radiation. Quasi amplitude contrast images are made by removing the ring near the condenser; the condenser area is then increased 2.5 fold, but because this added illumination is not attenuated in the phase ring, the direct radiation reaching the image field is increased 37 fold. Two objective–phase ring combinations have been used. The zone plates are made of germanium supported on thin silicon membranes. Zone plate MZP 53 has a diameter of 55 μm, 258 zones, an outer zone width of 53 nm, and an absolute diffraction efficiency of 11%. Its copper phase ring covers the annulus from 33.8 μm to 46.1 μm in diameter. Zone plate MZP30 has a diameter of 56 μm, 465 zones, an outermost zone width of 30 nm, and an absolute diffraction efficiency of 5.9%. Its phase ring covers the annulus from 19.4 μm to 26.5 μm in diameter.

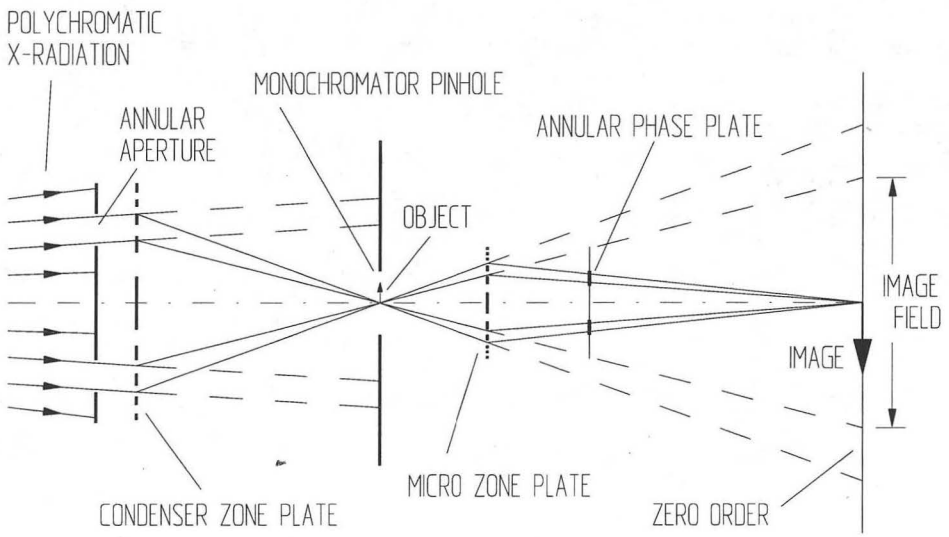

Figure 13: Schematic ray diagram of the Zernike phase contrast x-ray microscope with an annular aperture in front of the condenser and an x-ray objective with an annular phase plate. From Schmahl *et al.* [Schmahl 1994a].

3.2.2 The Göttingen laboratory microscope

The basic design of the Göttingen microscope is the basis of several other instruments planned, in operation, or under development. The Göttingen group itself has been involved in the construction of a "laboratory" microscope [Niemann 1990]. The instrument uses a gas plasma discharge x-ray source developed by Neff *et al.* [Neff 1988]. The purpose is on the one hand to make single-shot flash imaging possible, and on the other to develop a stand-alone

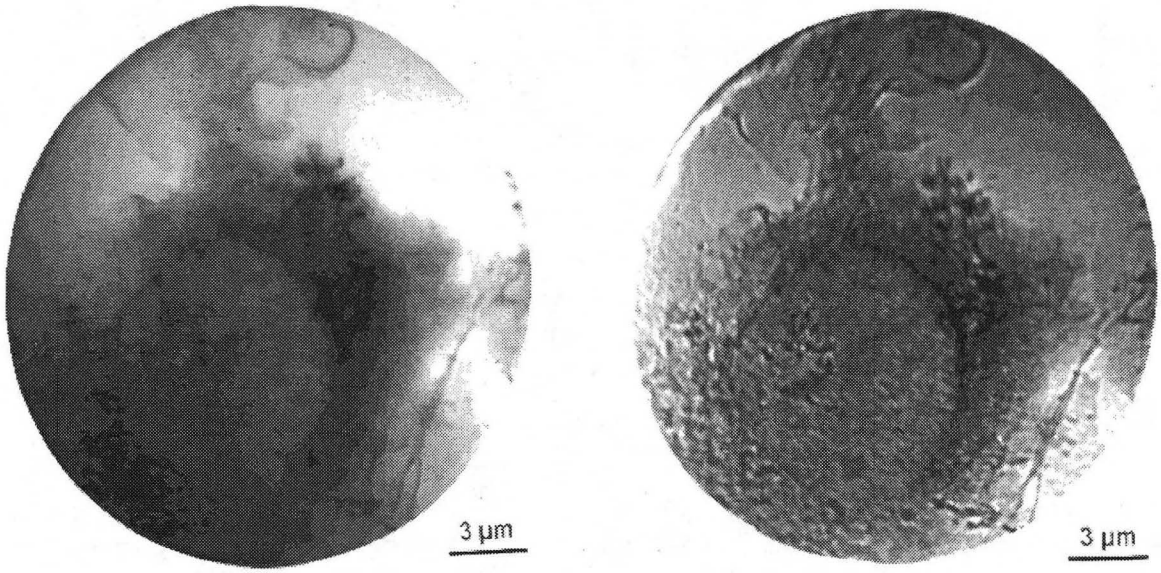

Figure 14: Images of cultured, glutaraldehyde-fixed Kupffer cells from rat liver, imaged in amplitude contrast (left) and phase contrast (right) using the Göttingen transmission x-ray microscope at BESSY. Macrophage-specific antigens on the cell surfaces have been stained using monoclonal antibodies ED1 and ED2, and a second peroxidase-conjugated antibody and silver staining; they appear emphasized in amplitude contrast, while unstained structures are more readily apparent in phase contrast. From Schmahl *et al.* [Schmahl 1994a].

soft x-ray microscope that could be placed into biology laboratories.

Quasi-monochromatic illumination at 2.48 nm is derived from hydrogen-like nitrogen ions under carfully controlled plasma conditions and filtered with a low pressure gas (oxygen) [Rothweiler 1994]. An ellipsoidal mirror is used as the condenser, but the rest of the optical system is very similar to the BESSY instrument. Mechanically it is the specimen and zone plate objective that swing out together for visible light microscopy and focusing, and swing back into precise alignment in the x-ray microscope (see Fig. 15). The optical performance of the instrument has been characterized by Diehl [Diehl 1994], and images of dry specimens have been obtained with a single pulse (see Fig. 16). To image wet specimens with the flux available in the pulse, the efficiency and the numerical aperture of the objective zone plate needs to be improved. Additional efforts may be directed towards integrated exposures from high-repetition-rate laser plasma sources [Rymell 1993, Rymell 1994].

3.3 Scanning x-ray microscopes

The basic idea in scanning microscopy is simple: form a microprobe and use it to examine the specimen one pixel at a time. In most applications the best resolution is set by the size of the microprobe. The speed of image acquisition is typically limited by the desire to collect statistically meaningful information for each pixel, which in turn is limited by the x-ray flux (photons/sec) in the microprobe.

The first successful scanning x-ray microscope was built by Horowitz and Howell at the Cambridge Electron Accelerator in 1972 [Horowitz 1972, Horowitz 1978]. They used synchrotron radiation focused onto a 1–2 μm diameter pinhole to define the microprobe, and formed images of a variety of specimens detecting either the x-ray fluorescence from the specimen or the transmitted x-rays. More recently, Bilderback *et al.* have used tapered capillary optics to carry this same approach to the 50 nm resolution level [Bilderback 1994]. The $\sim \sqrt{\lambda d}$ blurring due to Fresnel diffraction limits the probe-to-sample distance to an acceptable ~ 20 μm distance at the 8 keV energies used; such an approach is less practical at "water window" soft x-ray wavelengths, where the sample would have to be scanned at $\lesssim 1$ μm distances from the capillary tip.

To reach submicron resolution while maintaining a finite working distance with soft x-rays, it is necessary to use a focusing element to form the microprobe. Zone plates have been the most widely used focusing elements

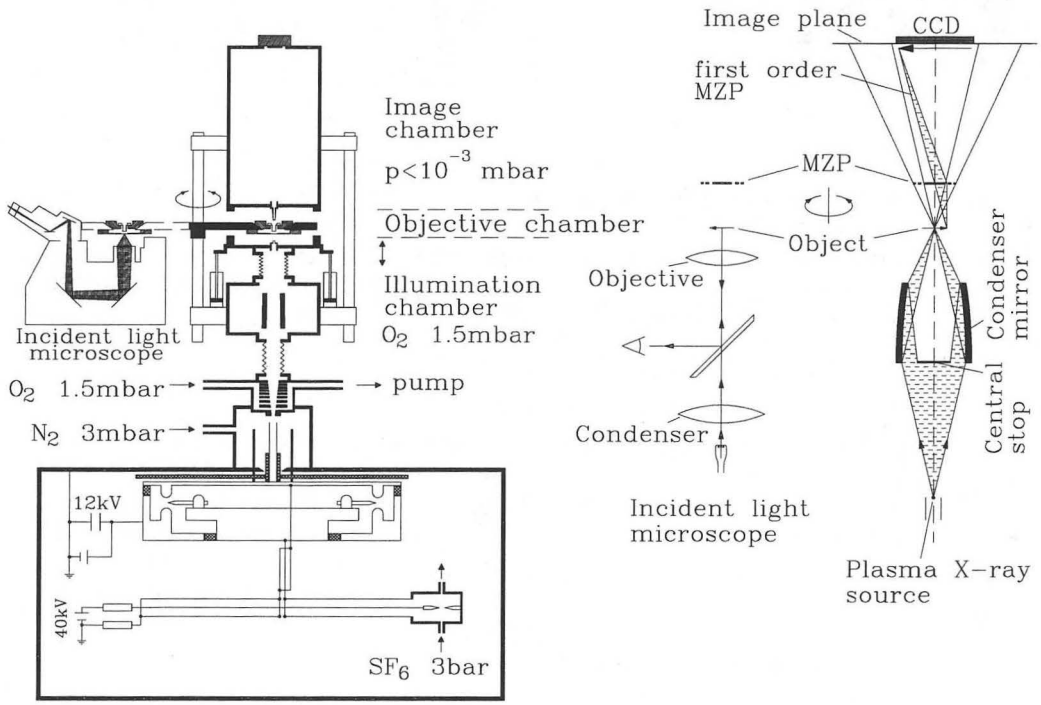

Figure 15: Layout of the Göttingen laboratory x-ray microscope. From Diehl [Diehl 1994].

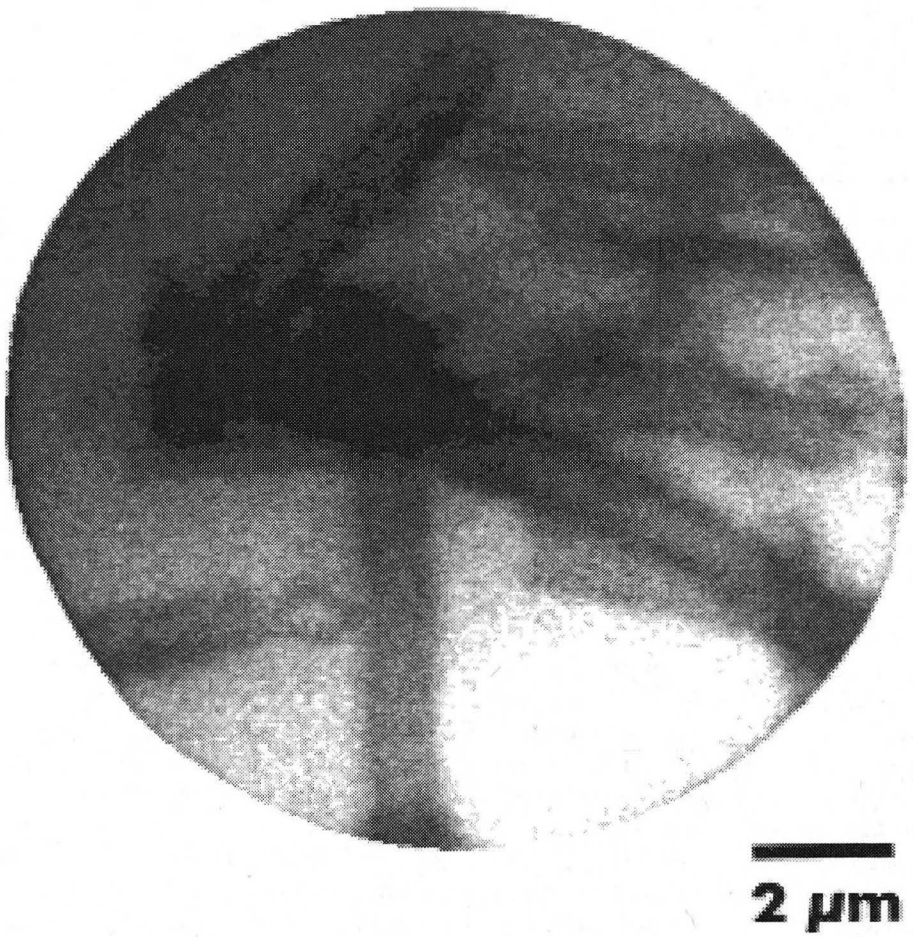

Figure 16: X-ray image of dry tubular sheaths of the bacterium *lepthotrix ochracea* taken with the Göttingen laboratory x-ray microscope using a single 5 nanosecond x-ray pulse. Figure courtesy G. Schmahl, Institute of X-ray Physics, Universität Göttingen.

(although mirrors both at normal and at grazing incidence have also been used; see Sec. 3.6). The optical problem is simplified relative to full field microscopes in that the focusing element need only work well for one image point (the focus), and off-axis aberrations are therefore of no concern. If a diffraction-limited (i.e., free of detectable aberrations) focusing element is coherently illuminated, it provides the smallest possible microprobe with a Rayleigh resolution of $\delta_t = 0.61\lambda/\text{N.A.}$, illustrating the reciprocity between imaging and scanning microscopy [Zeitler 1970, Sheppard 1986, Morrison 1989]. The actual probe size is given by a convolution of the demagnified image of the illumination source, and the point spread function of the objective lens. It can be shown that the modulation transfer function (a measure of the contrast for feature sizes approaching the resolution limit of an optical system) is seriously affected when the product of source diameter times full angle accepted by the optic approaches λ in each dimension [Rarback 1983, Buckley 1987, Jacobsen 1992b]. In laser terms, a scanning microscope requires single-mode illumination; other modes (such as are present in lower brightness sources such as laser produced plasmas [Michette 1988b, Michette 1993, Michette 1994] and synchrotron bending magnets) must be rejected with a spatial filter such as a focusing element and pinhole.

3.4 The Stony Brook scanning microscope at the NSLS

The first scanning transmission microscope (STXM) to use a zone plate objective was built in 1982 by Rarback *et al.* [Rarback 1984]. It used a bending magnet beamline with a grating monochromator at the 0.7 GeV ring at the National Synchrotron Light Source at Brookhaven National Laboratory. A small pinhole placed near the monochromator exit slit defined the beam to illuminate the zone plate, which focused the beam to a spot of about 0.3 μm. The zone plate was made by electron beam writing in Dieter Kern's laboratory at IBM [Kern 1984]. The specimen was placed in the focal plane and scanned using piezoelectric translators under computer control. Transmitted x-rays were detected using a proportional counter and used to form a digital image on the computer screen. The microscope was used for imaging both dry and hydrated biological specimens [Jacobsen 1987], and for experiments in elemental mapping [Kenney 1985]. The basic scheme of STXM has not changed over the years, although every aspect has been dramatically improved.

The current microscope hardware and its performance has been described by Jacobsen *et al.* [Jacobsen 1991, Jacobsen 1994a]. The beam is derived from a high brightness soft x-ray undulator on the 2.5 GeV ring of the National Synchrotron Light Source and its associated beamline [Buckley 1989, Rarback 1990]. At present, the properties of the storage ring electron beam are such that the undulator radiates into about 100 spatial modes in the horizontal, and about 3 modes in the vertical (storage ring upgrades are underway which should put more flux into fewer modes), and the spectral bandwidth of the first undulator harmonic is about 8%. (By adjusting the mechanical gap of the undulator, the first harmonic can be tuned throughout the "water window" spectral range). A spherical grating monochromator is used to spectrally filter the beam to $\lambda/\Delta\lambda$ =200–1500 (the experimenter can make a tradeoff between more flux or better spectral resolution). The sizes of the beamline optics and of the beam defining apertures are chosen so that the ones which occlude the beam (remove spatial modes) do so with a large enough overfilling factor that the throughput is stable against beam shifts. The beamline thus also serves as a spatial filter to deliver single-mode illumination to the zone plate. A 200 μm wide, 100 nm thick silicon nitride window is used as a $> 60\%$ transmissive vacuum window through which the x-ray beam is brought from the ultrahigh vacuum of the beamline to atmospheric pressure air. The x-ray air path can be filled with helium to minimize absorption losses. The zone plates in current use have been fabricated by Erik Anderson of Lawrence Berleley Laboratory in Dieter Kern's laboratory at IBM Yorktown Heights. The finest zone width is 45 nm, the outer diameter is 90 μm, and the central stop diameter is 40 μm. From Eq. 38, the focal length for 3.64 nm x-rays is found to be 1.11 mm. The 100 nm thick nickel zones, supported on a 100 nm silicon nitride membrane, result in a diffractive efficiency in excess of 12% at wavelengths above about 3 nm. The central stop is used in conjunction with an order sorting aperture (OSA) to cut out the portion of the beam that is not directed toward the first order focus (see Fig. 17); the typical working distance between a 35 μm OSA and the sample is about 350 μm. The typical flux delivered into a diffraction-limited focal spot is about 10^6 photons per second at present, although storage ring and beamline upgrades now underway promise an increase by more than a factor of five.

The specimen is mounted on a scanning stage in the focal plane of the zone plate. Fine scanning is provided by Queensgate piezoelectric positioners which operate with a least step size of 4.3 nm and drive a flexure stage [Browne 1992], while coarse scanning and positioning is performed using stepper motors. This arrangement makes large area survey scans easy. Transmitted x rays are detected using a proportional counter which is linear to about 1 MHz, and saturates at around 2.5 MHz. Wet specimens are imaged in wet cells with silicon nitride entry and exit

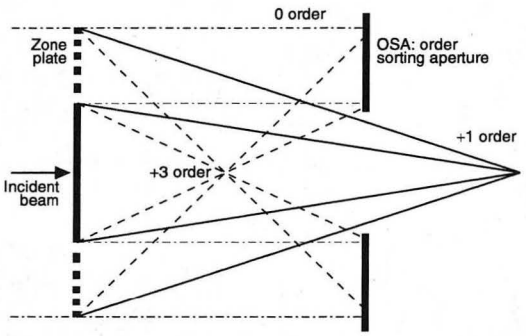

Figure 17: Schematic diagram showing the role of a central stop and an order sorting aperture in isolating the radiation focused in the first diffractive order of a Fresnel zone plate. Note that zone plates with alternate zones of equal area have only odd order foci.

windows. One such wet cell, shown in Fig. 18, was developed by Pine and Gilbert [Pine 1992, Gilbert 1992a]. The specimen is placed or cultured on the entrance window which can be rapidly mounted and dismounted; the window is sealed to the rest of the chamber using a gasket and held by a screwed-on frame, and the exit window (about 1 mm away) is glued in place. By draining the chamber of culture medium for no more than about 20 minutes at a time and then refilling through the syringe tubes provided, live cell cultures can be maintained for many hours [Pine 1992], and cultured cells are easily imaged (see Figs. 19 and 20). After draining, about 1 μm of liquid remains covering the sample as a result of surface tension, and the air within the chamber is maintained at 100% humidity by a "puddle" of buffer at the bottom of the chamber. Another type of wet cell, developed by Goncz *et al.* [Goncz 1992a], has permanent windows spaced just a few μm apart. The specimens in their buffer are introduced through the small tubes, and are exposed that way (see Sec. 4.5).

The microscope is run from a VAXstation 4000/90 using CAMAC-based electronics, and the mouse-driven graphical user interface and image processing software is based on the commercial package IDL. The system is designed so that the electronics operate without computer intervention on a pixel-by-pixel basis; data is transferred to the computer at the end of each scan line and is displayed at that time. Contrast levels, color maps can be changed at will, and the mouse can select pixels and lines through marked pixels for digital display of count rates and coordinates.

A resolution test pattern (also fabricated by Erik Anderson) was used to study the optical performance of the STXM. The measurements are in good agreement with calculated values (see Fig. 21). Based on the good agreement between calculated and theoretical modulation transfer functions, the theoretical point spread function can be deconvolved from oversampled images [Jacobsen 1991, Zhang 1992], as is illustrated in Fig. 22.

In the standard mode of operation, the specimen is mounted on a holder which attaches magnetically to the scanning stage. The specimen is positioned using a visible light microscope with the x-ray detector retracted (at present, the detector is the proportional counter mentioned above, although avalanche photodiodes have been used [Palmer 1992b] and a cooled avalanche photodiode will soon be installed). With the detector re-inserted, the operator is free to select the number of pixels in the image (up to 500×500), the pixel size, and the dwell time for each pixel. A typical large scale orientation scan involves 400×400 pixels with 1 μm steps and 1 ms dwell time using the stepper motors; such a scan takes about 7 minutes and delivers a dose of about 200 Gray to the sample (when the $\sim 50\%$ absorption losses between the sample and the active detector area are accounted for). Fine focusing is accomplished in a special operating mode where the horizontal dimension of an "image" corresponds to horizontal motion of the scanning stage as normal, but the vertical dimension corresponds to varying the focus position. This mode, examples of which are shown elsewhere [Jacobsen 1994a], allows the focal position to be rapidly located. The operator will then usually switch over to making high resolution images with a pixel size of about 50 nm, and a dwell time in the 1–10 ms range depending on the wavelength and the desired signal-to-noise ratio. For example, a 300×300 pixel scan with 5 msec dwell or about 5000 incident photons/pixel will take about 8 minutes and impart a dose of about 4×10^5 Gray to the sample.

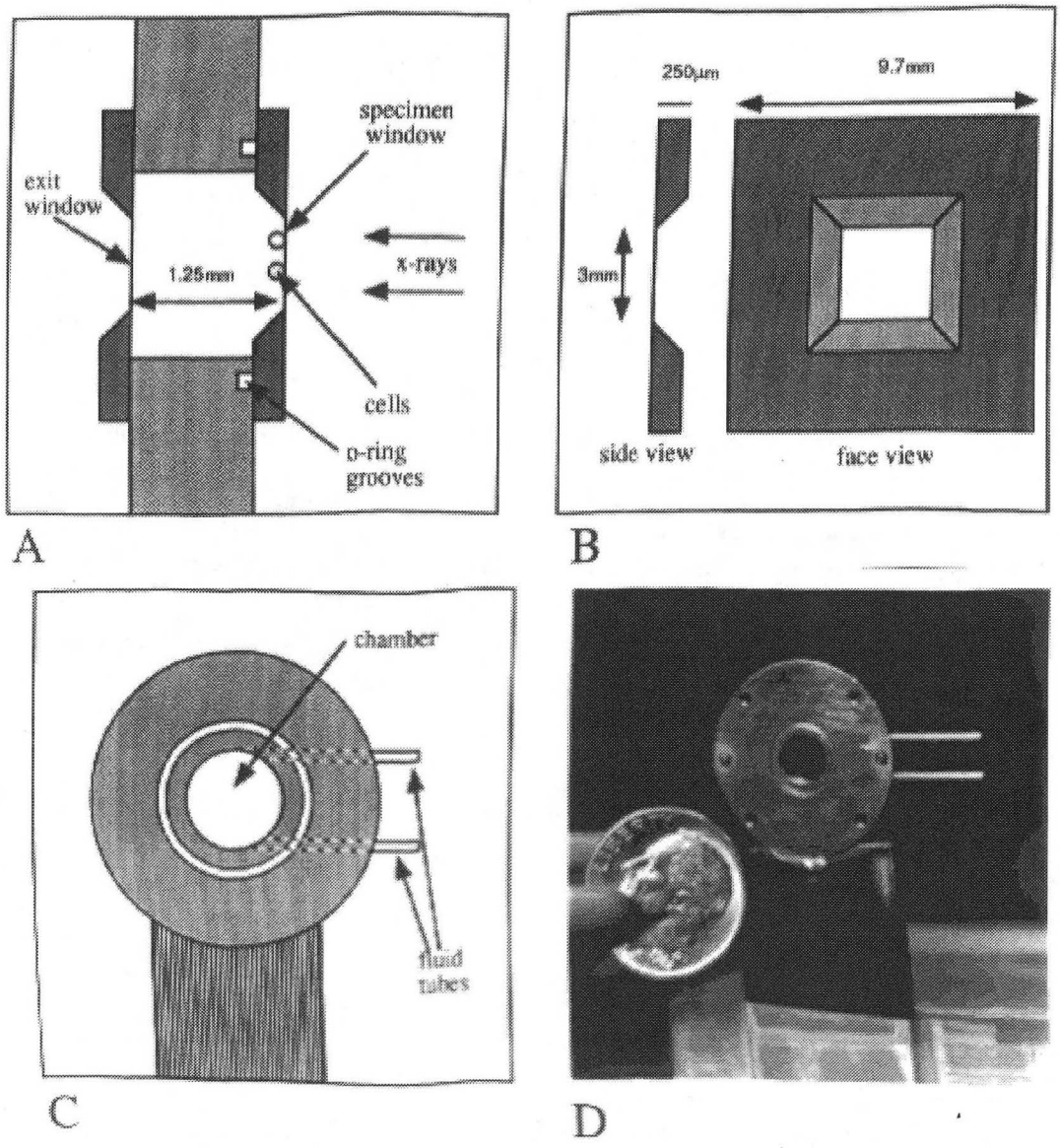

Figure 18: The Caltech wet specimen chamber. Samples are deposited on silicon nitride windows in silicon wafer frames (**b**); a clamping frame (not shown) is used to clamp the wafer frame against an O-ring in the groove shown in **C**. Cultured cells can be maintained for hours by flushing the chamber with fresh medium every 20–30 minutes; surface tension keeps a μm-thick medium layer around the samples when the chamber is drained. From Pine and Gilbert [Pine 1992].

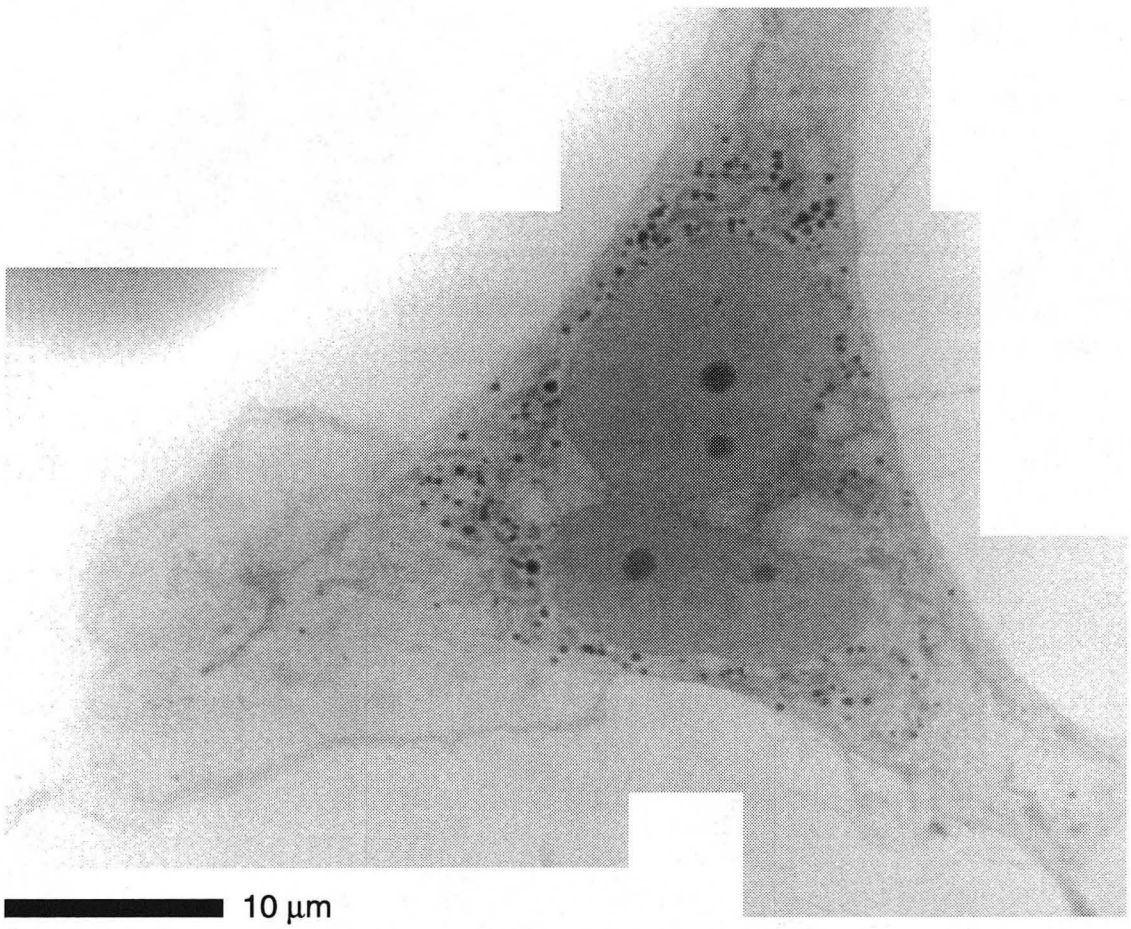

Figure 19: Scanning x-ray micrograph of a wet, glutaraldehyde-fixed chick embryo skin tissue fibroblast. Figure courtesy J. Gilbert and J. Pine (Caltech) and C. Buckley (King's College, London); from [Gilbert 1992a].

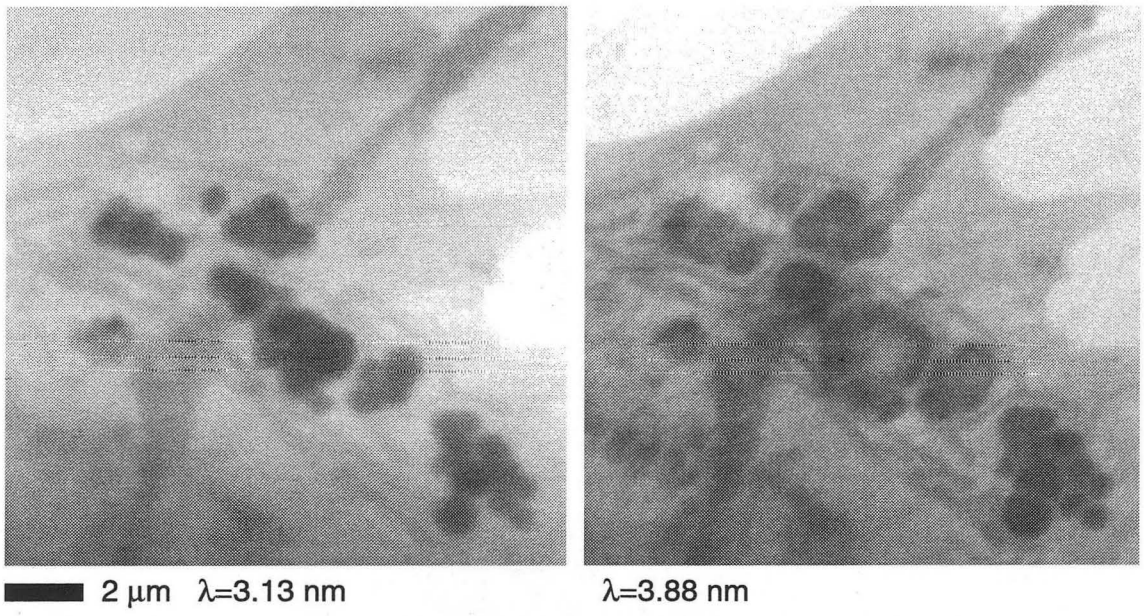

Figure 20: Detail from an fibroblast cell image similar to Fig. 19, showing organelles at two x-ray wavelengths. Figure courtesy J. Gilbert and J. Pine (Caltech) and C. Buckley (King's College, London); from [Gilbert 1992a].

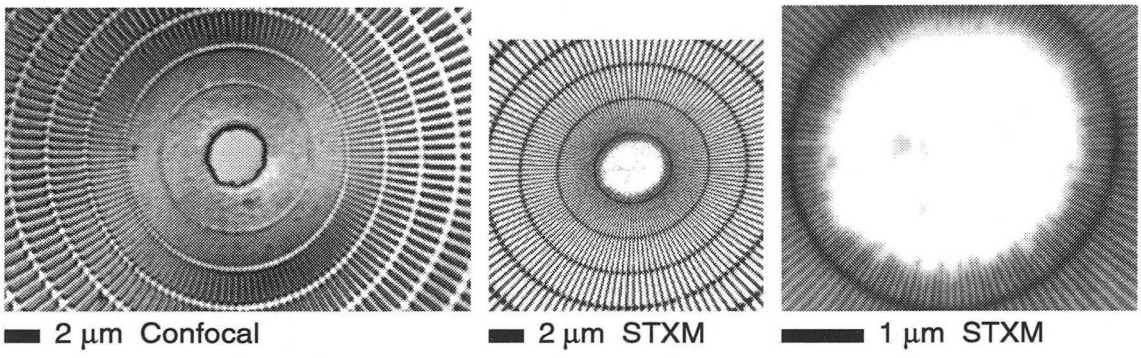

Figure 21: Resolution of confocal (left) and scanning transmission x-ray (center, right) microscopes. The **same** test pattern (gold lines on silicon nitride; *e*-beam fabricated by Erik Anderson, Lawrence Berkeley Laboratory) was viewed in both microscopes. Left: BioRad MRC-600 confocal microscope in reflection mode with a Zeiss Neofluor 1.2 N.A. water immersion objective (taken with the assistance of Barry Burbach, Stony Brook); features to about 150 nm size can be observed. Transmission imaging with the X1A STXM reveals finer detail at the same magnification (center); at higher magnification (right), features to about 35 nm can be observed. From Jacobsen *et al.* [Jacobsen 1992b].

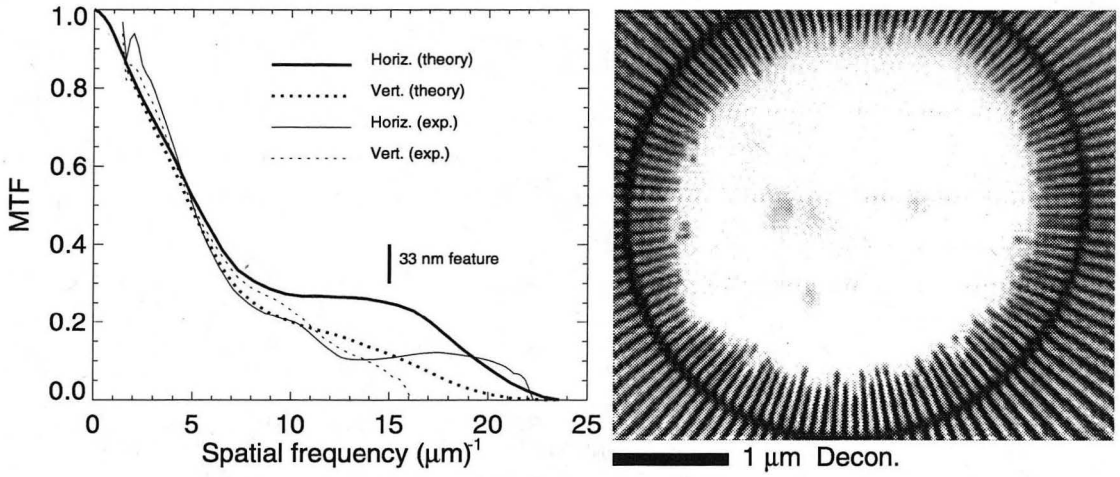

Figure 22: By comparison of electron and x-ray microscope images of the test pattern shown in Fig. 21, the modulation transfer function MTF of the microscope can be calculated (left). Based on the good agreement between theoretical and experimental MTF, the theoretical point spread function can then be deconvolved from oversampled images, yielding the test pattern image shown at right. From Jacobsen *et al.* [Jacobsen 1991] and Zhang *et al.* [Zhang 1992].

3.4.1 Elemental and chemical mapping

The information recorded by a STXM for any given pixel reflects the specimen absorptivity at that point. To the extent that the composition is known, this information can be directly interpreted as a measure of specimen mass (and thickness, if the density is known) at that location [Henke 1993]. Conversely, if the thickness is known, or is at least uniform (as in case of a section), the information may be used to find the absorption coefficient, from which composition may frequently be inferred.

In the neighborhood of an absorption edge, the absorption coefficient of one element changes dramatically. Whereas the absorption edge is based on the threshold energy for completely removing an inner shell electron, near-edge resonances are based on the energy for promoting an inner shell electron to a near-vacuum molecular energy level. As a result, spectral features due to such x-ray absorption near-edge structure (XANES)—also known as near-edge x-ray absorption fine structure (NEXAFS)—resonances often strongly reflect the chemical environment of the atom, for the nature of the bonding to neighboring atoms affects these outer-lying states. This principle can be seen in the comparison between carbon near-edge spectra of polycarbonate and poly(ethylene terephthalate) shown in Fig. 23.

To obtain the absorption spectrum from one spot on the specimen, one scans the monochromator instead of scanning the specimen. (The location is typically selected using the mouse on a previous image). Since the focal length of the zone plate depends on the wavelength, the scan of the monochromator must be tracked with the focus adjustment; the contol system does this automatically. For radiation sensitive specimens one may wish to take the spectrum with a defocused probe, while for more robust specimens one can get the spectrum from 1/4 μm regions in the specimen as limited by wobble in the current focusing mechanism [Ade 1992]. A spectrum with 512 points is collected in tens of seconds. This spectral scan can be used to identify the components present at the given location, or to select the wavelength of highest contrast for subsequent imaging, as will be described in Secs. 4.4 and 4.12.

The distribution of an element can be mapped by means of a pair of images collected at x-ray energies above and below an absorption edge [Engström 1946, Bigler 1983, Kenney 1985]. Buckley *et al.* have used absorption differences to map calcium in bone and cartilage [Buckley 1992d, Buckley 1992a] (see Sec. 4.3), and developed a technique for accurately mapping the calcium concentration in mineralized tissues by combining images collected above and below the calcium L and carbon K edges with images collected at the calcium NEXAFS peaks [Buckley 1995a].

Near-edge resonances can also be used to identify the chemical state. Ade *et al.* developed this method for the analysis of polymer blends [Ade 1992] (Sec. 4.12.1), but it has found much broader application (see e.g., Sec. 4.13). In biological specimens, where different chemical constituents (such as protein and DNA) are frequently not compartmentalized, several near-edge images and more complex analysis are required to map the distribution

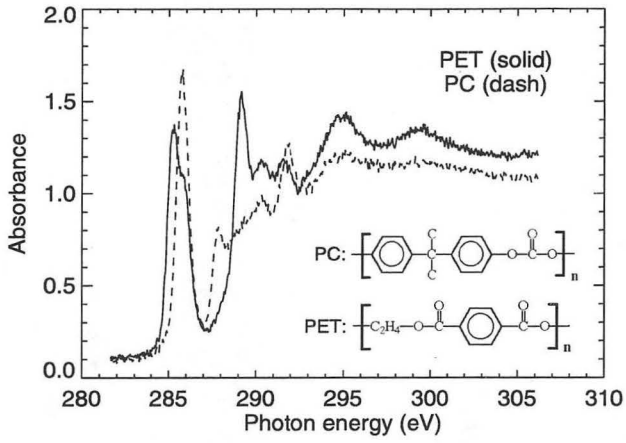

Figure 23: Near-edge absorption spectra of uniform $(0.1\ \mu\text{m})^2$ regions of a thin film with both polycarbonate (PC) and poly(ethylene terephthalate) (PET) polymers. The spectra were acquired by H. Ade (NCSU) using the Stony Brook scanning x-ray microscope. The two monomers have very different near-edge spectroscopic signatures. From Ade *et al.* [Ade 1994b].

quantitatively. This technique has been developed by Zhang *et al.* [Zhang 1994b], and will be discussed further in Secs. 4.4 and 4.6.

3.4.2 Dark field and differential phase contrast

Although most of the applications of scanning microscopy to date have been with the transmitted x-ray flux as the signal, the scanning technique lends itself to the development of a variety of additional imaging modalities.

With a large detector, the STXM delivers an incoherent brightfield image, just as in a TXM (or, indeed, in a conventional optical microscope) [Zeitler 1970, Morrison 1989]. This approximation, wherein the image is assumed to result entirely from the attenuation μt at each pixel, is good for most situations. However, consider two example cases shown in Fig. 24 where this is not so: a grating with a periodicity $d < (\lambda/\text{N.A.})$, or a prism. If a stop is used to block the undeviated transmitted beam, the sub-resolution grating (or arbitrary feature with considerable high-contrast information at sub-resolution spatial frequencies) will diffract part of the incident intensity beyond the stop to be detected as a dark field image signal by a large angle detector. If part of the sample instead can be regarded as a prism, the beam will be refracted and a variety of techniques including differential detection [Palmer 1992a] and Nomarski interference [Polack 1994] can be used to document its differential phase response. Dark field and differential phase contrast techniques have been demonstrated by Morrison *et al.* [Morrison 1992b, Morrison 1992a, Morrison 1994a], and Polack and collaborators are carrying out experiments in Nomarski interference contrast. In addition, Chapman *et al.* have used a CCD to collect the entire 2D pattern in the far-field of the specimen. This allows after-the-fact processing of the data for extraction of the dark field and differential phase contrast signals [Chapman ress]. In dark field mode with special attention paid to reducing spurious backgrounds, they have been able to image 30 nm gold spheres in complete correlation with electron micrographs of the same sample [Chapman 1994]. This observation, especially if it can be extended to even smaller objects, may lead to an important labeling technique for biological specimens.

The two methods of differential phase detection and Nomarski interference contrast have different characteristics for phase gradient imaging. To estimate the refraction due to phase difference, we will assume that features at the transverse resolution limit δ_t will typically have thickness differences which are also about δ_t. The refractive index change over the focused probe width δ_t is then approximately linear, so the sample will appear as a small prism. We can then calculate the refraction angle θ_{refr} for this prism. From Eq. 22, the phase difference φ between rays exiting

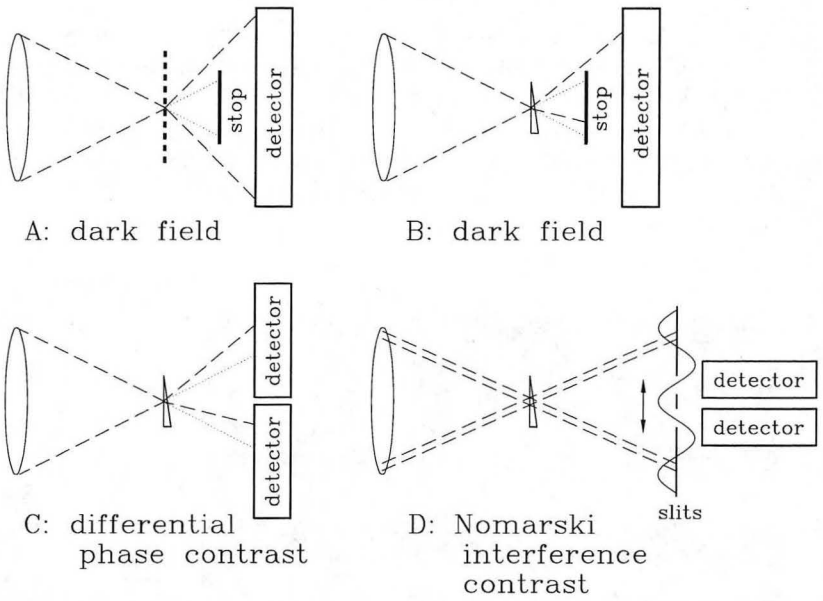

Figure 24: Some of the contrast modes available in scanning transmission x-ray microscopes. In dark field, sub-resolution periodicities can be detected (**A**), as can phase gradients (**B**) which would otherwise not be detected in a bright field image. Phase gradients (shown here as prisms) can also be detected using differential detectors (**C**) which also deliver bright field images from detector element sums, or in Nomarski interference contrast (**D**), where one or more slits are used to detect fringe pattern shifts caused by the difference in optical path length at the two nearby focal spots.

the feature and rays exiting a same thickness of background material is

$$|\varphi| = \frac{2\pi|\delta_{\text{feature}} - \delta_{\text{background}}|\delta_t}{\lambda}. \tag{40}$$

The refraction angle θ_{refr} is then given by the phase-lead-induced optical path difference divided by the δ_t separation between the two points, or

$$|\theta_{\text{refr}}| = \sin^{-1}\left[\frac{(|\varphi|/2\pi)\lambda}{\delta_t}\right] \simeq |\delta_{\text{feature}} - \delta_{\text{background}}|. \tag{41}$$

Since $\delta \approx 10^{-3}$ for organic materials in the "water window" spectral region, while N.A.=0.1 is typical for the best zone plates now available, the STXM beam is refracted by a small fraction of its total angular extent. The consequence of this is that split detector schemes must record small variations in a bright signal, which is bad from a photon statistics point of view; on the other hand, one can simply sum up the signals to obtain an uncompromised bright field image signal in addition to obtaining the differential phase contrast image. If quadrant detectors are used, one can also record phase gradients in two orthogonal directions [Palmer 1992a, Morrison 1994a]. In Nomarski interference contrast, first proposed for x-rays by Polack and Joyeux [Polack 1994], two slits are used to illuminate the zone plate with two beams from slightly different angles. The zone plate produces two closely-spaced focal spots from these beams, and interference fringes result in the far field downstream of the sample. As the optical path length changes in one spot relative to the other (i.e., a relative phase change), the interference pattern is shifted; the intensity measured through one or two slits in the far field can therefore be made to change dramatically with relatively slight phase variations, which is likely to be favorable from a photon statistics (and thus dose) point of view. A disadvantage of the approach is that phase gradients can be imaged in only one direction, and a bright field image is *not* simultaneously recorded (although the two detector slit version records a partial bright field image). Both approaches are under active development.

Central stop, quadrant and slit detectors represent specific, few-detector-element geometries for measuring the attenuation, diffraction, and refraction of the scanned focused beam. A more general approach is to record the entire 2-D far field diffraction pattern at each pixel of the scan. Rodenburg *et al.* have pointed out that this Wigner

phase approach can in principle be used to reconstruct both the magnitude and phase response of the specimen at a resolution exceeding $\lambda/(2\text{N.A.})$ [Rodenburg 1992, Rodenburg 1993], and experiments with visible light microscopy have successfully confirmed the general validity of the method. Recently, Chapman has recorded Wigner phase datasets using soft x-rays; an example is shown in Fig. 25. Wigner phase microscopy offers great potential for very high resolution imaging, although the sample must be radiation-tough and the data collection requirements of recording a 2-D diffraction pattern at each 2-D scan point are formidable.

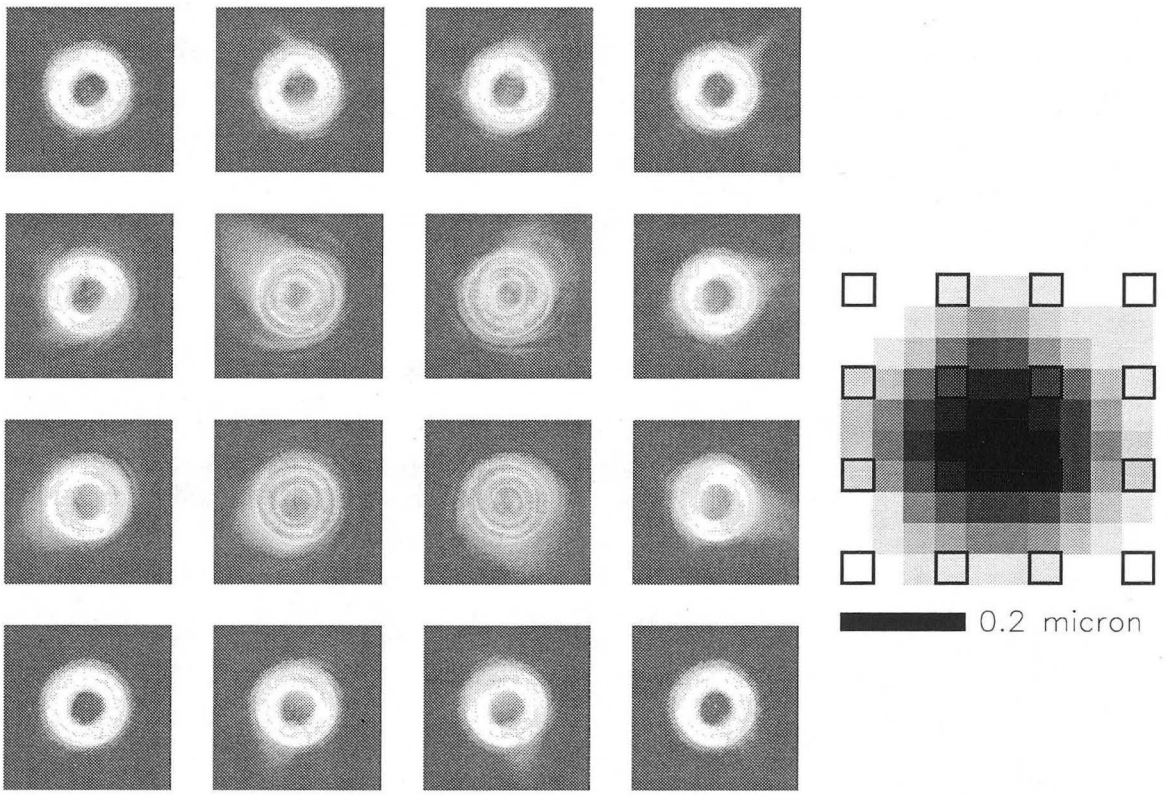

Figure 25: Diffraction plane data (left) and image (right) obtained by scanning a focused x-ray spot across a μm-size polystyrene sphere. The diffraction patterns at left (the logarithm of the logarithm of intensity is shown) were measured by Chapman using a soft x-ray CCD camera for each outlined pixel in the image, while the image itself was derived from the total signal in its respective diffraction plane dataset. The hollow center of the diffraction patterns is due to the use of a central stop on the Fresnel zone plate (see Fig. 17). This data can be interpreted using the methods of Wigner phase microscopy. Figure courtesy H. Chapman (Stony Brook).

3.4.3 Microtomography

The limited information content of an optical wavefront of given N.A. and wavelength λ implies that true three-dimensional imaging intrinsically requires multiple views (the use of holography does not avoid this requirement). One can gain insight into the three-dimensional structure using stereo pairs (see Fig. 41). Some progress has been made toward the goal of full three-dimensional imaging by McNulty *et al.* [McNulty 1992b, McNulty 1994] using multiview Fourier transform holography. However, the most successful experiment so far has been carried out by

the same team using the X-1A STXM [Haddad 1994b, Haddad 1994a]. Provided that the depth of focus of the zone plate probe is greater than the sample thickness, the STXM projections can be treated in the same way as the data from a standard straight-ray tomography experiment. This approach was applied by Haddad *et al.* to image a model object of about $2 \times 2 \times 5$ μm^3 microfabricated from gold bars supported on silicon nitride windows. Nine projections were recorded from -50° to +55° using 3.6 nm x-rays. The data were combined using an agebraic reconstruction technique (ART) algorithm to give a three-dimensional reconstruction of excellent fidelity (see Fig. 26). The transverse resolution was about 0.1 μm and the depth resolution varied between 0.1–0.6 μm for different parts of the structure. When this technique is optimized and applied to (presumably cryofixed) biological samples of similar size, it promises to provide a unique investigative tool.

3.4.4 Photoemission

So far we have discussed microscopies based on detecting those x-ray photons which were not absorbed by the specimen. In this section we discuss microscopes based on the detection of the products generated by absorption.

Primary products of the absorption event are a photoelectron and an ion with a core hole. Subsequent transitions lead to Auger electrons or x-ray fluorescence, and in some molecules the subsequent rearrangement also involves the emission of visible light (luminescence). Each of these phenomena can be used to advantage.

The energy of photoelectrons and Auger electrons is characteristic of the energy levels involved in the transition. Their detection and analysis therefore leads to positive identification of the absorbing species and their chemical environments. However, since the mean free path of these electrons in matter is only a few nanometers, only absorption near the surface leads to the correct electron energy. This limitation can be put to good advantage in surface analysis. Scanning Photoelectron Microscopy (SPEM) using a zone plate to form the microprobe was developed at the NSLS X1A beamline by Ade *et al.* [Ade 1990]. (Photoemission microscopes using mirrors to form the microprobe will be discussed in the following sections). Because only a small fraction of the x-rays are absorbed near the surface, and the electron energy analyzer accepts only a small fraction of the resulting products, photoemission microscopy with good spatial resolution involves a dose to the specimen that is orders of magnitude higher than in STXM. In addition, the electron spectroscopy must be carried out in ultrahigh vacuum. Photoemission microscopy is especially suited to the study of radiation-hard materials science or microelectronics specimens [Tonner 1988, Pianetta 1989, Stöhr 1993]; in biology, photoemission microscopy studies on dried samples in ultra-high vacuum [De Stasio 1993] must deal with sample preparation and radiation dose issues.

3.4.5 Luminescence

In biological imaging, one often wishes to image biochemically-selected structures within an larger object, such as is routinely done in fluorescence microscopy. In recognition of this, Jacobsen *et al.* developed scanning luminescence x-ray microscopy (SLXM) as an x-ray analog of scanning confocal fluorescence microscopy [Jacobsen 1992c, Jacobsen 1993]. The idea is to use the x-ray probe to excite visible light emission; if the visible light is emitted on a timescale shorter than the pixel dwell time, the resolution is determined by the x-ray probe size rather than the resolution of the visible light collection and detection system (the range of secondary electrons is small compared to the probe size). The fact that a bright signal is sought over a dark background leads to the potential for reduced radiation dose relative to bright field microscopy; in addition, confocal or segmented optical microscope systems can in principle be used for three dimensional imaging [Jacobsen 1993]. Jacobsen *et al.* demonstrated the resolution of the technique for imaging phosphor grains, and showed that organic dyes in polystyrene spheres gave good luminescence yields and adequate bleaching resistance for several images to be recorded (Fig. 27). More recently, Moronne *et al.* have developed avidin and secondary antibodies coupled to lanthanide polychelates with good luminescence yield and superior bleaching properties, and have begun efforts towards demonstrating high resolution selective staining of actin filaments [von Brenndorff 1994, Moronne 1994]. The prospects are quite exciting for imaging at the resolution of the x-ray microscope with florescence-microscopy-like labelling techniques.

3.5 Other microscopes with zone plate optics

3.5.1 The Advanced Light Source microscopes

A microscope based on the Göttingen model is being constructed by Meyer-Ilse *et al.* [Meyer-Ilse 1992, Meyer-Ilse 1994b] for the Advanced Light Source (ALS) at Lawrence Berkeley Laboratory. A great deal of thought has gone into the

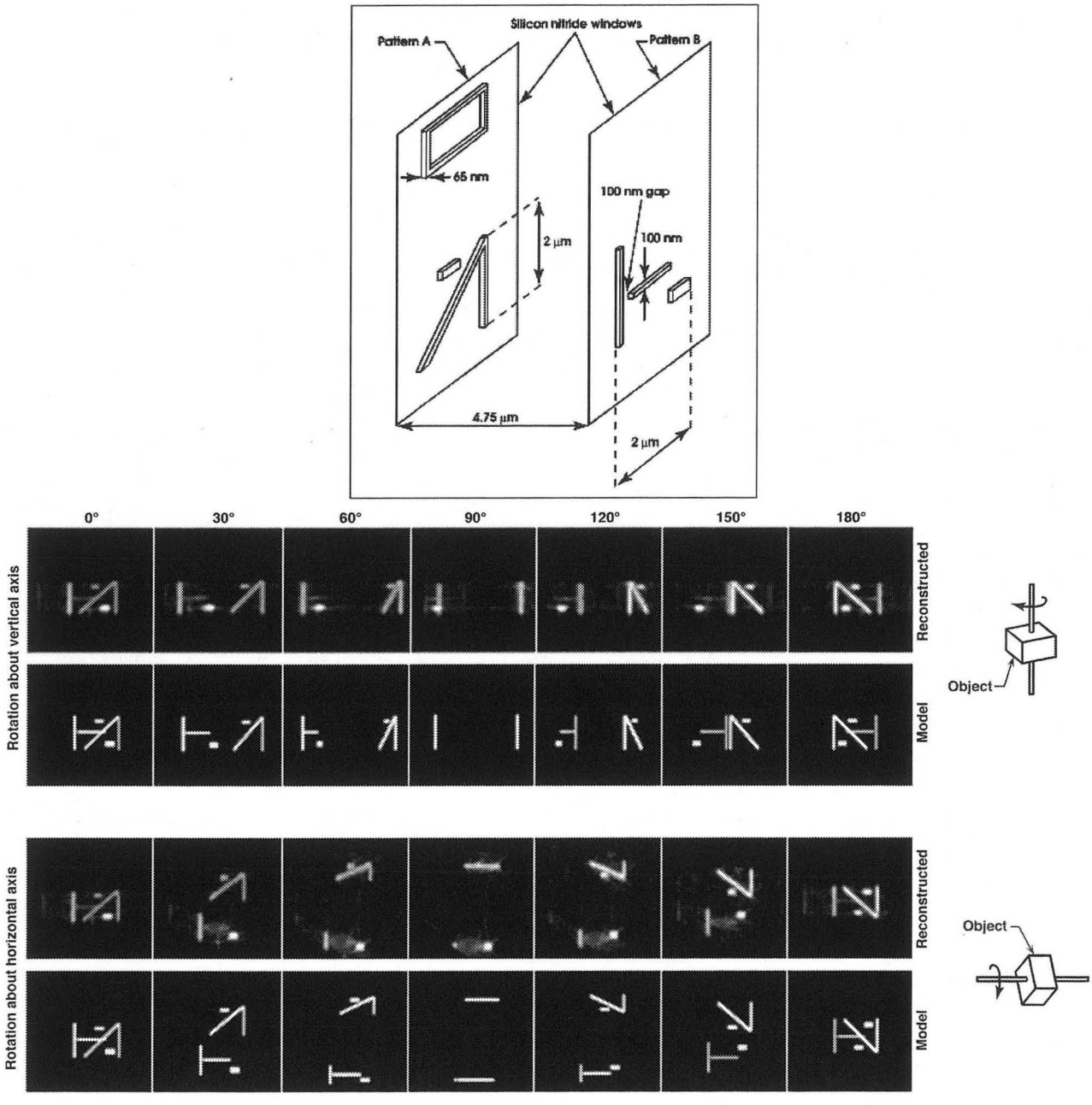

Figure 26: Microtomography in STXM. **Top:** sketch of the 3-D microscopic test object. The two gold patterns were written on thin windows using electron beam lithography. **Bottom:** views of the 3-D reconstruction at various orientations. Each image in the figure is a perspective, not a simple projection, of the object with a rotation of 30° between images. Two pairs of rows of images are presented, rotating about the vertical and horizontal axes, respectively. The top row of each pair contains images of the actual reconstructed data, while the bottom row of each pair shows identical views of a simulated model. From Haddad *et al.* [Haddad 1994a].

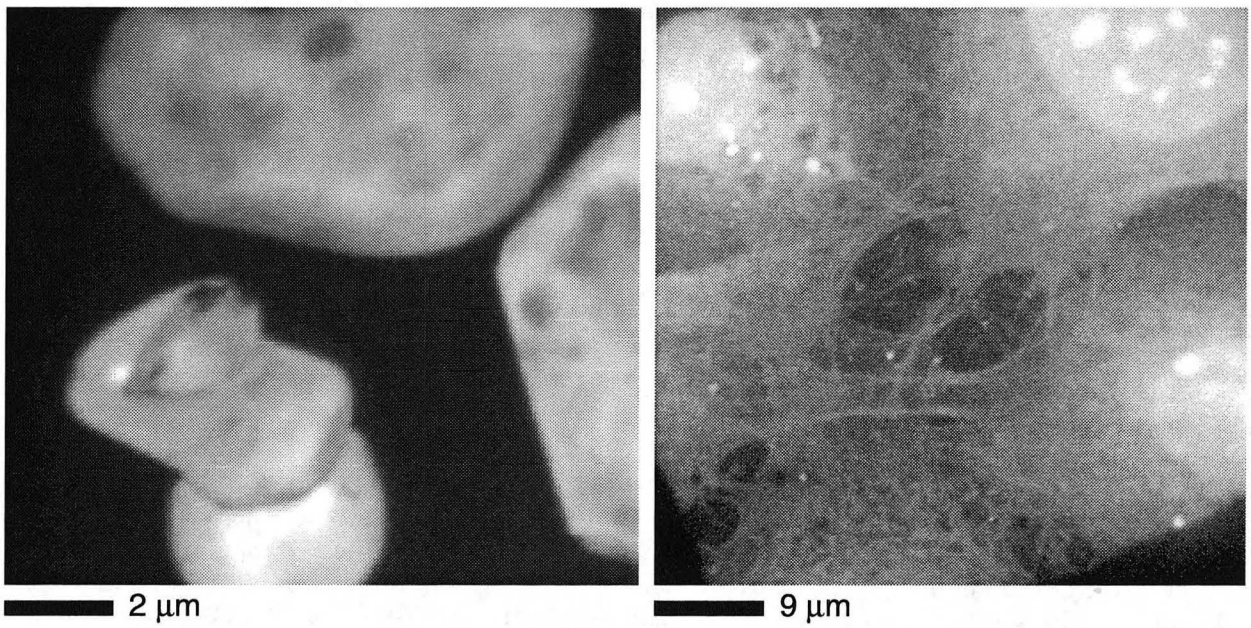

Figure 27: In scanning luminescence x-ray microscopy, visible light emission is excited by the focused x-ray probe. **Left:** P31 phosphor grains have been imaged at < 70 nm resolution. From C. Jacobsen *et al.* [Jacobsen 1993]. **Right:** experiments aimed at actin filament labelling using terbium conjugated to avidin. From M. Moronne *et al.* [Moronne 1994].

design of this instrument which started operation in the second half of 1994. The system combines visible light microscopy with x-ray microscopy. The sample is mounted on a sample carrier, which can be precisely moved from the visible light microscope to the x-ray microscope and vice versa, while maintaining registration of sample position and focus. The instrument allows multi-wavelength imaging with high spatial resolution and modest spectral resolution ($\lambda/\Delta\lambda \simeq 300$). The specimen holder has been designed to accommodate multiple angular orientations for stereo imaging or tomography.

Three soft x-ray scanning microscopes are planned for the Advanced Light Source. One of these will be specifically dedicated to biological applications [Meyer-Ilse 1992, Meyer-Ilse 1994b]. Another one, which should start operations around the end of 1994, will also include an x-ray fluorescence detector for materials science applications, and a scanning photoemission microscope is expected to begin operations in 1995 [Ade 1994a]. Although x-ray fluorescence induced by hard x-rays is a major field of investigation and a leading form of trace element mapping, soft x-ray induced fluorescence has not been widely exploited due to the relatively low fluorescence yield (only about 0.1–5% of absorption events produce fluorescent x-rays for $Z < 16$; the yield rises roughly as Z^3 [Krause 1979]). Nevertheless, detection of the fluorescent x-rays can be used for elemental mapping as will be discussed below, and fluorescence detection has also been used in absorption spectroscopy (see e.g., [Cramer 1992]).

3.5.2 The ESRF and APS microscopes

At third-generation synchrotron radiation facilities with higher electron beam energies, x-ray microscopes will operate at somewhat shorter wavelengths. It is only recently that these "harder" x-rays have been focused to submicron spots [Yun 1992, Lai 1992, Krasnoperova 1993, Bilderback 1994]. This opens up new capabilities, such as the ability to examine thicker specimens, and to use x-ray fluorescence for trace element mapping at high resolution [Howells 1985a]. In operations outside the water window, absorption imaging of wet specimens in amplitude contrast is unattractive due to low intrinsic contrast and concommitant high radiation dose, and other schemes such as phase or differential phase contrast need to be considered [Schmahl 1987, Jacobsen 1992a].

At the European Synchrotron Radiation Facility (ESRF) in Grenoble, two microscopes are to be constructed [Howells 1992]. One of these follows the Göttingen design for Zernike phase contrast. To accommodate the longer

interaction lengths at higher x-ray energies, the zone plates must be made considerably thicker. For some time, the Göttingen group has been working on a jelly-roll scheme [Rudolph 1982]. In this approach, a thin and accurately round wire is rotated about its axis while alternate layers of material corresponding to zone plate zones are deposited to precisely calibrated thicknesses. This cylinder is then to be "sliced" and etched to produce thick zone plates [Hilkenbach 1992, Witt 1994]. Such a scheme has been used by Bionta *et al.* to make zone plates for use at 8 keV [Bionta 1988].

The other microscope at the ESRF will be a scanning microscope. It will follow the King's College (London) design for imaging by x-ray fluorescence [Buckley 1992c], and will also incorporate other image modes such as differential phase contrast [Palmer 1992a, Morrison 1994a]. The zone plates will be fabricated at King's College using their contamination writing scheme followed by reactive ion etching [Charalambous 1994].

At the Advanced Photon Source (APS) at Argonne National Laboratory, several experimental stations are being built for x-ray microscopy. Sector 2 of the storage ring will have two undulator beamlines devoted primarily to this purpose. One of these will operate between 0.5 and 4 keV (λ = 2.5 to 0.3 nm), while the other one will cover the 4–30 keV range (λ = 0.3 to 0.03 nm). Both beamlines will be equipped with a transmission x-ray microscope and a scanning transmission x-ray microscope, and the low energy beamline will also have Fourier transform holography capabilities (Sec. 3.7.1). These beamlines will use zone plates with stepped profiles for high efficiency; such zone plates are made using x-ray lithographic reproduction of electron beam lithography defined zone plates [Krasnoperova 1993, Di Fabrizio 1994, Yun 1995]. The planned experimental program includes microspectroscopy, differential absorption contrast microscopy, microdiffraction, microanalysis, and microtomography. Several other facilities are being built where the microprobe will be formed by tapered capillaries [Bilderback 1994] or other focusing devices, mostly for fluorescence microanalysis.

3.5.3 Other zone plate microscopes

A microscope based closely on the BESSY design has been built in collaboration with the Göttingen group and installed at the Aarhus University storage ring in Denmark. It uses Göttingen zone plates, and has recently started operation [Medenwaldt 1994b].

Two microscopes similar to the one at BESSY have been constructed at the Photon Factory (Japan). One of these has been tested on the undulator beam line 2B, while the other one is to be used with polarized beams at the accumulator ring [Kagoshima 1992]. They use zone plates fabricated by Erik Anderson [Anderson 1992], as does a microscope at the UVSOR storage ring in Japan [Watanabe 1994].

A unique microscope that uses flash illumination is based on an x-ray laser developed at Lawrence Livermore National Laboratory. It uses a multilayer-coated condenser to illuminate the specimen, which in turn is imaged using a high resolution zone plate made by Erik Anderson. Images of test patterns and of dry biological specimens have been obtained using 200 picosecond exposures at a wavelength of 4.483 nm [DaSilva 1992b], and experiments with wet specimens in the water window are imminent [Trebes 1994].

Zone plate scanning microscopes have been built by Niemann *et al.* [Niemann 1988, Niemann 1987, Niemann 1992] for use at BESSY, and by the King's College group for use at Daresbury, UK [Kenney 1989, Morrison 1992d]. Both instruments have many attractive characteristics. The performance of the BESSY microscope has been limited by lack of an undulator source, although this will be remedied when the microscope is moved to the BESSY II source now under construction (a new transmission x-ray microscope is planned for BESSY II as well). The Daresbury microscope has recently benefitted from a beamline upgrade which has led to a twelvefold increase in focused flux, so that images can now be taken with exposure times of about 10 minutes. A scanning photoemission microscope has recently begun operation at the ELETTRA storage ring in Trieste, delivering 2×10^9 photons/sec into the 0.2 μm focus of a zone plate. Scanning microscopes are also under construction at the Hefei synchrotron radiation laboratory [Lei 1992] and in Beijing [Shu 1992], and one is planned for the SRRC in Hsinchu. Michette *et al.* [Michette 1988b, Michette 1993, Michette 1994] have developed a scanning x-ray microscope in which one x-ray pulse from a laser-produced-plasma is used for each pixel of a scan; this may lead to scanning microscopes which do not depend on synchrotron sources.

3.6 Other types of soft x-ray microscopes

3.6.1 Microscopes with Schwarzschild objectives

Normal incidence reflectivity R varies with the index of refraction as $R = [(1-\tilde{n})/(1+\tilde{n})]^2$. For x-rays with $\tilde{n} = 1 - \delta - i\beta$, we have $R \simeq (\delta/2)^2$; since $\delta \sim 10^{-3}$ for most materials in the soft x-ray wavelength range, there is very little normal incidence reflectivity from a single interface. However, all is not lost; with a series of weak reflecting interfaces spaced $\lambda/2$ apart, the weak amplitude reflectivities can add up coherently. The reflected intensity is the square of the amplitude, so the enhancement is proportional to the square of the number of reflectors, giving a net reflectivity which can be quite high (see e.g., [Spiller 1994]). The possibilities of synthetic multilayer mirrors for x-rays were first put forward by Spiller in 1972 [Spiller 1972] and by Barbee in 1978 [Barbee 1978, Barbee 1981], who pointed out that the materials in the multilayer stack must alternate between high and low absorptivity, and must have smooth boundaries. In the soft x-ray range, typically about 50 layers contribute to the reflectivity, so these optics have a spectral passband of about $\lambda/\Delta\lambda = 50$. The normal incidence reflectivity can exceed 60% at $\lambda = 13$ nm, and reflectivities of up to 3.4% have been reported within the "water window" spectral region [Kozhevnikov 1994, Seely 1993, Gutman 1994]. These efforts face real challenges in surface roughness and interlayer diffusion, since individual layers are $\sim \lambda/4$ thick, corresponding to only a half dozen or so atoms for $\lambda = 4$ nm.

Normal incidence mirror objectives are commercially available in the Schwarzschild configuration for good performance over a wide spectral range in visible light and UV microscopy, and have proven to be the geometry of choice for normal incidence mirror focusing of soft x-rays as well. Although Schwarzschild designed both spherical and aspherical mirror schemes, we consider only the former in what follows. The popularity of the Schwarzschild geometry is based on the fact that it is stigmatic and aplanatic to third order and it uses only two *spherical* surfaces. Its limitation is that diffraction-limited resolution is not achieved for N.A.$\gtrsim 0.15$ [Shealy 1992]. The Head configuration delivers better off-axis performance for large N.A. at the cost of requiring aspherical mirror surfaces[Head 1957, Shealy 1992]. In experiments in soft x-ray projection lithography, lines as fine as 50 nm have been printed with $\lambda = 13$ nm radiation [Bjorkholm 1990], and in microscopy applications features as small as about 90 nm have been imaged [Ng 1992, Underwood 1994]. The limited spectral passband means that for microscopes that are designed to operate at a wide range of wavelengths, multiple objectives must be fabricated, and high numerical aperture optics require graded multilayers (multilayers where the layer spacing is adjusted to account for the variation in incidence angle with distance from the optical axis). On the other hand, within its operating range the mirror is achromatic, quite long (2–10 mm) working distances are common, and the limited spectral passband means that broadband sources can be used without a separate monochromator. Because *two* reflecting surfaces are required, the best water-window Schwarzschild objectives with 3% reflective coatings will have a combined throughput of only 0.09%.

The first multilayer coated Schwarzschild objectives for x-ray microscopy were made by Haelbich, Spiller, and Kunz [Haelbich 1980a, Haelbich 1980b]. More recent versions have been made by the ATT/GCA Tropel group [Bjorkholm 1990], by Underwood *et al.* [Underwood 1994] for the MAXIMUM microscope at Wisconsin [Capasso 1991], Artyukov *et al.* [Artyukov 1993], and by researchers at Olympus [Horikawa 1993, Mochimaru 1994]. Most of these are designed to operate at around 13 nm (where, as noted above, reflectivities in excess of 60% can be obtained), although a successful microscope was made to operate with carbon K radiation at 4.48 nm [Murakami 1992].

Schwarzschild objectives have demonstrated diffraction-limited spatial resolution of 50 nm at $\lambda = 13$ nm wavelengths [Bjorkholm 1990]. They can also be fabricated to collect light over a large numerical aperture. This enhanced light-gathering capability makes Schwarzschild objectives attractive for use in scanning microscopy with high repetition rate, pulsed laboratory sources. One scheme involves one pulse of the source for each pixel. The first such microscope was built by Trail and Byer [Trail 1989] using a slab laser to create a pulsed plasma as the x-ray source. Similar sources are under development by Rymell *et al.* [Rymell 1993, Rymell 1994]. Laser produced plasma devices need to deal with the problem of the mirror-fouling debris which accompanies the plasma created from a solid surface; Rymell *et al.* address this problem by using tiny alcohol droplets as the target.

The 7–13 nm wavelength range within which multilayer reflectors presently work well is suited to EUV/soft x-ray projection lithography, and to photoemission microscopy of surfaces in materials science. The limited peformance at shorter wavelengths has not yet enabled any demonstrations of wet biological specimen imaging, in spite of ambitious efforts in that direction [Shealy 1992, Hoover 1993, NASA 1993].

3.6.2 Contact microscopy

The earliest attempts to use x-rays in microscopy involved the exposure of a specimen in contact with a photographic plate (as described in Sec. 1.3). The developed plate was then examined or enlarged using a visible light microscope. Various improvements have been made in this general approach as reviewed by Cheng [Cheng 1987a], including the use of higher resolution crystalline [Ladd 1956] or polymer resists [Feder 1976] instead of film, and the use of the scanning electron microscope to examine or enlarge the image [Ladd 1956, Asunmaa 1963, Feder 1976]. Modern developments have profited from the development of the related technique of x-ray lithography in the early 1970s by Feder [Feder 1970, Spiller 1993] and by Spears and Smith [Spears 1972a, Spears 1972b]. In current practice, the detector generally is the photoresist PMMA (polymethyl methacrylate), which has a long tradition as a high resolution resist in electron beam lithography [Hatzakis 1969]. When exposed to ionizing radiation, bonds along the polymer chain are broken, effectively reducing the local molecular weight. Development in a solvent leads to a surface topography which is based on the x-ray dose deposited in the resist [Shinozaki 1988]. Recent improvements include the use of flash sources such as x-ray lasers [Skinner 1990] or laser produced plasmas [Rosser 1985] to capture the image on a nanosecond time scale before specimen motion or radiation damage can interfere, relay optics to allow for specimen irradiation without the associated debris of a laser plasma source [Rosser 1985]. Improved ways to "read" the resist recording include the use of atomic force microscopes [Tomie 1991, Cotton 1992] (see Fig. 28), and transmission electron microscopy of carbon [Cheng 1987a] and plasma-polymer [Shinohara 1986] surface replicas.

Contact microscopy holds tremendous appeal as a relatively straightforward way to carry out x-ray microscopy experiments in a laboratory which has a high peak power laser and atomic force microscope available. Large fields can be exposed, and in principle the resolution limit of the photoresists employed is < 10 nm due to the range of the secondary electrons which result from x-ray absorption [Spiller 1977, Early 1990]. However, the actual resolution of contact microscopy is in most cases likely to be limited by Fresnel diffraction, liquid development, and/or shot noise in the exposure. Fresnel diffraction scales as $\sqrt{\lambda d}$, suggesting that < 50 nm resolution may be difficult to obtain with sample-to-resist separations d of 1 μm or more [Hare 1994] (although scalar diffraction theory gives an imperfect guide to this limit [Schattenburg 1991], and the use of polychromatic x-rays such as from a laser produced plasma source is likely to be of help). Wet development acts on the surface normal of a photoresist, leading to sidecutting of fine exposure patterns [Sayre 1979]. We have seen in Sec. 2.5.1 that high resolution requires high dose, but not all contact microscopy experiments deliver the necessary photon exposure to reduce surface noise on the resist to a sufficient level [Shinozaki 1992]. Wang and Jacobsen have modelled these effects in contact microscopy, and find that it is difficult to obtain sub-40 nm resolution [Wang 1994, Wang 1995]. With those caveats in mind, the simplicity and accessibility of the technique suggest that with further effort it may yet become widely available and useful.

As an alternative to photoresist recording, Polack *et al.* have developed a contact microscope where a photoemitting surface is used instead of a resist detector. The electrons from the photoemitter pass through an electron optical column to yield a magnified image [Polack 1981, Polack 1988]. This scheme is the basis of a commercially available instrument called the zooming tube [Kinoshita 1992, Matsumura 1994].

3.6.3 Projection microscopy

During the 1950s, x-ray microscopy enjoyed a period of considerable popularity which was largely due to the success of the x-ray projection microscope. During this time dedicated projection microscopes were sold commercially by General Electric, Phillips, and Microray, and kits were available for conversion of the electron microscopes made by Jeol, Shimadzu, RCA and others to x-ray projection imaging at various hard-x-ray wavelengths. The technique had originated in Germany in 1939 with the ideas of Malsch and Ardenne but the first projection microscope to show results was that of Cosslett and Nixon [Cosslett 1951, Cosslett 1960]. The principle of the method is to use an exceedingly small x-ray source to cast a magnified shadow of the object onto photographic film or an electronic detector. The source is a transmission anode illuminated by a microfocused electron beam. For soft x-rays, Fresnel diffraction can play a role in limiting the resolution; however, for hard enough x-rays, the image resolution/speed trade-off is determined entirely by the x-ray-emitting volume at the anode [Yada 1990] and the electron beam current. As an example, the General-Electric instrument [Newberry 1956], which was based on the Cosslett-Nixon design, could deliver 1 μm resolution images with a 20-minute exposure time. A later variant gave the same resolution at the 1.56 keV energy of the aluminum K line. Although the usual resolution of this generation of instruments was not less than 0.5 μm, Nixon [Nixon 1955] demonstrated that 0.1 μm was possible.

A great many striking pictures with high information content were taken during this period, often in stereo pairs (see, for example, the book by Hall *et al.* [Hall 1972]). Nevertheless, the technique lost popularity around the early

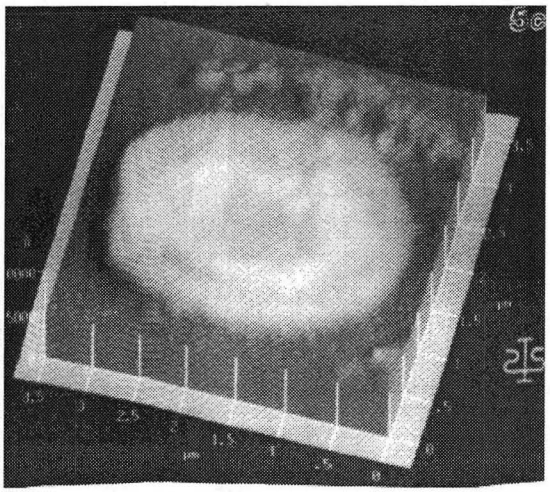

We are to receive a figure along these lines from Prof. Stead.

Figure 28: Contact x-ray micrograph of a living *Chlamydomonas* cell showing the two anterior flagella, numerous large spherical carbon-dense inclusions, and an outer region which is much lower in carbon density. The image was obtained using a Nd:glass laser operating at 1.053 μm with approximately 6 Joules of energy on an ytterbium target. An atomic force microscope was used to read the developed photoresist and provide the image shown. Figure courtesy A. D. Stead, Royal Holloway and Bedford New College, UK.

1960s apparently because of competition from the scanning electron microscope and electron probe microanalyser, both of which offered high resolution elemental maps (based on x-ray fluorescence) superimposed on structural images. However, both of these latter instruments give information about near-surface layers, so that they do not replace the x-ray projection system's potential for three-dimensional imaging, as has been pointed out by Newberry [Newberry 1987a]. Remarkably, Newberry has continued to operate and refine his projection instrument from the 1950's to the present time. In collaboration with Cheng and others [Newberry 1987b], he has introduced several innovations such as time-lapsed movie photography [Newberry 1992]. Moreover, his argument that the x-ray projection system offers a unique three-dimensional capability is gaining acceptance, leading to a resurgence of interest and some new improvements in the technique. For example, electronic detectors such as CCDs can now replace film to record the image [Thomas 1992] (although the magnification can not yet be made large enough to maintain submicron resolution with currently available CCDs). Among the currently active efforts to exploit the projection scheme, there is an established group under K. Yada in Japan [Yada 1990, Yada 1992] (see Fig. 29), and new instruments have been constructed at Buffalo (USA) by Cheng *et al.* [Cheng 1992] and at Reims (France) by Cazaux and coworkers [Thomas 1992]. Both the latter systems are being used in three-dimensional imaging experiments employing tomographic reconstruction techniques [Lin 1992, Zolfghari 1994].

3.6.4 Other microscopes

A particularly appealing way to form the microprobe is with an ellipsoidal mirror at grazing incidence. Although ellipsoids are not suitable for imaging of extended objects, they do have the special property that all the light emitted from one focus is collected at the other. At grazing incidence the focus is achromatic, so the wavelength is freely tuneable by use of a monochromator from the infrared to the x-ray range. Kunz and his group [Voss 1992, Voss 1994] have built a microscope of this type at HASYLAB. Imperfections of the mirror have limited the resolution to 0.4 μm so far, but even at this resolution the microscope has been productive, especially in materials science [Moewes 1994]. Another microscope of this type is being built at MAX II in Sweden [Johansson 1994], and a transmission x-ray microscope using ellipsoidal mirrors has been demonstrated by Aoki *et al.* [Aoki 1994] with a resolution reported to be in the 0.1 μm range.

Biological microscopy based on the reflection of 10–20 nm soft x-rays has been proposed by DiCicco *et al.* [DiCicco 1992].

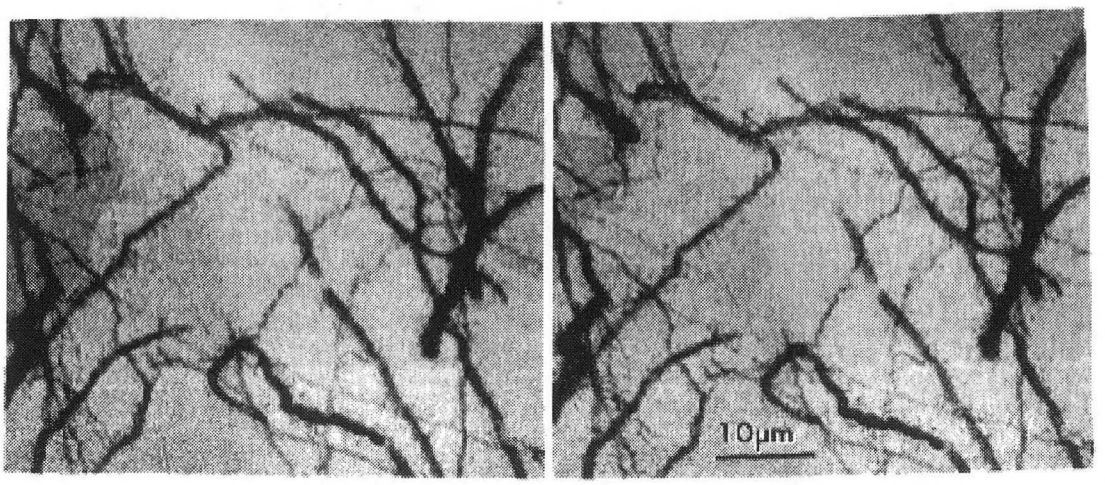

We are to receive a print of this image from Prof. Yada.

Figure 29: Stereo image pair of Golgi-stained neuronal tissue of rat hippocampus. The 100–200 μm dehydrated thick section was viewed using a projection x-ray microscope with a 10 keV beam on a 0.3 μm thick Ge target and an exposure time of 30 minutes. From Yada *et al.* [Yada 1992].

3.7 Holography and diffraction

3.7.1 X-ray holography

In conventional microscopes, lenses are used to process the wavefield emerging from an object so as to form an image on a detector. In holography, the same wavefield is captured by recording its interference with a reference wave. This registers both the amplitude and phase information and allows the image-forming role of the lens to be replaced either by using the hologram itself as a diffracting lens in the laboratory, or by digitizing the hologram and calculating its image.

X-ray holography has a long history (as reviewed for example by Jacobsen [Jacobsen 1990a]). It was first proposed as a form of microscopy by Baez in 1952 [Baez 1952] but it was some time before even the simplest objects were successfully imaged by reconstruction of an x-ray hologram [Giles 1969, Aoki 1974]. An important step forward was the use of synchrotron radiation, as pioneered in 1972 by Aoki and Kikuta [Aoki 1972]. The advent in the 1980's of even brighter storage ring undulator sources [Brown 1983, Krinsky 1983] and x-ray lasers [Matthews 1985, Suckewer 1985] stimulated a significant increase in the level of activity [Solem 1982, Howells 1983] and led to the modern improvements in the technique.

The principal motivation that has sustained both historical and current interest in the technique is the prospect of a lensless three-dimensional microscope of resolution superior to that of conventional visible light systems. Such a "microscope" would also have other attractive features including simultaneous recording of both the phase and amplitude images and, in certain geometries, an unusually large field of view. Furthermore, the image is "focused" in the reconstruction stage, so that holography is particularly well suited to flash imaging with x-ray laser sources [Solem 1982], thus providing a means to circumvent radiation damage limits [Solem 1986, London 1989, London 1992b]. The feasibility of x-ray laser holography has been demonstrated by Trebes *et al.* [Trebes 1987], although more coherent power is still needed at shorter wavelengths to fully realize the potential of this approach.

Although there is not yet a working holographic microscope with all of the above features, the prototype systems that have been demonstrated do show progress toward all of the capabilities mentioned. During the 1980's, high resolution (0.5–0.05 μm) was achieved at both the Brookhaven and Orsay storage rings using undulator sources and polymer resists as recording media [Howells 1987, Jacobsen 1990b, Joyeux 1988b]. More recently, better techniques for reading the resist recording have been designed by both of these two groups enabling more rapid and convenient delivery of the final image. Specifically, Lindaas *et al.* have obtained $\sim$ 40 nm resolution images of dried biological samples using an atomic force microscope for hologram readout [Lindaas 1992, Lindaas 1994, Howells 1994] (see Fig. 30). Joyeux and Polack have developed a holographic-microscope system wherein Gabor holograms, recorded on

photoresist [Joyeux 1988a, Joyeux 1988b], are reconstructed using a special UV reflection microscope designed for rapid image turnaround [Joyeux 1989, Joyeux 1994].

Holography texts [Collier 1971] describe two types of holography which are suitable for implementation with x-rays. The above-mentioned experiments all used in-line (Gabor-type) recording geometry. An alternative approach, based on Fourier-transform holography, has been used by McNulty *et al.* Their technique [McNulty 1992a] provided almost instantaneous readout and reconstruction of the hologram by means of a charge-coupled-device (CCD) system and was used to deliver 50 nm resolution images of microfabricated test patterns. McNulty and collaborators have also demonstrated 3-dimensional imaging of a gold-bar pattern [McNulty 1992b, McNulty 1994].

It is of interest to try to understand how these methods may contribute to life-science investigations in the future. First, in its two-dimensional form, x-ray holography is simple to do, is suited to flash exposures, and promises to be competitive in resolution. Second, by means of tomographic techniques, it offers a route to true three-dimensional imaging. On the other hand it requires high radiation doses and is lacking the analytical and spectroscopic capabilities of some of the other x-ray techniques. Consequently one must ask how the required doses which are $\sim 10^6$ Gray can be tolerated. It would appear that two-dimensional (single-shot) experiments on wet natural material can be done by means of flash exposure, and that either two- or three-dimensional holographic imaging can be done by means of cryofixation.

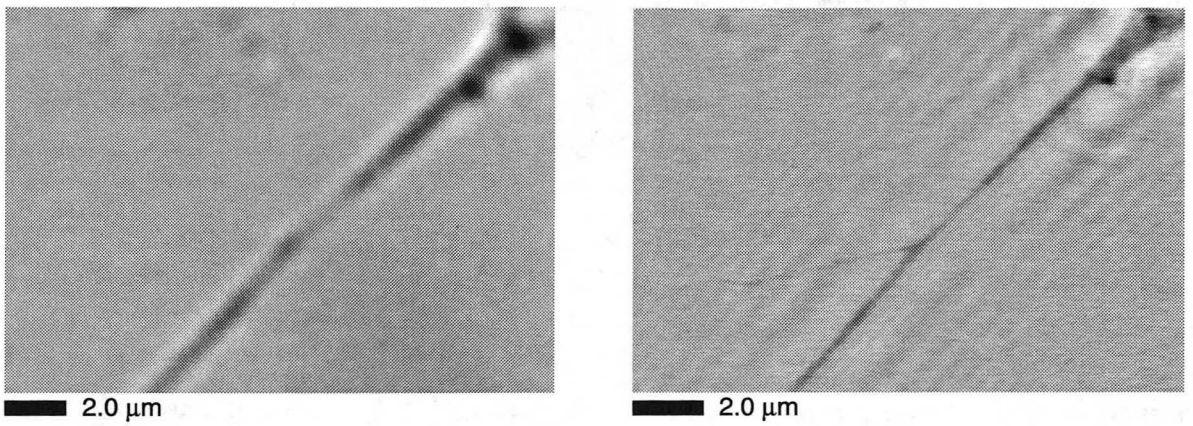

Figure 30: Optical micrograph (left; 100×, N.A.=0.9 Nikon dry Nomarski lens) and image reconstructed from an x-ray hologram (right; $\lambda = 1.8$ nm) of a tendril from a NIL 8 fibroblast. From Lindaas *et al.* [Lindaas 1994, Howells 1994].

3.7.2 Diffraction

Microscopy by diffraction in the absence of a holographic reference signal was suggested by Sayre [Sayre 1980], and has been pursued in several subsequent papers [Yun 1987, Sayre 1991]. The technique may be thought of as a variant of x-ray crystallography in which the crystal, with its very large number of copies of the unknown structure, is replaced by a single copy of the structure. Sayre considers that the holographic reference signal, although convenient for phasing the diffraction signal, is not required for that purpose. Instead, the continuous nature of the signal in the single-copy case allows phasing to be done via the oversampling theorem of Bates [Bates 1982] or Hayes [Hayes 1982]. In fact, use of the reference signal can add an additional noise source in the recording of the faint diffraction signal, and it reintroduces the quality of lenses or detectors, etc. as factors limiting achievable resolution. The correctness of these latter points has been somewhat confirmed by the fact that the soft x-ray diffraction patterns of single biological cells have been recorded by this method to angles corresponding to 14 nm resolution; at present this is perhaps the highest resolution data obtained by any x-ray microscopy technique. (With stronger scatterers, such as small diatoms, patterns have been recorded by the method to angles corresponding to 7 nm resolution). Part of the pattern recorded from *Minutocellus polymorphus* is shown in Fig. 31. The apparatus used for these experiments has been described by Sayre and Chapman [Sayre 1995], together with calculations which indicate that the observed resolutions are approximately those which can be expected on the basis of radiation-induced damage in the specimen.

To date, inversion of the diffraction pattern to an image has not been done. A characteristic of the oversampling

technique proposed for phasing is that three-dimensional diffraction data are needed for the phasing of a three dimensional structure, and the diffraction apparatus used to date does not provide the specimen motions needed to record such data. Instead, Chapman and Sayre plan to use the apparatus with two-dimensional structures to test the phasing and image-generation technique, followed by extension to three-dimensional data collection.

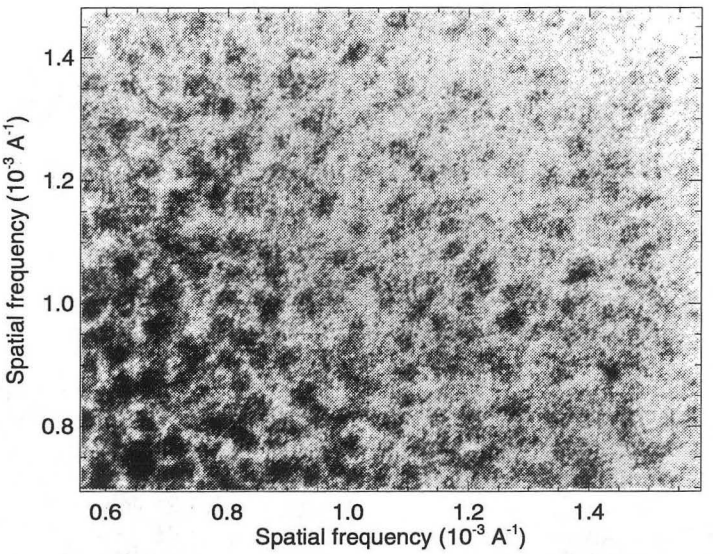

Figure 31: A small portion of the diffraction pattern from a single *Minutocellus polymorphus* cell. The pattern was recorded at Brookhaven with 1.8 nm x-rays and recorded on silver halide film. The pattern is continuous and contains a large amount of information extending to a spatial frequency of 33 μm^{-1}. From Sayre and Chapman, [Sayre 1995].

3.8 Relative merits of the different soft x-ray microscopies

The microscope of choice is generally determined by the specimen and the observation to be made on it.

For live biological specimens to be imaged at high resolution, the dose is inevitably lethal and disruptive. With a short duration flash exposure one may nevertheless capture the image before the specimen has had a chance to alter its appearance [Solem 1986, London 1989]. A single flash exposure is not compatible with any sort of scanning microscopy, but is well suited to contact microscopy, transmission microscopy with zone plate objectives, and holography.

In fixed, wet specimens, both theoretical considerations [Schneider 1994a] and experimental observations indicate that the time scale for visible damage appears to be in the range of many milliseconds. This is time enough for making single high resolution images by scanning as well as the other techniques, given a powerful enough source. To be able to make a meaningful series of images with an x-ray microscope (or, indeed, with any microscope using ionizing radiation), the wet specimen would need to be very well fixed, or particularly radiation hard.

Dry or frozen hydrated specimens can withstand higher doses of radiation, and are well suited to multiple imaging, as is required for microtomography, or elemental/chemical analysis by multiple wavelength imaging.

The Göttingen transmission microscope at BESSY and the scanning transmission microscope at the NSLS represent generic types with complementary capabilities. In looking at not only their present capabilities but possible future improvements in these devices, and installations of similar types, it is useful to keep in mind the special advantages of each.

Transmission microscopes take the image faster, with exposure times of seconds using synchrotron radiation sources, compared to minutes with the scanning systems. They are well suited to Zernike phase contrast, and are

insensitive to rapid fluctuations in the illumination intensity.

Scanning transmission microscopes minimize the radiation dose to the specimen with (**1**) no lossy optics between specimen and detector and (**2**) complete flexibility in scan parameters. The microprobe in scanning microscopes can be used to obtain spectral information from small specimen areas, or elicit other signals such as luminescence, fluorescence, etc. Scanning microscopes are naturally compatible with quantitative analysis of image data, including mass and thickness measurements, elemental and chemical information. They offer ready access to low dose, large area exploratory scans, and easy zoom capability.

In considering eventual laboratory versions of transmission and scanning transmission microscopes, the major attraction of the transmission microscope is the prospect of single-shot flash imaging. For either type, one is likely to lose the free choice of x-ray wavelength, as laboratory sources usually provide only one or a few characteristic emission lines.

Contact microscopy offers experimental simplicity, and is well suited to the use of polychromatic radiation from broadband sources. Gabor holography is suited to coherent flash sources such as x-ray lasers or undulator sources with cryopreparation.

Table 1 summarizes these considerations.

4 Applications

In this section we shall describe some of the biological applications of soft x-ray microscopes. Most of these projects are continuing, and many of the results are preliminary. Nevertheless they should illustrate the range of problems in which biologists have found these instruments to be of value.

4.1 Chromosomes

What is known about the morphology and architecture of chromosomes comes partly from visible light microscopy, partly from electron microscopy, and partly from x-ray scattering studies. The architecture on the nanometer scale is well understood: the structure of the nucleosome is known, much has been learned about chromatin, and it has been suggested that the 30 nm fiber forms loops attached to a protein backbone. Nevertheless, the organization at the 30–300 nm size range has been difficult to determine. Current methods include chemical removal of all histones for structural visualization of the remaining protein scaffold by TEM [Paulson 1977], or intermediate voltage electron microscopy studies of 0.3 μm sectioned, heavy-metal-stained, plastic-embedded chromosomes in which a cumulative exposure of between 1400 and 2.4×10^5 e^-/nm^2 (corresponding to an estimated dose of between 9×10^7 and 2×10^{10} Gray; c.f. Sec. 2.5.2.4) is delivered in the acquisition of a tomographic dataset [Koster 1993]. These efforts can be carried out at the high resolution of the electron microscope, and have yielded considerable information; however, they generally involve dehydrated chromosomes, with no capability for checking structural preservation against hydrated chromosomes at the desired resolution (see Fig. 32). Furthermore, there are limited data on structural variability within a species, or characteristics that are conserved as one compares chromosomes from different species.

Williams *et al.* have undertaken a study of lightly fixed, wet metaphase chromosomes from the broad bean *Vicia faba*, the pea *Pisum sativum*, the sweet pea *Lathyrus odoratus*, and the JU56 cell line from the wallaby, an Australian marsupial. Radiation dose was kept to 3×10^5 Gray in all cases to keep mass loss below 3% [Williams 1993] (see Sec. 2.5.2). This study was aimed at determining the ratio of DNA mass to other organic mass (e.g., histones); if constant among species, it would indicate commonalities of mechansims for folding of chromatin into metaphase chromosomes. Previous measurements for this ratio range from 0.16 to 0.32, with a twofold variation seen for different measurements on a single species. Based on over a thousand micrographs from the STXM at Brookhaven and published total DNA measurements, they report that the DNA mass fraction is 0.38 in all cases [Williams 1994a, Williams 1994b]. However, chromosome length and diameter change from species to species in a manner which suggests that different arrangement mechanisms are brought into play as the amount of chromatin is increased (although more data is needed to firmly establish this trend). The JU56 chromosomes were also used to examine the effects of fixation. Images of fixed and unfixed chromosomes were collected under otherwise identical conditions. Fixation leads to substantial shrinkage in both length and diameter, leading to a 50% decrease in volume. There appears to be some net increase in mass as well, presumably due to the binding of the fixative.

Giant chromosomes from *Chironomus thummi* have been studied in the Göttingen microscope [Guttmann 1992a] (Fig. 33); structural details are beautifully revealed when imaged in a salt solution which causes partial chromosome

	TXM	**STXM**	**Contact**	**Gabor**	**Diffraction**
Detection	parallel (CCD)	serial (counter)	parallel	parallel	parallel
Field size	fixed by objective lens	selected by operator	large (illumination & readout)	large (illumination & readout)	small
Resolution	set by objective (zone plate)	set by objective (zone plate)	set by resist & diffraction	set by resist & coherence	not limited by technology
Dose	See (•) below	lowest	Resist DQE ~ 10%	Resist DQE ~ 10%	
Image time	fast overall	fast per pixel	fast overall	fast overall (laser?)	slow for 3D
Temporal coherence	monochromatic (zone plate)	monochromatic (zone plate)	polychromatic OK	monochromatic	monochromatic
Source acceptance∗	multimode	single mode	multimode	single mode	single mode
Intensity fluctuation sensitivity	low (integrates)	high (per pixel)	low (integrates)	low (integrates)	low (integrates)
Flash imaging?	yes	no	yes	yes	not for 3D
Modes besides bright field amplitude contrast					
Phase contrast	Zernike	differential, Nomarski	no	intrinsic	intrinsic
Dark field	possible†	yes	no	no	no
Photoemission	yes (electron optics)	yes (electron spectrometer)	no	no	no no
Fluorescence	no	yes	no	no	no
Luminescence	no	yes	no	no	no
Elemental maps	possible†	yes	quantitation?	quantitation?	quantitation?
XANES maps	possible?†	yes	very hard	very hard	very hard
Polarization	possible†	yes	possible†	possible†	possible†
Micro-spectroscopy	hard	yes	no	no	no

Table 1: Comparison of the features of four classes of x-ray microscopes: transmission x-ray microscopy (TXM), scanning transmission x-ray microscopy (STXM), contact microscopy or microradiography, Gabor holography, and diffraction (from which reconstructed images have not yet been obtained).
∗: Single mode corresponds to coherent, laser-like illumination, in which case undulators or x-ray lasers are required. A greater range of x-ray sources deliver multimode illumination.
†: Not yet demonstrated, but expected to be available in the future.
•: There is a dose penalty due to the inefficiency of the zone plate. However, in Zernike or optimized phase contrast this penalty is compensated to a large degree, especially near the oxygen K edge and outside the water window [Schmahl 1994a].

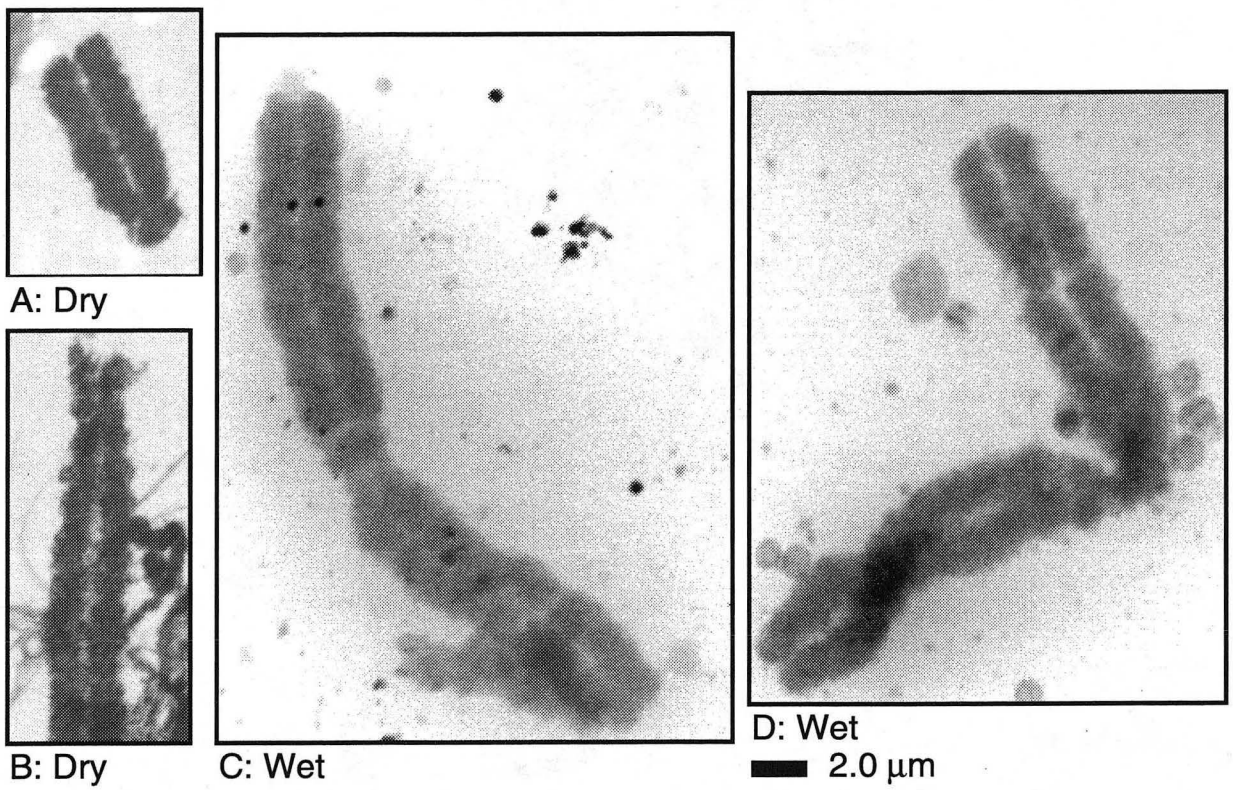

Figure 32: Dry and wet, 0.1% glutaraldehyde-fixed chromosomes of the bean *Vicia faba*. Images B, C, and D are all of the *M* chromosome type. Note that while the freeze-dried specimens appear to show more structure, their morphology is considerably altered compared to the chromosomes which were viewed hydrated in 65 mM 1/2x McLeish buffer. From data of Williams *et al.* [Williams 1993]).

decondensation. Human chromosome spreads have also been viewed in the Göttingen microscope by Hearst and collaborators [Meyer-Ilse 1994b]. Shinohara *et al.* have viewed dried [Shinohara 1990a] and wet [Shinohara 1992, Kinjo 1994] human chromosomes using contact x-ray microscopy, aiming to study high resolution structural organization.

Future studies of the structure of whole, hydrated chromosomes will certainly benefit from the further development of flash and cryogenic x-ray microscopes.

Figure 33: Part of a condensed polytene chromosome of *Chironomus thummi* imaged in a physiological salt solution using the Göttingen x-ray microscope at BESSY. From Guttmann *et al.* [Guttmann 1992a].

4.2 Malaria

Human erythrocytes infected with *P. falciparum*, the organism that causes the most lethal form of human malaria, were first imaged using both TXM and STXM by Moronne *et al.* [Meyer-Ilse 1994b] (see Fig. 2). Their studies are aimed at characterizing the extensive tubulovesicle system of the parasite, and localizing important parasite antigens with luminescent probes.

Mangel, McGrath, Williams, and collaborators have begun x-ray microscopy studies of malaria aimed in part at addressing a question concerning the possibility of a parasitophorous duct in the trophozoite stage of *P. falciparum*. Pouvelle *et al.* [Pouvelle 1991] have published confocal microscope observations which they interpret as evidence of a duct that appears to connect the vacuole in which the parasite resides with the surface of the red blood cell. The

duct would provide a path by which antimalarial agents could reach the parasite, and provide a new approach to the development of a vaccine against the disease. The existence of the duct remains an issue of some controversy (see e.g., [Taraschi 1994] plus exchange of letters which follows in the same issue of *Parisitology Today*), in part because of the resolution limitations of visible light microscopes on the one hand and questions over fluorescence labeling and conventional EM preparation and sectioning on the other hand. Present x-ray microscopy studies require glutaraldehyde fixation (cryofixation will be used in the future), but they have allowed the study of the morphology of the whole, unsectioned parasite at various stages of the erythrocytic life cycle (see Fig. 34). If the duct is a common characteristic of the system, STXM with its 50 nm resolution should see it easily. In over a hundred micrographs of infected erythrocytes (wet and fixed), no duct has been found. If further observations still do not provide positive evidence, one would have to question the original observation. The development of soft x-ray tomographic imaging of frozen hydrated samples (as suggested by R. Glaeser of Lawrence Berkeley Laboratory) should have a large impact on malaria studies, including malaria from other species (Fig. 35).

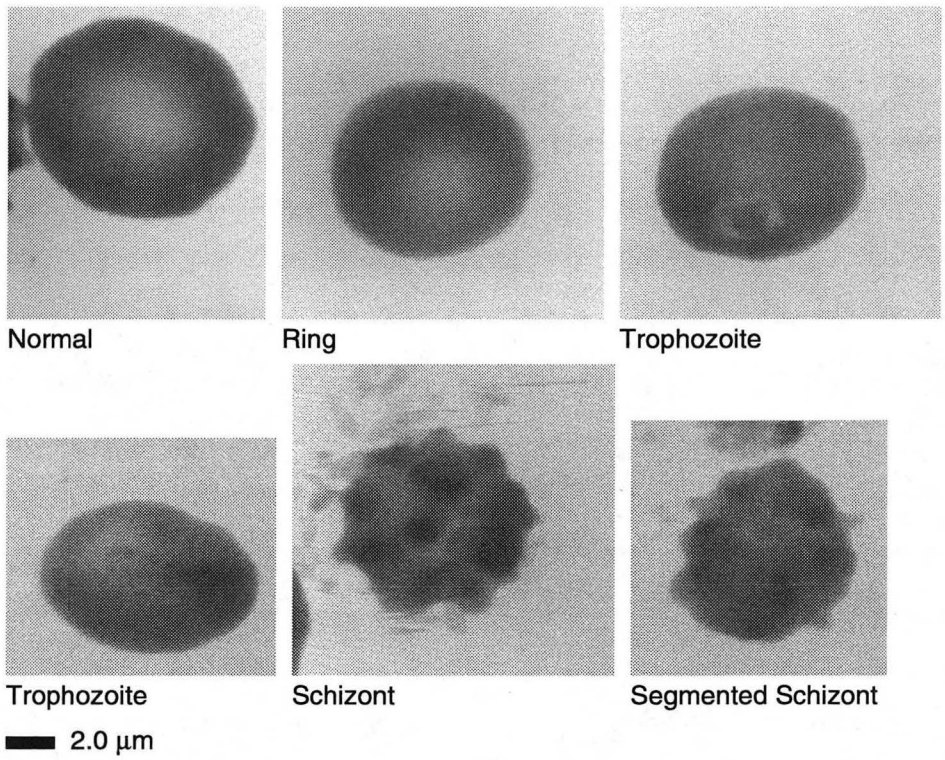

Figure 34: Stages in the life cycle of the human malarial parasite *Plasmodium falciparum* in whole, wet, 1% glutaraldehyde-fixed erythrocytes viewed using the X1A STXM. Samples from a culture generously provided by Dr. William Trager, Rockefeller University. Figure courtesy S. Williams, C. Jacobsen, and X. Zhang (Stony Brook) and W. Mangel and W. McGrath (Brookhaven).

4.3 Mapping Calcium deposits and calcified tissue

Calcification or decalcification are involved in a large variety of biological phenomena in development, aging, normal physiology and disease. STXM offers a convenient way to measure the distribution and concentration of calcium in tissue sections, cell cultures, etc. The absorption spectrum of calcified tissue (Fig. 36) shows a prominent resonance structure near the calcium L absorption edges around 3.5 nm. From a pair of images, one on a resonance peak, and another away from resonance, the distribution of the element can be determined. This approach was used by Kenney, Cinotti, and collaborators [Kenney 1985, Cinotti 1987] to map bone calcium distribution in biopsy sections from patients suffering from osteoporosis. Recently, Buckley has further developed the calcium mapping technique on

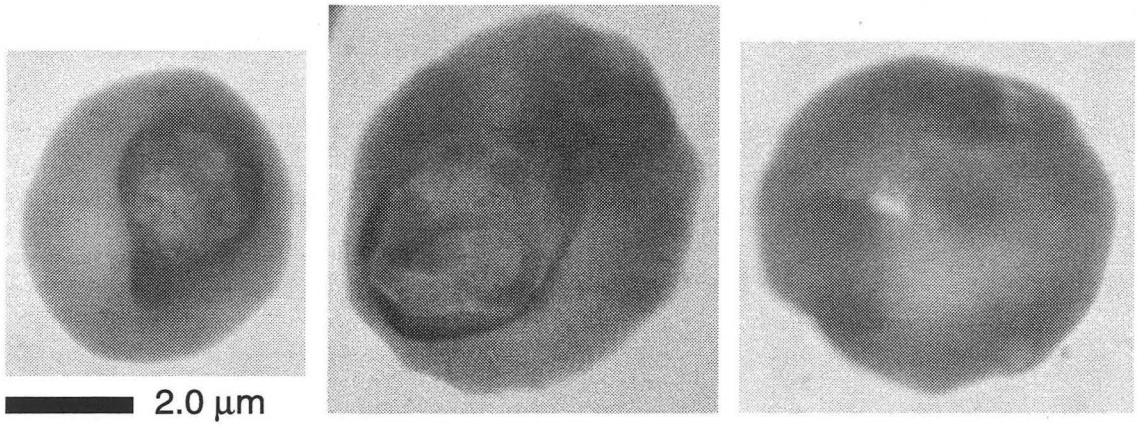

Figure 35: Mouse malaria *P. vinkei* from the lab of P. G. Kremsner, Landesinstitut für Tropenmedizin, Berlin. The samples were fixed in 2% glutaraldehyde and imaged the same day using a 30 nm zone plate in the Göttingen microscope at BESSY. Figure courtesy S. Williams, C. Jacobsen, and J. Maser (Stony Brook) and P. Guttmann and G. Schneider (Universität Göttingen).

mineralized tissues to provide high signal-to-noise maps with improved quantification and sensitivity [Buckley 1995a].

Calcium mapping has also been used to study both normal and pathological calcification in tendon, cartilage and bone [Buckley 1992d, Buckley 1992a, Buckley 1992b]. In 0.1 μm thick fixed but unstained tissue sections, they find that small crystallites nucleate in the immediate surroundings of chondrocyte cells, consistent with the idea that these deposits develop in response to secretions from the cells into the surrounding matrix (see Fig. 37). The precise shape of the absorption spectrum, and the positions of the resonances can be further interpreted in terms of the chemical environment of the calcium atom [Buckley 1995a, Buckley 1995b]. It is hoped that this work will lead to a determination of the mineral phase of these deposits to ascertain their relation to destructive pathogenic phases, and provide an insight into the likely formation mechanism.

Studies of the reaction of the body to bone implants are also being pursued [Buckley 1994]. It appears that if the implant (often made of titanium) is coated with a well bonded layer of calcium apatite, the host makes use of this coating, and incorporates it into the remodeled bone structure.

4.4 Mapping protein and DNA

Although individual proteins and nucleic acid molecules show characteristic spectra near x-ray absorption edges [Kirtley 1992], it does not follow that in the complexity of a biological specimen these characteristics survive to provide useful signatures for mapping the distribution of chemical types. A study was undertaken, nevertheless, by Zhang *et al.* [Zhang 1994a, Zhang 1994b] on critical point dried CHO fibroblasts. They find that some of the resonant peaks observed in pure DNA near the carbon K absorption edge are particularly prominent in spectra taken from the nucleus. Similarly, some of the peaks observed in protein standards (see Fig. 38) are much stronger in the cytoplasm than in the nucleus. Based on the analysis of these spectra, Zhang *et al.* have performed a preliminary analysis on the distribution of protein and DNA within the cells. By imaging the cells at several wavelengths corresponding to the characteristic absorption peaks of protein and DNA, it was found that DNA is located in the nucleus, while protein is spread more evenly throughout the cell. This reassuring result has then allowed the technique to be applied to the study of protamine in sperm (Sec. 4.6 and Fig. 40). By extending the analysis to the nitrogen and oxygen edges, one should be able to create separate maps of other constituents, such as carbohydrates and lipids.

4.5 Zymogen granules

Zymogen granules are membrane-bound vesicles, approximately 1 μm in diameter, that store proteins manufactured and secreted by the acinar cells of the pancreas. Questions concerning the protein content and structure of these

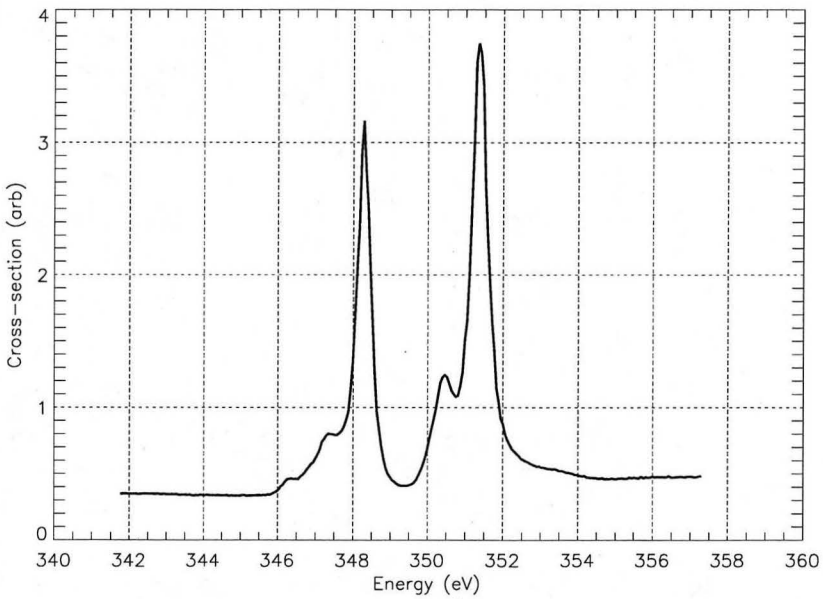

Figure 36: Absorption spectrum from calcium in bone. Figure courtesy C. J. Buckley (King's College, London).

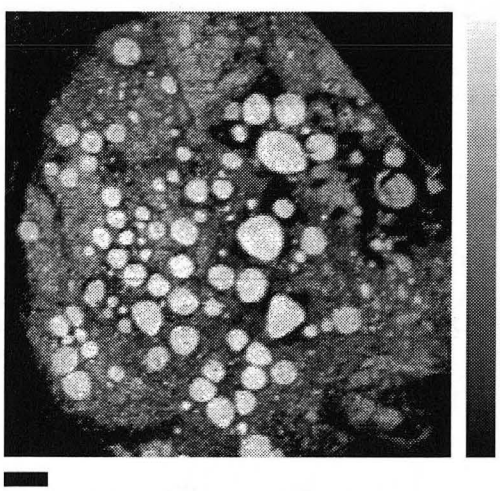

Figure 37: Quantitative calcium map of a 0.1 μm thick section of tendon from a human with tendonitis. The calcium concentration map shows the distribution and density of the pathogenic mineral deposits, enabling the study of possible processes responsible for isolating the calcification in rounded islands. Scale bar: 20 μm. Peak brightness: calcium concentration 5.5 μg/cm^2. From Buckley *et al.* [Buckley 1995a].

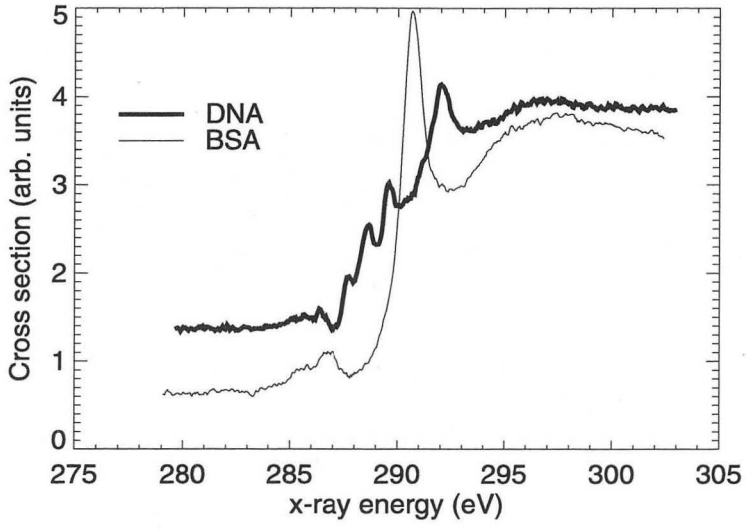

Figure 38: Carbon edge NEXAFS spectra of protein (BSA; bovine serum albumin) and DNA thin films taken using the X1A STXM. The relative strengths of the signals at various absorption resonances are used for chemical mapping. From X. Zhang *et al.* (Stony Brook) [Zhang 1994b].

secretion granules, as well as the way in which the proteins enter and leave the granule, have been examined by Rothman, Goncz and collaborators. Since the chemical makeup of the proteins are reasonably well-known, the STXM x-ray transmission map provides a quantitative measure of both the protein concentration and the total content of the granules with femtogram accuracy. Using a specially designed sample chamber [Goncz 1992a], they were able to repeatedly image both fixed and freshly isolated granules suspended in aqueous environments. By this means, the authors performed a study of the time evolution of the content-size relationship of the granules as a function of their preparative treatment and chemical surroundings. The thousands of granules that have now been observed in this way [Goncz 1994a] reveal two distinct types, both of which are reported to either gain or lose protein or stay in equilibrium according to the protein concentration of the buffer. The measured protein fluxes are much greater than could cross a continuous lipid membrane barrier but much less than the free-diffusion flux in the absence of a barrier. A major fraction of the granules release their protein gradually and without a catastrophic loss (lysis) event [Goncz 1992b]. The protein concentration of fresh granules varies about 600% for different (fasted) rats but only about 20% for a particular rat [Goncz 1994b].

One might suppose that radiation damage to the membrane would be a factor in these experiments and this is indeed observed. When a sequence of images using both low and high dose is taken of a number of nominally similar granules, the content versus time curve is initially the same for both high and low dose x-ray images and also the same as recorded by non-x-ray methodologies. However, when the high-dose granules reach about 6×10^5 Gray, they begin to show an increase in effective permeability and the curves diverge. Below the 6×10^5 Gray limit, the release/uptake behavior in the x-ray microscope appears to be independent of dose and is assumed to be representative of the behavior of unilluminated granules.

These measurements exploit the capabilities of the x-ray microscope to effectively "weigh" a small sample or feature in an aqueous environment with a precisely known x-ray illumination. The complex body of evidence that has now been accumulated in this way is being interpreted by Rothman and coworkers in terms of their theory of protein transport by mass action across the granule membrane. In the opinion of some, such interpretations are unconventional, but Rothman *et al.* point to a growing literature describing membrane transport processes for proteins across many biomembranes and to granule images taken by freeze-fracture/SEM [Cabana 1988] which seem to indicate a protein "pore" with a permeability in agreement with the STXM-derived values [Goncz 1995].

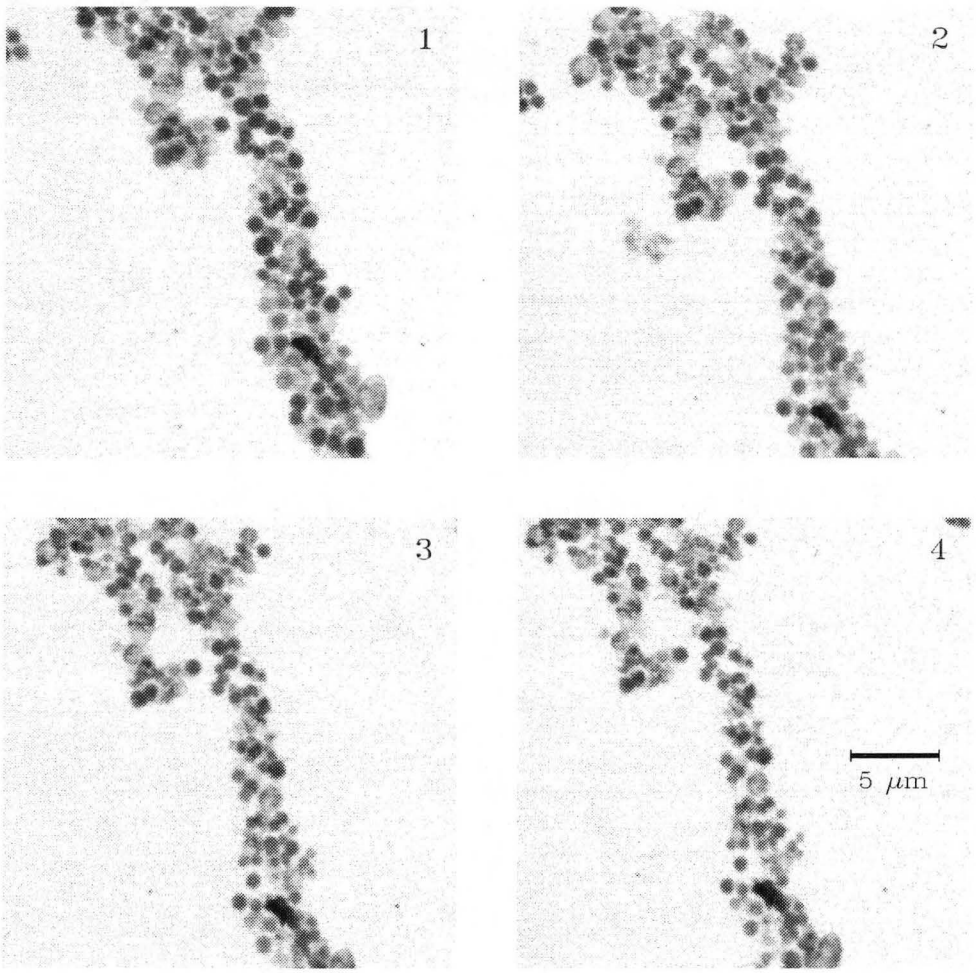

Figure 39: STXM images of a group of wet, unfixed zymogen granules taken over a period of 4 hours, while fluid was perfused past the granules. Over that time interval, the same granules can be seen as they become smaller and lose their protein contents, as determined by quantitative analysis of the images. The experiment shows that the great majority of granules are losing protein slowly over time and not via a sudden rupture or "lysis". The four low-power STXM images were taken with 3.4 nm x-rays and a pixel size of 63 nm. From Goncz *et al.* [Goncz 1992b].

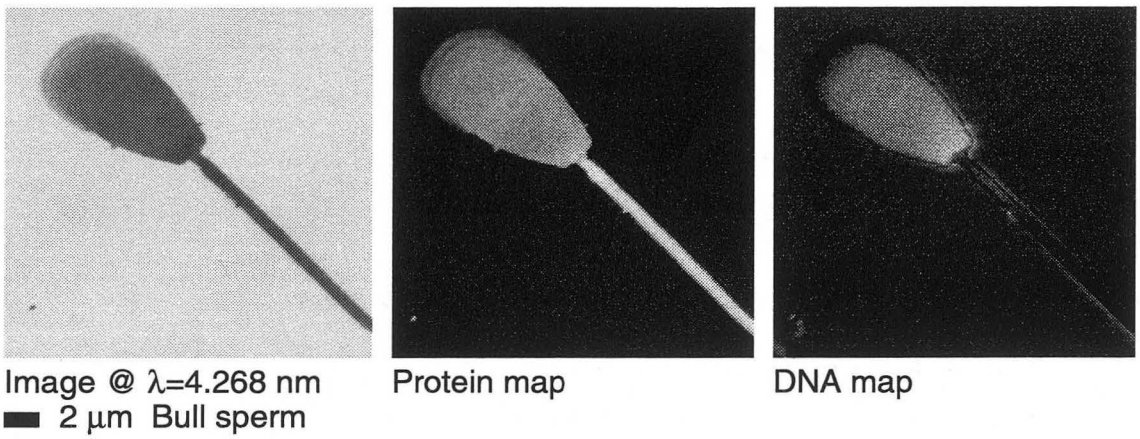

Figure 40: STXM image, and protein and DNA map, of air-dried bull sperm (prepared by R. Balhorn, LLNL). STXM images were taken by X. Zhang (Stony Brook) at six wavelengths in the NEXAFS resonance spectral region. One of these images is shown at the left, next to the protein and DNA maps derived from the series of images. From Zhang *et al.* [Zhang 1994b].

4.6 Sperm

There are several unsolved problems associated with the structure of sperm. Maybe the most important has to do with the packing of the DNA in the sperm head, proposed to be in layered sheets each of which contain arrays of coiled portions of the genome. Balhorn has been studying this system using a variety of techniques [Balhorn 1992], including x-ray microscopy. In this continuing study, micrographs of bull sperm were made using the Livermore x-ray laser by Da Silva *et al.* [DaSilva 1992a], with the microscope at BESSY by Meyer-Ilse *et al.* [Meyer-Ilse 1994a], and with the microscope at Brookhaven [Balhorn 1992].

Recently Zhang *et al.* have started to use carbon edge XANES mapping (Sec. 4.4) to measure total protein content and protein distribution within dried sperm heads. Specimens from bull, human, hamster, stallion, and mouse have been examined in collaboration with Balhorn. These differ not only in size and shape, but also in protamine I and protamine II content. Previous studies have given population-averaged values of these parameters, but what is less clear is the protamine content in individual, morphologically normal sperm. The work of Zhang *et al.* provides information on the variability from cell to cell, and has produced detailed maps of the overall protein distribution. Changes in protamine II content are related to infertility; however, it is not known whether infertile males produce sperm with uniformly defective protamine II content, or whether there is a broad variation among cells from a single individual.

Other aspects of sperm structure have been investigated by Tomie *et al.* using contact microscopy with AFM read-out [Tomie 1991, Tomie 1992], and by Loo *et al.* [Loo 1992b, Loo 1992a] with the help of a stereo stage attached to the STXM at Brookhaven (see Fig. 41).

4.7 Muscle

The structure of muscle has been the subject of extensive research. The sliding filament model is generally accepted to explain the main features of vertebrate skeletal muscle, and much information has been gathered regarding the motor mechanism in terms of cross bridge motion from x-ray crystallography, scattering, and electron microscopy. There is nevertheless much more to learn, and many groups around the world are approaching the problem with all available tools.

The King's College group has been studying vertebrate skeletal muscle using scanning transmission x-ray microscopy. In their work at Daresbury they have shown that myofibrils maintain their ability to contract on addition of ATP to the buffer up to a radiation dose of about 10^4 Gray, and that this limit can be somewhat extended with the use of radiation protectants [Bennett 1993]. Based on additional imaging studies at the Brookhaven STXM they

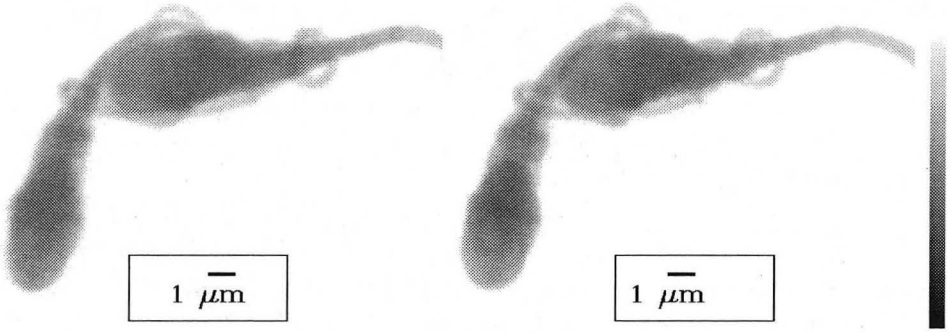

Figure 41: Stereo image pair (20° separation) of human spermatozoa. Of interest in these images is the area of increased density in the posterior half of the head which may represent the post acrosomal sheath. This feature is not seen in electron microscope thin sections, but is seen by phase contrast light microscopy. Images acquired using a 60 nm zone plate (fabricated by E. Anderson, Lawrence Berkeley Laboratory) in the Stony Brook microscope at Brookhaven. From Loo *et al.* [Loo 1992b, Loo 1992a].

provide detailed mass density maps along the length of the sarcomere (see Fig. 42), and document the changes in these maps due to radiation exposure.

Soft x-ray contact microscopy has also been used to investigate the structure of intact cardiac muscle cells. In these studies, the existence of the major bands within the sarcomere is reported to be observable without the need to isolate the myofibrils [Stead 1994b].

There are significant differences between the vertebrate and the insect flight muscle [Tregear 1977]. The structure of the honey bee flight muscle has been extensively studied by electron microscopy, and more recently Yeh and Fan have embarked on a program of study using scanning x-ray microscopy and diffraction at Brookhaven.

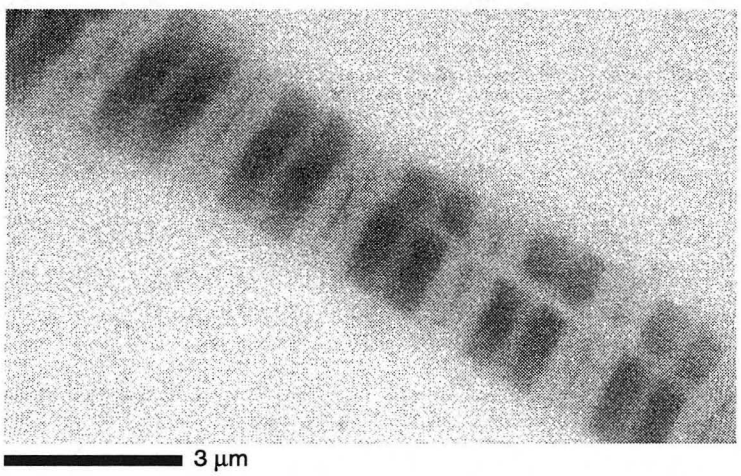

Figure 42: An unfixed and unstained rabbit myofibril imaged by the STXM at Brookhaven using 3.53 nm x-rays. The sarcomere repeat length is 2.45 μm. From Bennett *et al.* [Bennett 1993].

4.8 Study of macrophages

The Göttingen group, in collaboration with J. Scharf, has been studying Kupffer cells from the liver of the rat. In their study of phagocytosis, the accumulation of ingested 80 nm hematite particles in intracellular phagosomes is clearly seen in phase contrast.

In their study aimed at locating macrophage specific antigens on the surface of these cells, they used monoclonal antibodies ED1 and ED2. To render the sites visible, a second, peroxidase conjugated antibody and silver stain was applied. Both the amplitude and phase contrast images (Fig. 14) provide useful, detailed and complementary information [Schmahl 1994a, Schmahl 1994b].

4.9 Lipid membranes

Guttmann and Klögsen have used the Göttingen microscope at BESSY to study artificial lipid membranes (palmitoyl-oleyl-phosphatidyl-choline, or POPC) in a wet cell [Guttmann 1994]. The study of this model system by amplitude and phase contrast x-ray microscopy provides an opportunity to visualize the adhesion of adjacent membranes, and to look for the postulated microroughness of unstressed membranes at a resolution superior to that of the visible light microscope (see Fig. 43). Unilamellar and paucilamellar vesicles are seen with good contrast due to enhanced absorption and phase shift when the membrane is roughly parallel to the x-ray beam. Spherical vesicles were seen to be quite stable in the x-ray beam, and irregular structures in membrane surfaces were observed. This ongoing study is expected to lead to a better understanding of artificial and, finally, biological membranes.

A. B.

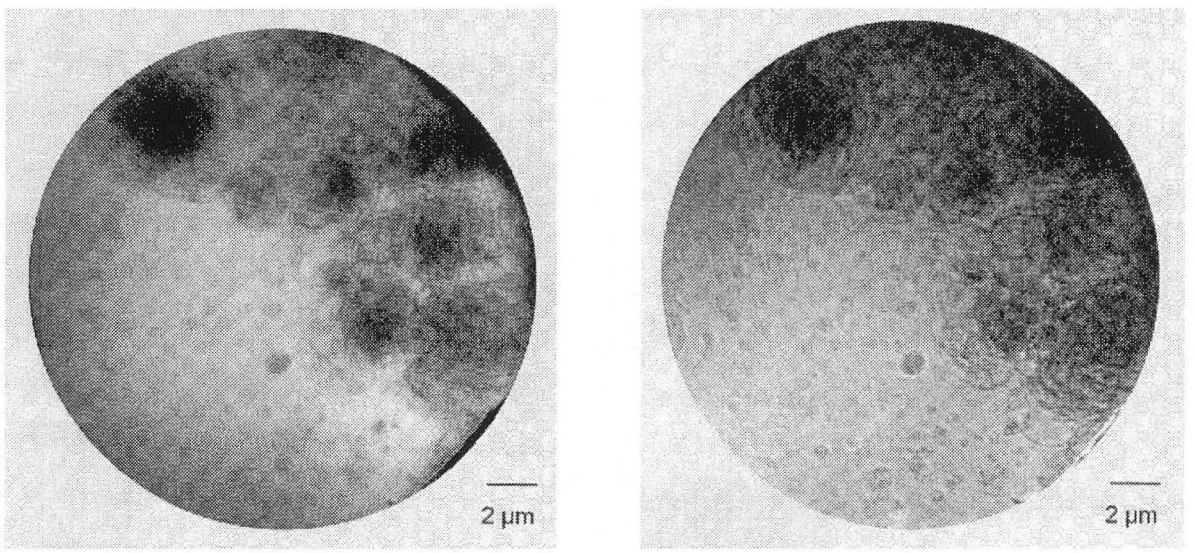

lipidp.eps lipida.eps

Figure 43: Artificial lipid vesicles, prepared by B. Klösgen, Freie Universität Berlin, imaged at $\lambda = 2.4$ nm with the Göttingen x-ray microscope at BESSY. Both amplitude (left) and phase (right) contrast images are shown. From Guttmann and Klösgen [Guttmann 1994].

4.10 Plant cells

Plant cells have thick cell walls, so the high penetration of soft x-rays relative to electrons becomes particularly relevant. Stead, Ford, and collaborators have undertaken a series of studies on plant cell ultrastructure. These studies have examined image fidelity and resolution of contact microscopy relative to light and electron microscopy for algal cells [Stead 1987] and for the floral epidermal hairs of *Digitalis purpurea* [Stead 1989]. More recently, they have used a laser plasma x-ray source for exposure and atomic force microscope for readout of the developed photoresist (see Fig. 28), and find that this combination offers improved characteristics for contact microscopy [Cotton 1992, Cotton 1994]. Using this approach, they are undertaking studies on the carbon density in membranes of the alga *Microthamnion* and the structure of the flagellar apparatus of *Chlamydomonas* [Ford 1994] (see Fig. 28), and the fate of cellulose fibrils in the protonemal cell wall of the moss *Bryum tenuisetum* during abscission cell formation [Stead 1994a].

4.11 Iron- and manganese-accumulating microorganisms

Thieme *et al.* have been using the Göttingen microscope at BESSY for the study of microorganisms which accumulate metals [Thieme 1994b]. The microorganisms live in wet environments where metal containing ions are present in low concentrations. They create internal or external deposits which eventually become minerals. The x-ray microscope is well suited to the study of the this process, as the microorganisms can be imaged wet, and the regions with high metal content show up in excellent contrast. In samples of slime from a mine, Thieme *et al.* find metal containing aggregations in the form of tubules, helical bands and also in bacteria. Fig. 44 shows fine slime fibrils originating on the concave side of the bean shaped cell of the bacterium *Gallionella ferruginea.*

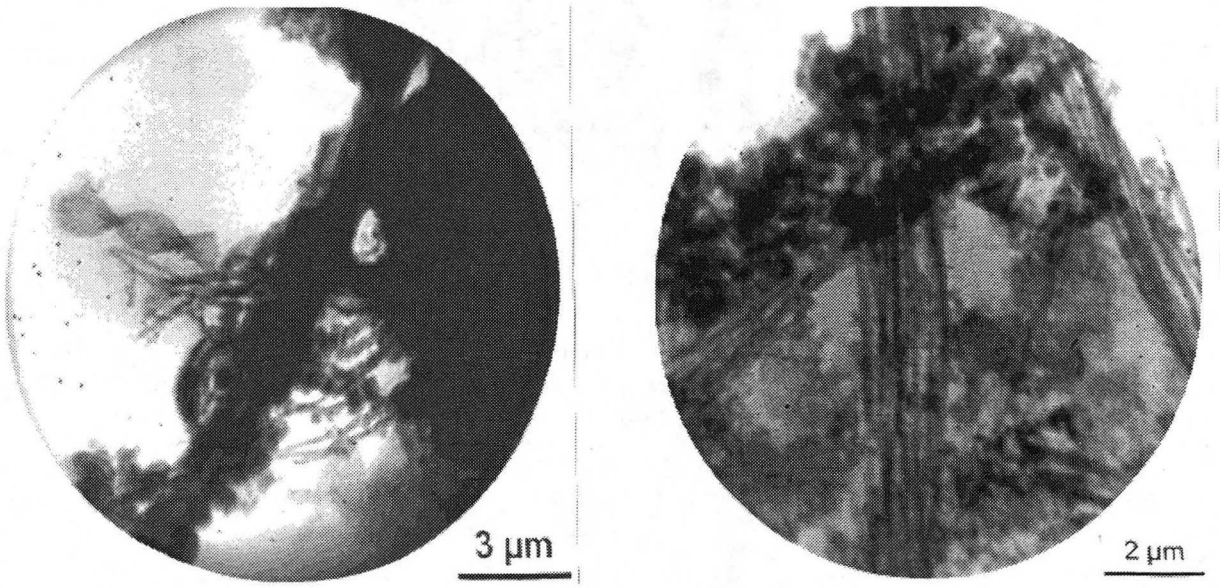

Figure 44: X-ray images of iron- and manganese-accumulating bacteria in soil. **Left:** tubular sheaths packed with other aggregates and a helical band. **Right:** helical bands, bacteria, and other forms of aggregation. From Thieme *et al.* [Thieme 1994b].

4.12 Non-biological applications

4.12.1 Polymers and polymer blends

The study of polymeric materials is of considerable interest in the design and understanding of advanced plastics, fibers, and related materials. X-ray microscopy offers unique capabilities for the characterization of such materials on the submicron scale. Using the STXM at Brookhaven, Ade *et al.* developed the capabilities required for their analysis [Ade 1992]. Since these materials are built from simple monomers, their near edge absorption spectra provide specific fingerprints, useful in identification. Such spectra can be acquired from 250 nm size areas in a few seconds (see e.g., Fig. 23), and most polymers are sufficiently radiation resistant that the associated radiation dose does not result in observable damage.

If one selects a specific x-ray energy associated with a sharp peak in the absorption spectrum of a particular polymer, then that polymer is highlighted, as shown in Fig. 45. The technique is useful in characterizing the distribution of phases in polymer blends, in assessing the effect of compatibilizers, which are designed to promote the adhesion of dissimilar phases, and in finding and identifying contaminating precipitates [Ade 1994c].

More recently, Ade and Hsiao have utilized the polarization of the x-ray beam in mapping the orientation of polymer molecules in Kevlar fiber [Ade 1993] (Fig. 46).

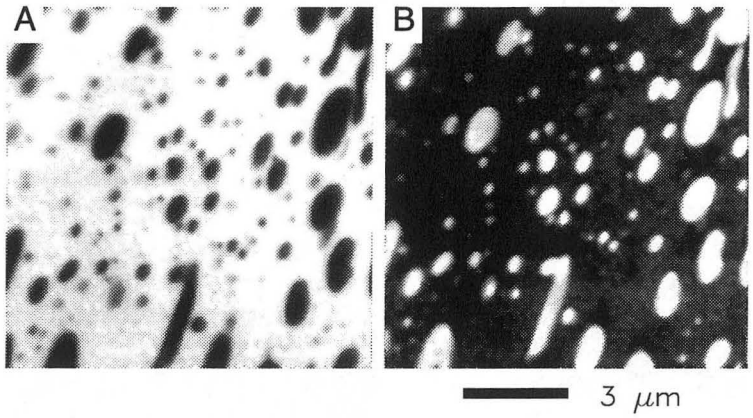

Figure 45: Scanning transmission x-ray micrographs of a thin section of a polycarbonate/poly(ethylene terephthalate) polymer blend acquired at a photon energy of 285.36 eV (**A**) and 285.69 eV (**B**). The photon energies were chosen to distinguish the two materials, based on the x-ray absorption spectra of the two polymers (see Fig. 23). From Ade *et al.* [Ade 1994b].

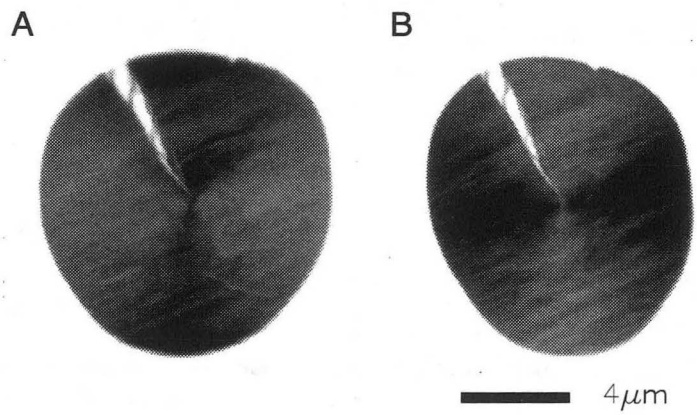

Figure 46: X-ray linear dichroism images of a 200 nm thick section of Kevlar 149 fiber cut at 45° to the fiber axis. The section was imaged with the electric field vector in the left-right direction (**A**) and in the up-down direction (**B**) at a photon energy of 285.5 eV. This energy selects the aromatic group of the fiber polymer; the butterfly patterns are due to linear dichroism contrast caused by the radial symmetry and orientational order of the fiber. From Ade *et al.* [Ade 1993].

4.12.2 Soil colloids

The structure of clay and similar minerals is strongly influenced by the presence of water, and cations in the aqueous environment. The movement of nutrients and toxic materials in the soil, as well as weathering and erosion, are strongly influenced by this environment. Such systems must be studied wet in a special sample cell (see Fig. 11), and x-ray microscopy provides the first opportunity to obtain morphological information at the high resolution level. The Göttingen group studied the behavior of montmorillonite. They found evidence for both the "cardhouse" and "bookhouse" structures previously postulated [Thieme 1992]. More recently [Niemeyer 1994], they examined the changes these clay minerals undergo when the ionic environment changes. They find that non-covalent cations, such as Na^+, lead to the delamination of the structure, while the addition of organic surfactants leads to a compaction of the aggregates (Fig. 47).

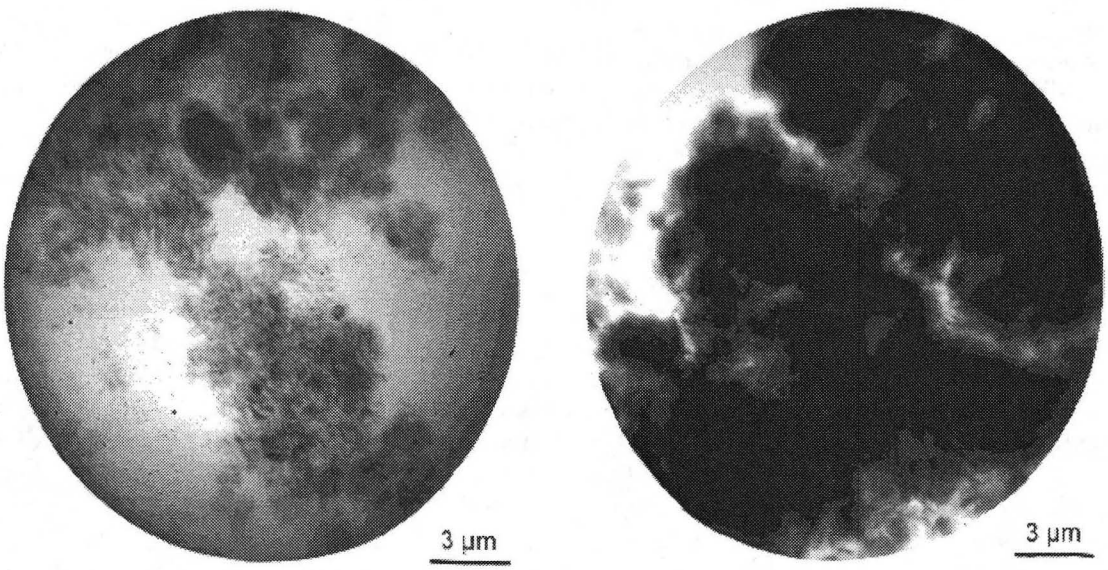

Figure 47: X-ray images of a 0.1% suspension of a naturally-Ca^{2+}-coated montmorillionite (left) and the same preparation with aggregates formed after the addition of a cationic organic surfactant (right). The Göttingen microscope at BESSY was used with $\lambda = 2.4$ nm x-rays. From Niemeyer *et al.* [Niemeyer 1994].

4.12.3 Aggregation in silica and zeolitic precursors

The structure of silica and the zeolites is of great practical importance to the chemical industry. Such materials often appear in an aqueous form, where the mechanisms of aggregation determine their ultimate effectiveness in applications. X-ray microscopy of hydrated specimens offers a unique route to obtain images of these structures which usually cannot exist outside of the aqueous environment.

The complex porous structure of silicas has led to their application both as selective catalysts and as catalyst supports in the petrochemical industry. They are also used as filters, absorbers, and molecular sieves. In addition, the synthesis of special glasses and ceramics by the sol-gel process is an area of increasing interest, in which it is important to understand the factors that affect the homogeneity and microporous structure of the material. The development of a porous structure is strongly influenced by the factors that affect the aggregation, gelation, aging and drying of the material, including the pH and the concentration of the silica system. Such systems have conventionally been studied by indirect methods, such as small-angle scattering techniques (*e.g.*, SAXS and SANS) [Wijnen 1991], which give information on the average mass-density distribution for length scales up to about 200 nm. The STXM has a spatial resolution of ~ 50 nm and is capable of imaging hydrated samples under normal ambient conditions, so it can provide direct, spatially-resolved data on the developing gel structures over length scales that overlap and extend those accessible with SAXS.

The King's College group used their scanning microscope at Daresbury to study these systems [Morrison 1992c, Morrison 1994b] and has reported clear evidence for fractal aggregates (Fig. 48).

Significant structural differences were observed as the pH was varied over the range 3 to 8 [Shi 1994]. At low pH values a relatively dense structure was observed; this can be related to the small size of the primary particles. Larger aggregates were formed at intermediate pH values, but as the pH was increased still further a more open structure was formed that reflects the influence of increasing surface charge on the aggregates that inhibits the formation of large dense lumps of gel. At the highest pH values, the primary particles themselves are significantly larger, and the result is a loosely connected assembly of colloidal particles. In some cases the structure of the aggregates can be characterised by a fractal dimension that can be used to distinguish between different growth models.

4.13 Paleo-botany: microchemical characterization of coal

Chemically and morphologically, coal is a very complex, heterogeneous material. Its components derive from selective preservation of various biochemically resistant plant remains. Over geologic time scales, these plant remains are thermo-chemically modified. Coal's constituents are defined as macerals and are classified as liptinites with H/C ratios $\gtrsim 2.0$, vitrinites with H/C ratios $\simeq 1.0$, and inertinites with H/C ratios < 1.0. This classification is based primarily on characterization using reflected light microscopy.

Botto, Cody, and collaborators have initiated investigations into the microchemical analysis of coal macerals using the Stony Brook scanning microscope [Botto 1994, Cody 1994]. By imaging ultramicrotomed sections of coal at various wavelengths near the carbon K absorption edge, they were able to spatially resolve both intermaceral and intramaceral chemical heterogeneity. For example (see Fig. 49), the exinitic maceral, sporinite (derived from the exine of spores), is clearly resolved when an image is obtained with an x-ray energy corresponding to absorption due to aromatic carbon. The concentration of aromatic carbon within the outer rim of the spore is less than that of the matrix material (vitrinite). Intracellular material evident in the core of the smaller spore contains even less aromatic carbon. At x-ray energies where absorption is primarly due to aliphatic carbon, outer regions of the spore can be seen to contain approximately the same concentration of aliphatic carbon as the matrix vitrinite, while the intracellular material is clearly most aliphatic. Remarkably, compositionally-discrete intracellular material is preserved within these spores after 300 million years of thermal metamorphism.

5 Discussion

5.1 Critical hardware ingredients: ongoing developments in sources and optics

It is the dramatic improvements in the brightness of soft x-ray sources in combination with the improvements in optics (mainly zone plate) fabrication that have made the recent progress in soft x-ray microscopy possible. Early synchrotron radiation sources offered more than a 10^5 increase in spectral brightness, and undulators on modern storage rings produce beams with brightness about 10^9 higher than that of laboratory x-ray tubes. Additional improvements in these areas are already taking place.

Third generation synchrotron radiation sources have started operation in Berkeley (ALS), in Trieste (ELETTRA), in Hsinchu (SRRC), in Uppsala (MAX II), and with higher energy beams in Grenoble (ESRF). Other such sources are under construction in Berlin (BESSY II), in Pohang (PLS), in Campinas (LNLS) and at higher energies in Argonne (APS) and in Nishi-Harima (SPRing 8). These machines are designed to provide beams with between one and two orders of magnitude higher brightness than what we have been using at the X1A beamline at the NSLS. Programs in x-ray microscopy are starting up, or are planned at most of these facilities. Brightness at the NSLS is also being improved by about one order of magnitude.

X-ray lasers, useable as coherent sources for flash imaging, have been under development for some time at Livermore and elsewhere [Matthews 1985, Suckewer 1985, Trebes 1987]. Plans for a laser dedicated to applications in the wavelength range best suited for biological imaging have been put forward [London 1992a], and considerable technical progress toward its realization has been made [Trebes 1994].

A potential alternative to "conventional" x-ray lasers is the free electron laser, FEL. Such devices are in operation at visible and infrared wavelegths, and detailed plans have been put forward to build one for the soft x-ray range [Pellegrini 1993]. This ambitious plan would make use of part of the Stanford 2 mile accelerator, and would generate subpicosecond pulses with about 10^{14} coherent, tuneable x-ray photons, enough to make multiple x-ray images or holograms in a single shot.

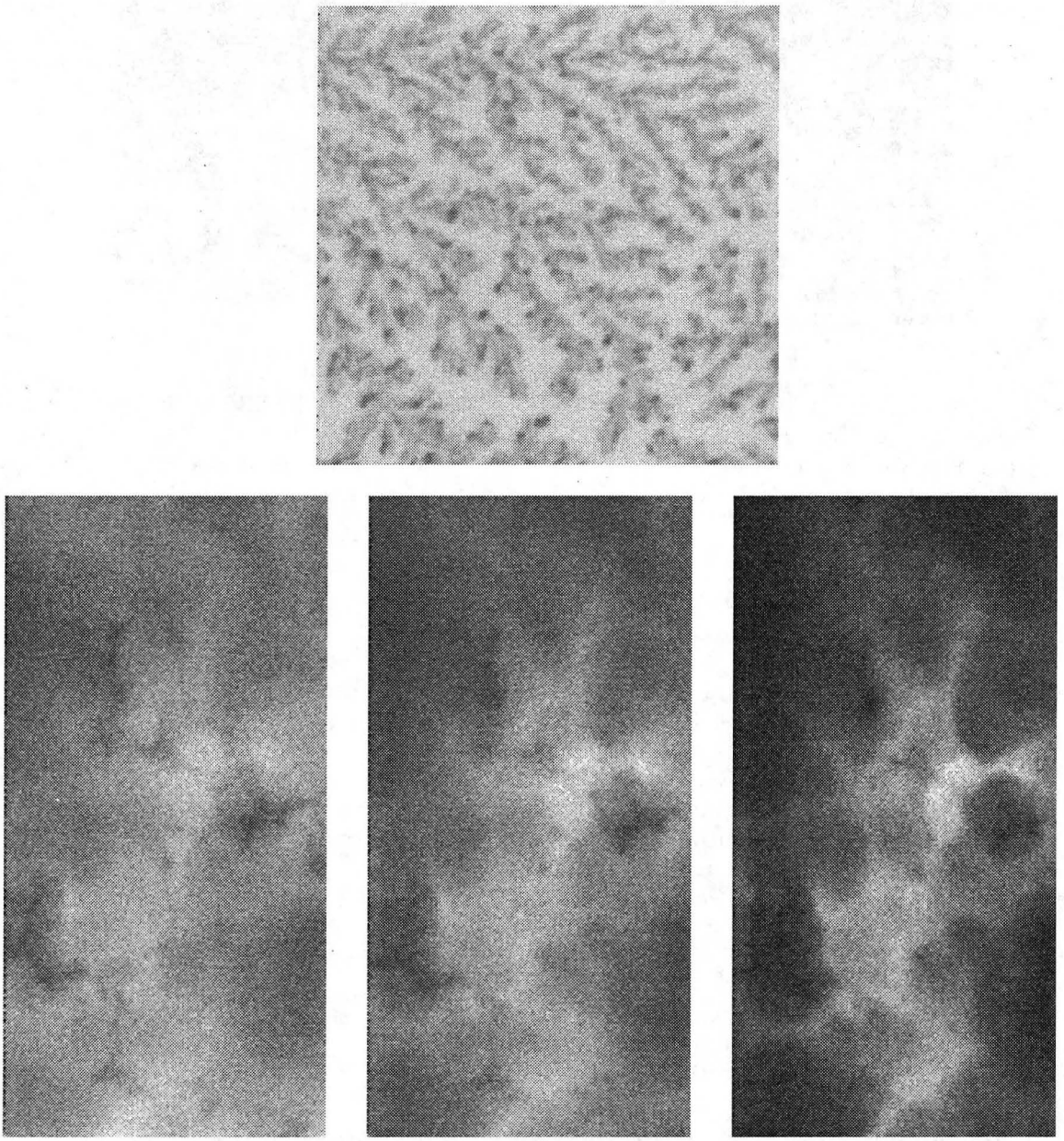

Figure 48: Silica gels imaged using the King's College STXM at Daresbury Laboratory. **Top:** silica gel aggregates from a sample prepared with 0.4% (by weight) silica concentration at pH=3 (18×18 μm image field). **Bottom:** time sequence of three images of the same area of a hydrated gel prepared with 0.4 weight % silica concentration at pH=7, with very obvious changes to the structure clearly visible. (Each image is of a 12.8×6.4 μm field). From Morrison *et al.* [Morrison 1992c, Morrison 1994b].

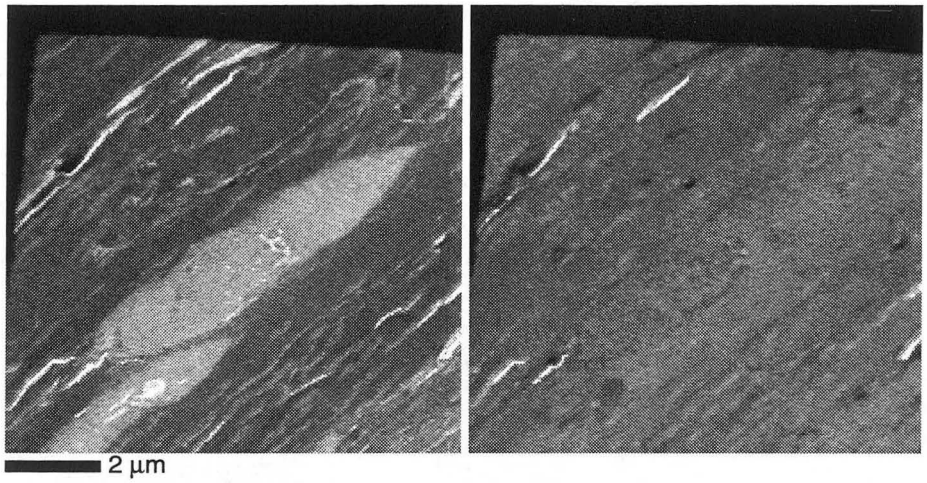

Figure 49: X-ray micrographs of Pittsburgh No. 8 high volatile A rank coal. **Left:** at an x-ray energy of 285.5 eV, aromatic carbons absorb strongly; the elliptical bodies are indentified as the maceral sporinite. **Right:** at an x-ray energy of 288.1 eV, contrast is based on the concentration of aliphatic carbon (see text). The contrast reversal between the two x-ray energies highlights intracellular material within the microspore at bottom. From Botto, Cody and collaborators [Botto 1994].

These sources are too large and expensive for the individual investigator. It is clearly desirable to develop smaller, cheaper alternatives that could form the basis of an x-ray microscope to be made commercially available. In fact a considerable amount of work has been done toward this goal, as were described in Secs. 3.2.2, 3.5.3, and 3.6.1. These developments are very encouraging because they promise a way to satisfy the demand for access to x-ray microscopes which is being generated by the results emerging from synchrotron radiation laboratories.

With the continuing development of microfabrication, one may expect continuing improvement in the performance of x-ray optical elements as well. Already zone plates with finest zone width in the 20–30 nm range have been fabricated [Attwood 1994, David 1994, Charalambous 1994]. With improvements in the technology one may look forward to not just finer linewidths, but also better control over thickness which affects efficiency and over zone profile, which affects both the efficiency and the point spread function.

There are continuing developments in normal incidence multilayer coated mirror technology as well. If the reflectivities reach levels above 10% (a level still well below ideal materials limits [Rosenbluth 1983]), one can begin to consider using these devices in water window microscopes, powered by the smaller laboratory sources mentioned above.

All in all, one may be looking forward to routine operation with small scale laboratory sources at selected wavelengths at around 50 nm resolution in the not too distant future. At the larger, state of the art facilities, the resolution should improve to 20 nm or better (at least in radiation resistant or cryo specimens).

5.2 Critical specimen handling ingredients: labels, environmental chambers, cryo, and tomography

It is the aim of microscopy to render visible the structures, sites, and interrelationships that are of interest to the microscopist. Beyond the basic requirements of resolution and illumination, specimen preparation, handling and image interpretation must support this goal for the microscope to be a useful instrument.

In the case of relatively thick biological specimens one must be concerned with complexity and overlap of features. One must also be concerned with motion and distortion due to radiation damage, and in the case of wet specimens due to diffusion and drift as well.

To deal with the complexity, the traditional way is to use labels or dyes to highlight structures of interest. We have seen (Sec. 3.4.5) that in scanning microscopy it is possible to use dyes in a way similar to that in UV fluorescence microscopy, but at considerably higher resolution. In addition, it should be possible to use the gold/silver microsphere

labeling methods used in electron microscopy.

Soft X-ray microscopy can also highlight specific elements or distinct molecular structures based on the spectroscopic signatures (absorption edges and XANES), as discussed earlier (Sec. 3.4.1). These techniques by themselves are useful for mapping components present with high local concentrations (1% or higher). For trace elements the techniques involving fluorescent x-ray detection tend to provide superior sensitivity.

To stabilize or immobilize the specimen, several techniques are available, depending on the specimen and the microscope. Many studies can employ dehydrated specimens (prepared by e.g., freeze drying and critical point drying) and exploit the unique spectral and thick sample capabilities of x-ray microscopes. Another approach is to use a single, sufficiently rapid flash exposure so that there is no need to take special precautions. For wet specimens imaged more slowly, rapid freezing appears to be the most suitable technique. There is considerable experience with samples in vitreous ice in the electron microscopy community [Dubochet 1988], where one can count on good structural preservation and immobilization up to a specimen exposure of 10^3–10^4 e^-/nm^2, or a dose of 10^7–10^8 Gray. The Göttingen group is the first to demonstrate cryo x-ray microscopy [Schneider 1994b], and their early experiments indicate a dose tolerance consistent with cryo electron microscopy data. A scanning cryomicroscope is also under construction at Stony Brook, and plans for cryomicroscopy are under development at Lawrence Berkeley Laboratory as well.

Given a well preserved specimen, it should be possible to collect a series of images using a tilt stage, and perform a tomographic reconstruction of the full three dimensional structure. First experiments using both microfabricated and biological specimens have already been performed (as described in Sec. 3.4.3), and the ALS microscopy facility is designed to accomodate such work on biological specimens [Meyer-Ilse 1994b]. It is important to note that, in principle, a full tomographic data set need not require more dose than a 2D image. A three dimensional reconstruction requires the same integral dose as a conventional two dimensional micrograph provided that the level of significance and the resolution are identical. The necessary dose D for one of the K projections in a reconstruction series is simply the integral dose divided by K [Hegerl 1976].

5.3 Extending the energy range covered: phase contrast and fluorescence

Much of the emphasis in the development of soft x-ray microscopy has been on the absorption contrast between relatively transparent water and absorbing organics afforded by the "water window". For problems involving thicker specimens (5–50 μm) or a desire to map trace elements, x rays of somewhat higher energy, 2–5 keV, offer significant advantages. In phase contrast, high resolution image formation appears possible at moderate dose levels [Rudolph 1990, Gölz 1992, Jacobsen 1992a], while if fluorescent x rays are detected, it should be possible to map trace concentrations of several important elements (including P, Cl, K, and Ca) [Howells 1985a, Buckley 1992c]. Both forms of microscopy will become possible at the facilities being constructed at the European Synchrotron Radiation Facility in Grenoble [Howells 1992] and at the Advanced Photon Source near Chicago. In both laboratories undulators will provide the x-ray beams, while zone plates will be used as focusing elements.

6 Conclusions

X-ray microscopy is emerging as a powerful form of biological investigation. It provides resolution intermediate between visible light microscopy on the one hand, and electron microscopy on the other. It is suitable for the study of wet or frozen hydrated specimens several micrometers thick, whereas scanned probe microscopes (such as scanning force or near field optical) are better suited to surfaces or very thin specimens. Typical specimens which have been studied by soft x-ray microscopy include chromosomes, sperm, malarial erythrocytes, myofibrils, fibroblasts, and tissue sections. Transmission microscopy routinely yields images which reveal 25–35 nm features with exposure times of a few seconds. In a variety of important cases, scanning microscopy can deliver maps of elemental composition and chemical states of major low-Z constituents of the specimen. Luminescent labels are being developed for use in scanning microscopy, while the recent introduction of phase contrast techniques in transmission microscopy has already yielded interesting results. The use of nanogold and similar labels is being developed for all forms of x-ray microscopy.

As with any microscope using ionizing radiation, radiation damage in x-ray microscopy is a serious concern. It precludes the possibility of following normal physiological events at high resolution within a single (live) specimen. In the case of dry exposures, radiation damage does not limit image fidelity even after multiple exposures, and it is expected that the same holds true for frozen hydrated specimens as well. Wet, fixed specimens are in the intermediate

situation, where it appears that only a single high resolution image can be obtained before damage leads to a change of morphology and mass in many cases.

The principal microscopes in operation today use synchrotron radiation as their source of x-rays. In addition to the established ones at BESSY (Berlin), Brookhaven (New York), and other places, several more are at various stages of construction or commissioning. There are important efforts toward the development of x-ray microscopes that do not require such large and expensive sources, and which may also be consistent with flash imaging.

X-ray microscopy has matured, yet we expect many new developments in the years to come.

7 Acknowledgements

We are grateful to our colleagues for sharing their results and for permission to publish their figures. In particular we wish to thank Günter Schmahl and his group for several figures and for numerous helpful comments. We are indebted to past and current members of the Stony Brook x-ray microscopy group for their contributions to the development of the facilities at the NSLS X-1A beamline at Brookhaven. Harald Ade (now at North Carolina State University), Chris Buckley (now at King's College, London), Henry Chapman, Steve Lindaas (now at Lawrence Berkeley Laboratory), Jörg Maser, Ian McNulty (now at Argonne National Laboratory), David Sayre, Shawn Williams (now at Yale University), and Xiaodong Zhang have provided material for and valuable comments on this review. Several collaborators and users from other institutions have also kindly provided material and comments for this review, including George Cody (Argonne National Laboratory), Walter Mangel, William McGrath, and Jack Van't Hof (Brookhaven National Laboratory), Jerry Pine (CalTech), Graeme Morrison (King's College, London), Mario Moronne (Lawrence Berkeley Laboratory), Rod Balhorn, Lee Haddad, and Jim Trebes (Lawrence Livermore National Laboratory), and Steven Rothman and Kaarin Goncz (UC San Francisco). We also thank Werner Meyer-Ilse (Lawrence Berkeley Laboratory), Tony Stead (Royal Holloway and Bedford New College), and Keiji Yada (Aomari Public College) for material from their work.

We thank Robert Glaeser and Richard Henderson for several instructive discussions regarding scattering theory and radiation damage.

This review was written in large part while one of the authors (JK) was a guest of the Experimental Systems Group, Advanced Light Source, Lawrence Berkeley Laboratory, and the group's hospitality is gratefully acknowledged. This work was supported by the Office of Health and Environmental Research, Department of Energy, under contract FG02-89ER60858, and by the National Science Foundation under grants BIR-9316594 and BIR-9112062, and Presidential Faculty Fellow award RCD-9253618 (CJ).

8 References

[Ade 1990] H. Ade, J. Kirz, S. L. Hulbert, E. Johnson, E. Anderson, and D. Kern. X-ray spectromicroscopy with a zone plate generated microprobe. *Applied Physics Letters*, **56**, pp. 1841–1843, (1990).

[Ade 1992] H. Ade, X. Zhang, S. Cameron, C. Costello, J. Kirz, and S. Williams. Chemical contrast in x-ray microscopy and spatially resolved XANES spectroscopy of organic specimens. *Science*, **258**, pp. 927–975, (1992).

[Ade 1993] H. Ade and B. Hsiao. X-ray linear dichroism microscopy. *Science*, **262**, pp. 1427–1429, (1993).

[Ade 1994a] H. Ade. NEXAFS microscopy of polymeric samples. *Synchrotron Radiation News*, **7**(2), pp. 11–15, (Mar. 1994).

[Ade 1994b] H. Ade, B. Hsiao, G. Mitchell, E. Rightor, A. P. Smith, and R. Cieslinski. Chemical contrast x-ray microscopy. In M. Sarikaya, M. Isaacson, and H. K. Wickramasinghe, editors, *Determining Nanoscale Physical Properties of Materials by Microscopy and Spectroscopy*, volume 332, Boston, (1994). Materials Research Society.

[Ade 1994c] H. Ade, A. P. Smith, S. Cameron, R. Cieslinski, C. Costello, B. Hsiao, G. Mitchell, and E. Rightor. X-ray microscopy in polymer science: prospects of a "new" imaging technique. *Polymer*, **accepted**, (1994).

[Anderson 1992] E. Anderson and D. Kern. Nanofabrication of zone plate lenses for high resolution x-ray microscopy. In Michette et al. [Michette 1992], pp. 75–78.

[Aoki 1972] S. Aoki, Y. Ichihara, and S. Kikuta. X-ray hologram obtained by using synchrotron radiation. *Japanese Journal of Applied Physics*, **11**, p. 1857, (1972).

[Aoki 1974] S. Aoki and S. Kikuta. X-ray holographic microscopy. *Japanese Journal of Applied Physics*, **13**, pp. 1385–1392, (1974).

[Aoki 1994] S. Aoki. Recent developments in x-ray microscopy at Photon Factory. In Erko and Aristov [Erko 1994].

[Artyukov 1993] I. A. Artyukov, A. I. Fedorenko, V. V. Kondtratenko, S. A. Yulin, and A. V. Vinogradov. Soft x-ray submicron imaging experiments with nanosecond exposure: *Optics Communications*, **102**, pp. 401–406, (1993).

[Aschoff 1994] H. Aschoff, (1994). Diplomarbeit, Universität Göttingen.

[Asunmaa 1963] S. K. Asunmaa. Electron microscopic enlargements of x-ray absorption micrographs. In Pattee et al. [Pattee 1963], pp. 33–51. Stanford, 1962.

[Attwood 1981] D. T. Attwood and B. L. Henke, editors. **Low Energy X-ray Diagnostics**, volume 75, New York, (1981). American Institute of Physics. Monterey, 1981.

[Attwood 1985] D. Attwood, K. Halbach, and K.-J. Kim. Tunable coherent x-rays. *Science*, **228**, pp. 1265–1272, (1985).

[Attwood 1994] D. Attwood. X-ray optics, microscopy and lithography in Berkeley. In Erko and Aristov [Erko 1994].

[Baez 1952] A. V. Baez. A study in diffraction microscopy with special reference to x-rays. *Journal of the Optical Society of America*, **42**, pp. 756–762, (1952).

[Baez 1961] A. V. Baez. Fresnel zone plate for optical image formation using extreme ultraviolet and soft X radiation. *Journal of the Optical Society of America*, **51**, pp. 405–412, (1961).

[Bailey 1994] G. W. Bailey and A. J. Garratt-Reed, editors. **Proceedings of the 52nd Annual Meeting of the Microscopy Society of America**, San Francisco, (1994). San Francisco Press.

[Balhorn 1992] R. Balhorn, M. Corzett, M. J. Allen, C. Lee, T. W. Barbee, Jr, J. A. Koch, B. J. MacGowan, D. L. Matthews, S. J. Mrowka, J. E. Trebes, I. McNulty, L. B. DaSilva, J. W. Gray, E. H. Anderson, D. Kern, and D. T. Attwood. Application of x-rays to the analysis of DNA packaging in mammalian sperm. In Jacobsen and Trebes [Jacobsen 1992d], pp. 374–385.

[Barbee 1978] T. W. Barbee and D. C. Keith. Synthetic structures layered on the atomic scale. In H. Winick and G. Brown, editors, *Workshop on Instrumentation for Synchrotron Radiation Research*, volume Report 78/04, pp. III–36–III–45. Stanford Synchrotron Radiation Laboratory, (1978).

[Barbee 1981] T. W. Barbee, Jr. Sputtered layered synthetic microstructure (LSM) dispersion elements. In Attwood and Henke [Attwood 1981], pp. 131–145. Monterey, 1981.

[Bates 1982] R. H. T. Bates. Fourier phase problems are uniquely solvable in more than one dimension. I. Underlying theory. *Optik*, **61**, pp. 247–262, (1982).

[Benattar 1989] R. Benattar, editor. **X-ray Instrumentation in Medicine and Biology, Plasma Physics, Astrophysics, and Synchrotron Radiation**, volume 1140, Bellingham, Washington, (1989). Society of Photo-Optical Instrumentation Engineers (SPIE).

[Bennett 1993] P. M. Bennett, G. F. Foster, C. J. Buckley, and R. E. Burge. The effect of soft X-radiation on myofibrils. *Journal of Microscopy*, **172**, pp. 109–119, (1993).

[Berger 1964] M. J. Berger and S. M. Seltzer. Tables of energy-losses and ranges of electrons and positrons. Technical Report Publication 1133, Committee on Nuclear Science, National Research Council, National Academy of Sciences, Washington, D.C., (1964). Chapter 10, pp. 205–268, Library of Congress catalogue number 64-60027.

[Bigler 1983] E. Bigler, F. Polack, and S. Lowenthal. Quantitative mapping of atomic species by x-ray absorption spectroscopy and contact microradiography. *Nuclear Instruments and Methods in Physics Research*, **208**, pp. 387–392, (1983).

[Bilderback 1994] D. H. Bilderback, S. A. Hoffman, and D. J. Thiel. Nanometer spatial resolution achieved in hard x-ray imaging and Laue diffraction experiments. *Science*, **263**, pp. 201–203, (1994).

[Bionta 1988] R. M. Bionta, A. F. Jankowski, and D. M. Makowiecki. Sputtered-sliced linear zone plates for 8 keV x-rays. In Sayre et al. [Sayre 1988a], pp. 142–145.

[Bjorkholm 1990] J. E. Bjorkholm, J. Bokor, L. Eichner, R. R. Freeman, J. Gregus, T. E. Jewell, W. M. Mansfield, A. A. MacDowell, E. L. Raab, W. T. Silfvast, L. H. Szeto, D. M. Tennant, W. K. Waskiewicz, D. L. White, D. L. Windt, O. R. Wood II, and J. H. Bruning. Reduction imaging at 14 nm using multilayer-coated optics: printing of features smaller than 0.1 μm. *Journal of Vacuum Science and Technology*, **B 8**, pp. 1509–1513, (1990).

[Born 1980] M. Born and E. Wolf. **Principles of Optics**. Pergamon Press, Oxford, sixth edition, (1980).

[Botto 1994] R. E. Botto, G. D. Cody, J. Kirz, H. Ade, S. Behal, and M. Disko. Selective chemical mapping of coal microheterogeneity by scanning transmission x-ray microscopy. *Energy and Fuels*, **8**, pp. 151–154, (1994).

[Brown 1983] G. Brown, K. Halbach, J. Harris, and H. Winick. Wiggler and undulator magnets—a review. *Nuclear Instruments and Methods*, **208**, pp. 65–77, (1983).

[Browne 1992] M. T. Browne. Aspects of nanopositioning in stage design for scanning x-ray microscopes. In Michette et al. [Michette 1992], pp. 355–358.

[Buckley 1987] C. J. Buckley. **The Fabrication of Gold Zone Plates and their use in Scanning X-ray Microscopy**. PhD thesis, Department of Physics, King's College, London, (1987).

[Buckley 1989] C. Buckley, H. Rarback, R. Alforque, D. Shu, H. Ade, S. Hellman, N. Iskander, J. Kirz, S. Lindaas, I. McNulty, M. Oversluizen, E. Tang, D. Attwood, R. DiGennaro, M. Howells, C. Jacobsen, Y. Vladimirsky, S. Rothman, D. Kern, and D. Sayre. Soft x-ray imaging with the 35 period undulator at the NSLS. *Reviews of Scientific Instruments*, **60**, pp. 2444–2447, (1989).

[Buckley 1992a] C. J. Buckley. Imaging of calcium deposits in cartilage by scanning x-ray microscopy. *Bone*, **13**, p. 100, (1992).

[Buckley 1992b] C. J. Buckley, R. E. Burge, G. F. Foster, S. Y. Ali, C. A. Scotchford, J. H. Dunsmuir, S. R. Ferguson, and M. L. Rivers. X-ray imaging of calcium deposits in human cartilage. In Jacobsen and Trebes [Jacobsen 1992d], pp. 363–373.

[Buckley 1992c] C. J. Buckley, R. E. Burge, G. F. Foster, M. R., S. Y. Ali, and C. A. Scotchford. X-ray probe mapping of calcium deposits in articular cartilage. In P. B. Kenway, P. J. Duke, G. W. Lorimer, T. Mulvey, I. W. Drummond, G. Love, A. G. Michette, and M. Stedman, editors, *X-Ray Optics and Microanalysis 1992*, pp. 621–626, Bristol, (1992). IOP Publishing.

[Buckley 1992d] C. J. Buckley, G. F. Foster, R. E. Burge, S. Y. Ali, C. A. Scotchford, J. Kirz, and M. L. Rivers. Elemental imaging of cartilage by scanning x-ray microscopy. *Review of Scientific Instruments*, **63**, pp. 588–590, (1992).

[Buckley 1994] C. J. Buckley, S. Downes, N. Khaleque, S. J. Bellamy, and X. Zhang. Mapping the density and mineral phase of calcium in bone at the interface with biomaterials using scanning x-ray microscopy. In Bailey and Garratt-Reed [Bailey 1994], pp. 44–45.

[Buckley 1995a] C. J. Buckley. The measuring and mapping of calcium in mineralised tissues by absorption difference imaging. *Reviews of Scientific Instruments*, **66**, p. to be published, (1995).

[Buckley 1995b] C. J. Buckley, S. J. Bellamy, X. Zhang, G. Dermody, and S. Hulbert. The NEXAFS of biological calcium phosphates. *Review of Scientific Instruments*, **(to be published)**, p. 0, (1995).

[Burge 1993] R. E. Burge. The interaction of x-rays. In A. G. Michette and C. J. Buckley, editors, *X-ray Science and Technology*, chapter 5, pp. 160–206. Institute of Physics, Bristol, (1993).

[Cabana 1988] C. Cabana, P. Magny, D. Nadeau, G. Grondin, and A. Beaudoin. Freeze-fracture study of the zymogen granule membrane of pancreas: two novel types of intramembrane particles. *European Journal of Cell Biology*, **42**, pp. 245–255, (1988).

[Capasso 1991] C. Capasso, A. K. Ray-Chaudhury, W. Ng, S. Liang, R. K. Cole, J. P. Wallace, F. Cerrina, G. Margaritondo, J. Underwood, J. B. Kortright, and R. C. C. Perera. High resolution x-ray microscopy using an undulator source: Photoelectron studies with MAXIMUM. *Journal of Vacuum Science and Technology*, **9 A**, pp. 1248–1253, (1991).

[Ceglio 1983] N. M. Ceglio, A. M. Hawryluk, and M. Schattenburg. X-ray phase lens design and fabrication. *Journal of Vacuum Science and Technology*, **B 1**, pp. 1285–1288, (1983).

[Chance 1994] B. Chance, D. Deisenhober, S. Ebashi, D. T. Goodhead, J. R. Helliwell, H. E. Huxley, T. Iizuka, J. Kirz, T. Mitsui, E. Rubenstein, N. Sakabe, T. Sasaki, G. Schmahl, H. Sturhmann, K. Wüthrich, and G. Zaccai, editors. **Synchrotron Radiation in the Biosciences**, Oxford, (1994). Clarendon Press.

[Chapman 1994] H. Chapman, S. Williams, and C. Jacobsen. Imaging of 30 nm gold spheres by dark-field scanning transmission x-ray microscopy. In Bailey and Garratt-Reed [Bailey 1994], pp. 52–53.

[Chapman ress] H. N. Chapman. Applications of a CCD detector in a scanning transmission x-ray microscope. *Review of Scientific Instruments*, **66**, (in press).

[Charalambous 1992] P. S. Charalambous and D. Morris. Status of zone plate fabrication at King's College, London. In Michette et al. [Michette 1992], pp. 79–82.

[Charalambous 1994] P. Charalambous. The fabrication of high resolution zone plates at King's College. In Erko and Aristov [Erko 1994].

[Cheng 1987a] P. C. Cheng. Recent advances in contact imaging of biological materials. In Cheng and Jan [Cheng 1987b], pp. 65–104.

[Cheng 1987b] P. C. Cheng and G. J. Jan, editors. **X-ray Microscopy: Instrumentation and Biological Applications**, Berlin, (1987). Springer-Verlag.

[Cheng 1992] P. C. Cheng, D. M. Shinozaki, T. H. Lin, S. P. Newberry, R. Sridhar, W. Tarng, M. T. Chen, and L. H. Chen. X-ray shadow projection microscopy and microtomography. In Michette et al. [Michette 1992], pp. 184–189.

[Cinotti 1987] F. Cinotti, M. C. Voisin, C. Jacobsen, J. M. Kenney, J. Kirz, I. McNulty, H. Rarback, R. Rosser, and D. Shu. Studies of calcium distribution in bone by scanning x-ray microscopy. In Cheng and Jan [Cheng 1987b], pp. 311–329.

[Cody 1994] G. D. Cody, R. E. Botto, H. Ade, S. Behal, M. Disko, and S. Wirick. C-NEXAFS microanalysis and scanning x-ray microscopy of microheterogeneities in a high volatile A bituminous coal. *Energy and Fuels*, **in press**, (1994).

[Collier 1971] R. J. Collier, C. B. Burckhardt, and L. H. Lin. **Optical Holography**. Academic Press, New York, (1971).

[Cosslett 1951] V. E. Cosslett and W. C. Nixon. X-ray shadow microscope. *Nature*, **168**, pp. 24–25, (1951).

[Cosslett 1957] V. E. Cosslett, A. Engström, and H. H. Pattee, Jr., editors. **International Symposium on X-ray Optics and X-ray Microanalysis**, New York, (1957). Academic Press. Cavendish Laboratory, Cambridge, 1956.

[Cosslett 1960] V. E. Cosslett and W. C. Nixon. **X-ray Microscopy**. Cambridge University Press, London, (1960).

[Cotton 1992] R. A. Cotton, M. D. Dooley, J. H. Fletcher, A. D. Stead, and T. W. Ford. Atomic force microscopy employed as the final imaging stage for soft x-ray contact microscopy. In Jacobsen and Trebes [Jacobsen 1992d], pp. 204–212.

[Cotton 1994] R. A. Cotton, J. H. Fletcher, A. D. Stead, T. W. Ford, and C. E. Webb. An investigation of the factors limiting the resolution in soft x-ray contact microscopy. In Erko and Aristov [Erko 1994].

[Cramer 1992] S. P. Cramer, J. Chen, S. J. George, J. v. Elp, J. Moore, O. Tensch, J. Colaresi, M. Yocum, O. C. Mullins, and C. T. Chen. Soft x-ray spectroscopy of metalloproteins using fluorescence detection. *Nuclear Instruments and Methods in Physics Research*, **A 319**, pp. 285–289, (1992).

[DaSilva 1992a] L. B. DaSilva, J. E. Trebes, R. Balhorn, S. Mrowka, E. Anderson, D. T. Attwood, T. W. Barbee, Jr, J. Brase, M. Corzett, J. Gray, J. A. Koch, C. Lee, D. Kern, R. A. London, B. J. MacGowan, D. L. Matthews, and G. Stone. X-ray laser microscopy of rat sperm nuclei. *Science*, **258**, pp. 269–271, (1992).

[DaSilva 1992b] L. B. DaSilva, J. E. Trebes, S. Mrowka, T. W. Barbee, Jr, J. Brase, J. A. Koch, R. A. London, B. J. McGowan, D. L. Matthews, D. Minyard, D. Stone, T. Yorkey, E. Anderson, D. T. Attwood, and D. Kern. Demonstration of x-ray microscopy with an x-ray laser operating near the carbon K edge. *Optics Letters*, **17**, pp. 754–756, (1992).

[David 1992] C. David, R. Medenwaldt, J. Thieme, P. Guttmann, D. Rudolph, and G. Schmahl. Electron beam generated phase zone plates with 30 nm zonewidth for high resolution x-ray microscopy. *Journal of Optics (Paris)*, **23**(6), pp. 255–258, (1992).

[David 1994] C. David, N. Fay, R. Medenwaldt, M. Diehl, and J. Thieme. Electron beam generated germanium zone plates with zone widths below 30 nm. In Erko and Aristov [Erko 1994].

[De Stasio 1993] G. De Stasio, S. Hardcastle, S. F. Koranda, B. P. Tonner, D. Mercanti, M. Teresa Ciotti, P. Perfetti, and G. Margaritondo. Photoemission spectromicroscopy of neurons. *Physical Review*, **E 47**, pp. 2117–2121, (1993).

[Devaney 1986] A. J. Devaney. Reconstructive tomography with diffracting wavefields. *Inverse Problems*, **2**, pp. 161–183, (1986).

[Di Fabrizio 1994] E. Di Fabrizio, M. Gentili, L. Grella, M. Baciocchi, A. Krasnoperova, and F. Cerrina. High-performance multilevel blazed x-ray microscopy Fresnel zone plates fabricated using x-ray lithography. *Journal of Vacuum Science and Technology*, **(in press)**, (1994).

[DiCicco 1992] D. S. DiCicco, D. Kim, R. Rosser, and S. Suckewer. First stage in the development of a soft-x-ray reflection imaging microscope in the Schwarzschild configuration using a soft-x-ray laser at 18.2 nm. *Optics Letters*, **17**, pp. 157–159, (1992).

[Diehl 1994] M. Diehl. Imaging properties of the x-ray microscope with a pulsed plasma source. In Erko and Aristov [Erko 1994].

[Dubochet 1988] J. Dubochet, M. Adrian, J. J. Chang, J.-C. Homo, J. Lepault, A. W. McDowell, and P. Schultz. Cryo-electron microscopy of vitrified specimens. *Quarterly Reviews of Biophysics*, **21**, pp. 129–228, (1988).

[Early 1990] K. Early, M. L. Shattenburg, and H. I. Smith. Absence of resolution degradation in x-ray lithography for λ from 4.5 nm to 0.83 nm. *Microelectronic Engineering*, **11**, pp. 317–321, (1990).

[Engström 1946] A. Engström. Quantitative micro- and histochemical elementary analysis by Roentgen absorption spectrography. *Acta Radiologica (Supplement)*, **63**, p. 1, (1946).

[Engström 1960] A. Engström, V. E. Cosslett, and H. H. Pattee, Jr., editors. **X-ray Microscopy and X-ray Microanalysis**, Amsterdam, (1960). Elsevier. Stockholm, 1959.

[Erko 1994] A. I. Erko and V. V. Aristov, editors. **X-ray Microscopy IV**, Chernogolovka, Moscow Region, (1994). Bogorodski Pechatnik.

[Feder 1970] R. Feder. X-ray projection printing of electrical circuit patterns. Technical Report IBM Technical Report TR 22.1065, IBM Components Division, East Fishkill facility, Hopewell Junction NY, (1970).

[Feder 1976] R. Feder, D. Sayre, E. Spiller, J. Topalian, and J. Kirz. Specimen replication for electron microscopy using x rays and x-ray resist. *Journal of Applied Physics*, **47**, pp. 1192–1193, (1976).

[Folkard 1992] M. Folkard. Radiation damage to cells by ultrasoft x-rays. In Michette et al. [Michette 1992], pp. 306–312.

[Ford 1992] T. W. Ford, A. M. Page, G. F. Foster, and A. D. Stead. Effects of soft x-ray irradiation on cell ultrastructure. In Jacobsen and Trebes [Jacobsen 1992d], pp. 325–332.

[Ford 1994] T. W. Ford, R. A. Cotton, A. M. Page, and A. D. Stead. The use of soft x-ray microscopy to study the internal ultrastructure of living cells and their cellular organelles. In Erko and Aristov [Erko 1994].

[Foster 1994] G. F. Foster, P. M. Bennett, C. J. Buckley, and R. E. Burge. Structural radiation damage to mammalian myofibrils. In Erko and Aristov [Erko 1994].

[Gilbert 1992a] J. R. Gilbert. **Soft x-ray microimaging of whole wet cells**. PhD thesis, California Institute of Technology, Pasadena, California, (1992).

[Gilbert 1992b] J. R. Gilbert and J. Pine. Imaging and etching: soft x-ray microscopy on whole wet cells. In Jacobsen and Trebes [Jacobsen 1992d], pp. 402–408.

[Gilbert 1992c] J. R. Gilbert, J. Pine, J. Kirz, C. Jacobsen, S. Williams, C. J. Buckley, and H. Rarback. Soft x-ray absorption imaging of whole wet tissue culture cells. In Michette et al. [Michette 1992], pp. 388–391.

[Giles 1969] J. W. Giles, Jr. Image reconstruction from a Fraunhofer x-ray hologram with visible light. *Journal of the Optical Society of America*, **59**, pp. 1179–1188, (1969).

[Glaeser 1971] R. M. Glaeser. Limitations to significant information in biological electron microscopy as a result of radiation damage. *Journal of Ultrastructure Research*, **36**, pp. 466–482, (1971).

[Glaeser 1975] R. M. Glaeser. Radiation damage and biological electron microscopy. In B. M. Siegel and D. R. Beaman, editors, *Physical aspects of electron microscopy and microbeam analysis*, pp. 205–227, New York, (1975). Wiley.

[Glaeser 1978] R. M. Glaeser and K. A. Taylor. Radiation damage relative to transmission electron microscopy of biological specimens at low temperature: a review. *Journal of Microscopy*, **112**, pp. 127–138, (1978).

[Goby 1913] P. Goby. Une application nouvelle des rayons x: la microradiographie. *Comptes Rendue de l'Academie des Sciences, Paris*, **156**, p. 686, (1913).

[Gölz 1992] P. Gölz. Calculations on radiation dosages of biological materials in phase contrast and amplitude contrast x-ray microscopy. In Michette et al. [Michette 1992], pp. 313–315.

[Goncz 1992a] K. K. Goncz, P. Batson, D. Ciarlo, B. W. Loo, Jr., and S. S. Rothman. An environmental sample chamber for x-ray microscopy. *Journal of Microscopy*, **168**, pp. 101–110, (1992).

[Goncz 1992b] K. K. Goncz and S. S. Rothman. Protein flux across the membrane of single secretion granules. *Biochimica et Biophysica Acta*, **1109**, pp. 7–16, (1992).

[Goncz 1994a] K. K. Goncz. **A comprehensive study of the physical properties of isolated zymogen granules using scanning transmission x-ray microscopy**. PhD thesis, Department of Biophysics, University of California, (1994). Lawrence Berkeley Laboratory report LBL-35088, UC-406/408.

[Goncz 1994b] K. K. Goncz, R. Bersing, and S. S. Rothman. The protein content and morphogenesis of zymogen granules. *Cell and Tissue Research*, **in press**, (1994).

[Goncz 1995] K. K. Goncz and S. S. Rothman. A trans-membrane pore can account for the movement of proteins across zymogen granule membranes. *Nature (submitted)*, (1995).

[Goodman 1968] J. W. Goodman. **An Introduction to Fourier Optics**. McGraw-Hill, San Francisco, (1968).

[Goodman 1985] J. W. Goodman. **Statistical Optics**. John Wiley & Sons, New York, (1985).

[Greinke 1992] B. Greinke and P. Gölz. Temperature rise of objects in x-ray microscopy—measurements and calculations. In Michette et al. [Michette 1992], pp. 316–318.

[Gutman 1994] G. Gutman. High-performance Mo/Si and W/B_4C multilayer mirrors for soft x-ray imaging optics. *Journal of X-ray Science and Technology*, **4**, pp. 142–150, (1994).

[Guttmann 1992a] P. Guttmann, G. Schneider, M. Robert-Nicoud, B. Niemann, D. Rudolph, J. Thieme, T. M. Jovin, and G. Schmahl. X-ray microscopic investigations on giant chromosomes isolated from salivary glands of *Chironomus Thummi* larvae. In Michette et al. [Michette 1992], pp. 404–407.

[Guttmann 1992b] P. Guttmann, G. Schneider, J. Thieme, C. David, M. Diehl, R. Medenwaldt, B. Niemann, D. H. Rudolph, and G. A. Schmahl. X-ray microscopy studies with the Göttingen x-ray microscopes. In Jacobsen and Trebes [Jacobsen 1992d], pp. 52–61.

[Guttmann 1994] P. Guttmann and B. Klösgen. X-ray microscopy studies of artificial lipid membranes. In Erko and Aristov [Erko 1994].

[Haddad 1994a] W. S. Haddad, I. McNulty, J. E. Trebes, E. H. Anderson, R. A. Levesque, and L. Yang. Ultra high resolution x-ray tomography. *Science*, **accepted**, (1994).

[Haddad 1994b] W. S. Haddad, I. McNulty, J. E. Trebes, E. H. Anderson, L. Yang, and J. M. Brase. Demonstration of ultra-high-resolution soft x-ray tomography using a scanning transmission x-ray microscope. In Bailey and Garratt-Reed [Bailey 1994], pp. 312–313.

[Haelbich 1980a] R.-P. Haelbich. A scanning ultrasoft x-ray microscope with multilayer coated reflection optics: first test with synchrotron radiation aaround 60 ev photon energy. In E. A. Ash, editor, *Scanned Image Microscopy*, pp. 413–433, London, (1980). Academic Press.

[Haelbich 1980b] R.-P. Haelbich, W. Staehr, and C. Kunz. A scanning ultrasoft x-ray microscope with large aperture reflection optics for use with synchrotron radiation. In Parsons [Parsons 1980], pp. 148–157.

[Hall 1972] T. A. Hall, H. O. E. Rockert, and R. L. deC. Saunders. **X-Ray Microscopy in Clinical and Experimental Medicine**. C. C. Thomas, Springfield, Illinois, (1972).

[Hare 1994] A. R. Hare and G. R. Morrison. Near-field soft X-ray diffraction modelled by the multislice method. *Journal of Modern Optics*, **41**(1), pp. 31–48, (1994).

[Hatzakis 1969] M. Hatzakis. Electron resists for microcircuit and mask production. *Journal of the Electrochemical Society*, **116**, pp. 1033–1037, (1969).

[Hayes 1982] M. H. Hayes. The reconstruction of a multidimensional sequence from the phase or magnitude of its fourier transform. *IEEE Transactions on Acoustics and Speech Signal Processing*, **ASSP-30**, pp. 140–154, (1982).

[Head 1957] A. K. Head. The two-mirror aplanat. *Proceedings of the Physical Society (London)*, **B 70**, pp. 945–949, (1957).

[Hegerl 1976] R. Hegerl and W. Hoppe. Influence of electron noise on three-dimensional image reconstruction. *Zeitschrift für Naturforschung*, **31 a**, pp. 1717–1721, (1976).

[Heitler 1954] W. Heitler. **The Quantum Theory of Radiation**. Dover, New York, (1954).

[Henderson 1992] R. Henderson. Image contrast in high-resolution electron microscopy of biological macromolecules: TMV in ice. *Ultramicroscopy*, **46**, pp. 1–18, (1992).

[Henke 1955] B. L. Henke and J. W. M. DuMond. Submicroscopic structure determination by long wavelength x-ray diffraction. *Journal of Applied Physics*, **26**, pp. 903–917, (1955).

[Henke 1981] B. L. Henke. Low energy x-ray interactions: photoionization, scattering, specular and Bragg reflection. In Attwood and Henke [Attwood 1981], pp. 146–155. Monterey, 1981.

[Henke 1993] B. L. Henke, E. M. Gullikson, and J. C. Davis. X-ray interactions: Photoabsorption, scattering, transmission, and reflection at E=50–30,000 eV, Z=1–92. *Atomic Data and Nuclear Data Tables*, **54**, pp. 181–342, (1993).

[Henke 1994] B. L. Henke, (1994). The data set of Henke *et al.* [Henke 1993] can be obtained on Internet using `anonymous ftp` to `xray1.physics.sunysb.edu` with `cd pub/henke`, or by `WWW` access to `http://xray1.physics.sunysb.edu/index.html`.

[Hilkenbach 1992] R. Hilkenbach. Experiments for the construction of sputtered sliced zone plates. In Michette et al. [Michette 1992], pp. 94–97.

[Hoover 1993] R. B. Hoover, P. C. Baker, D. L. Shealy, D. B. Gore, A. B. C. Walker, Jr., T. W. Barbee, Jr., and T. Kerstetter. Imaging Schwarzschild multilayer x-ray microscope. In R. B. Hoover and A. B. Walker, editors, *Multilayer and Grazing Incidence X-Ray/EUV Optics for Astronomy and Projection Lithography*, volume 1742, pp. 660–673. Society of Photo-Optical Instrumentation Engineers (SPIE), (1993).

[Horikawa 1993] Y. Horikawa, K. Nagai, S. Mochimaru, and Y. Iketaki. A compact Schwarzschild soft x-ray microscope with a laser-produced plasma source. *Journal of Microscopy*, **172**, pp. 189–194, (1993).

[Horowitz 1972] P. Horowitz and J. A. Howell. A scanning x-ray microscope using synchrotron radiation. *Science*, **178**, pp. 608–611, (1972).

[Horowitz 1978] P. Horowitz. Some experiences with x-ray and proton microscopes. In D. F. Parsons, editor, *Short Wavelength Microscopy (Annals of the New York Academy of Sciences)*, volume 306, pp. 203–222, New York, (1978).

[Howells 1983] M. R. Howells and J. Kirz. Coherent soft x-rays in high resolution imaging. In J. M. J. Madey and C. Pellegrini, editors, *Free Electron Generation of Extreme Ultraviolet Coherent Radiation*, volume 118, pp. 85–95, New York, (1983). American Institute of Physics.

[Howells 1985a] M. Howells, J. Kirz, and D. Sayre. Proposal for a 4.1 keV submicron microprobe at the 6 GeV ring. In *Report of the workshop on the scientific case for a 6 GeV synchrotron source*, pp. II–29–II–31, Argonne, Illinois, (1985). Argonne National Laboratory.

[Howells 1985b] M. Howells, J. Kirz, D. Sayre, and G. Schmahl. Soft-x-ray microscopes. *Physics Today*, **38**, pp. 22–32, (Aug. 1985).

[Howells 1987] M. Howells, C. Jacobsen, J. Kirz, R. Feder, K. McQuaid, and S. Rothman. X-ray holograms at improved resolution: a study of zymogen granules. *Science*, **238**, pp. 514–517, (1987).

[Howells 1990a] M. R. Howells. Soft x-ray imaging for the life sciences. In S. S. Hasnain, editor, *Biophysics and Synchrotron Radiation*, pp. 295–329. Ellis Horwood, Ltd., Chichester, UK, (1990). Also available as Lawrence Berkeley Laboratory report LBL-27420.

[Howells 1990b] M. R. Howells, C. Jacobsen, J. Kirz, K. McQuaid, and S. S. Rothman. Progress and prospects in soft x-ray holographic microscopy. In P. J. Duke and A. G. Michette, editors, *Modern Microscopies*, pp. 119–132. Plenum, New York, (1990).

[Howells 1991] M. R. Howells, J. Kirz, and D. Sayre. X-ray microscopes. *Scientific American*, **264**(2), pp. 88–94, (Feb. 1991).

[Howells 1992] M. R. Howells, R. Burge, C. J. Buckley, A. Miller, G. Morrison, D. Rudolph, G. Schmahl, J. Thieme, and M. Vollbrecht. Conceptional design for an x-ray microscopy facility at the ESRF. Technical report, European Synchrotron Radiation Facility, Grenoble, France, (1992).

[Howells 1994] M. R. Howells, C. J. Jacobsen, and S. Lindaas. X-ray holographic microscopy using the atomic-force microscope. In Erko and Aristov [Erko 1994].

[Hubbell 1980] J. H. Hubbell, H. A. Gimm, and I. Øverbø. Pair, triplet, and total atomic cross sections (and mass attenuation coefficients) for 1 MeV–100 GeV photons in elements Z=1–100. *Journal of Physical and Chemical Reference Data*, **9**, pp. 1023–1147, (1980).

[Isaacson 1976] M. S. Isaacson. Specimen damage in the electron microscope. In M. A. Hayat, editor, *Principles and Techniques of Electron Microscopy*, volume 7, pp. 1–78. Van-Nostrand Publishing, New York, (1976).

[Jackson 1962] J. D. Jackson. **Classical Electrodynamics**. John Wiley & Sons, New York, (1962).

[Jackson 1975] J. D. Jackson. **Classical Electrodynamics**. John Wiley & Sons, New York, second edition, (1975).

[Jacobsen 1987] C. Jacobsen, J. Kenney, J. Kirz, R. Rosser, F. Cinotti, H. Rarback, and J. Pine. Quantitative imaging and microanalysis with a scanning soft x-ray microscope. *Physics in Medicine and Biology*, **32**, pp. 431–437, (1987).

[Jacobsen 1990a] C. Jacobsen. X-ray holography: a history. In Shinohara et al. [Shinohara 1990b], pp. 167–177. Also Japan Scientific Societies Press, Tokyo.

[Jacobsen 1990b] C. Jacobsen, M. Howells, J. Kirz, and S. Rothman. X-ray holographic microscopy using photoresists. *Journal of the Optical Society of America*, **A 7**, pp. 1847–1861, (1990).

[Jacobsen 1991] C. Jacobsen, S. Williams, E. Anderson, M. T. Browne, C. J. Buckley, D. Kern, J. Kirz, M. Rivers, and X. Zhang. Diffraction-limited imaging in a scanning transmission x-ray microscope. *Optics Communications*, **86**, pp. 351–364, (1991).

[Jacobsen 1992a] C. Jacobsen. Making soft x-ray microscopy harder: considerations for sub-0.1 μm resolution imaging at $\sim$ 4 Å wavelengths. In Michette et al. [Michette 1992], pp. 274–277.

[Jacobsen 1992b] C. Jacobsen, J. Kirz, and S. Williams. Resolution in soft x-ray microscopes. *Ultramicroscopy*, **47**, pp. 55–79, (1992).

[Jacobsen 1992c] C. Jacobsen, S. Lindaas, V. Oehler, S. P. Williams, S. Wirick, X. Zhang, S. Guo, and I. Spector. Experiments in scanning luminescence x-ray microscopy. In Jacobsen and Trebes [Jacobsen 1992d], pp. 223–231.

[Jacobsen 1992d] C. Jacobsen and J. Trebes, editors. **Soft X-ray Microscopy**, volume 1741, Bellingham, Washington, (1992). Society of Photo-Optical Instrumentation Engineers (SPIE).

[Jacobsen 1992e] C. Jacobsen and S. Williams. X-ray microscopy and holography with third generation sources. In J. Arthur, editor, *Optics for High-Brightness Synchrotron Radiation Beamlines*, volume 1740, pp. 108–116. Society of Photo-Optical Instrumentation Engineers (SPIE), (1992).

[Jacobsen 1993] C. Jacobsen, S. Lindaas, S. Williams, and X. Zhang. Scanning luminescence x-ray microscopy: imaging fluorescence dyes at suboptical resolution. *J. Microscopy*, **172**, pp. 121–129, (1993).

[Jacobsen 1994a] C. Jacobsen, E. Anderson, H. Chapman, J. Kirz, S. Lindaas, M. Rivers, S. Wang, S. Williams, S. Wirick, and X. Zhang. The X-1A scanning transmission x-ray microscope: Optics and instrumentation. In Erko and Aristov [Erko 1994].

[Jacobsen 1994b] C. Jacobsen and S. Williams. Contrast and dose for ice-embedded biological specimens in electron and x-ray microscopy. *(to be submitted to Ultramicroscopy)*, (1994).

[James 1982] R. W. James. **The Optical Principles of the Diffraction of X-rays**. Ox Bow Press, Woodbridge, Connecticut, (1982). Originally published as **The Crystalline State**, Vol. **II**, ed. L. Bragg (1948).

[Jochum 1992] L. Jochum. The validity of the Born approximation for the imaging of 3-D objects in x-ray microscopy. In Michette et al. [Michette 1992], pp. 281–283.

[Jochum 1994] L. Jochum and W. Meyer-Ilse. Partially coherent image formation with x-ray microscopes. *Applied Optics*, **submitted**, (1994).

[Johansson 1994] U. Johansson, R. Nyholm, C. Tornevik, and A. Flodström. The VUV scanning spectromicroscope at MAX-LAB. In Erko and Aristov [Erko 1994].

[Joy 1973] R. T. Joy. The electron microscopical observation of aqueous biological specimens. In R. Barer and V. E. Cosslett, editors, *Advances in Electron and Optical Microscopy*, volume 5, pp. 297–352, London, (1973). Academic Press.

[Joyeux 1988a] D. Joyeux, S. Lowenthal, F. Polack, and A. Bernstein. X-ray microscopy by holography at LURE. In Sayre et al. [Sayre 1988a], pp. 246–252.

[Joyeux 1988b] D. Joyeux and F. Polack. Progress in optical reconstruction of submicron x-ray holograms. In R. W. Falcone and J. Kirz, editors, *OSA Proceedings on Short Wavelength Coherent Radiation: Generation and Applications*, volume 2, pp. 295–302, Washington, D. C., (1988). Optical Society of America.

[Joyeux 1989] D. Joyeux, F. Polack, and R. Mercier. Principle of a 'reconstruction microscope' for high resolution x-ray holography. In Benattar [Benattar 1989], pp. 399–405.

[Joyeux 1994] D. Joyeux, F. Polack, D. Phalippou, and R. Mercier. Status of the optical reconstruction microscope for x-ray holographic microscopy. In Erko and Aristov [Erko 1994].

[Kagoshima 1989] Y. Kagoshima, S. Aoki, M. Kakuchi, M. Sekimoto, H. Maezawa, K. Hyodo, and M. Ando. Soft x-ray microscope at the undulator beamline of the Photon Factory. *Reviews of Scientific Instruments*, **60**, pp. 2448–2451, (1989).

[Kagoshima 1992] Y. Kagoshima, T. Miyahara, M. Ando, and S. Aoki. Present status and future plan for x-ray microscopy at the Photon Factory. *Reviews of Scientific Instruments*, **63**, pp. 605–608, (1992).

[Kenney 1985] J. M. Kenney, C. Jacobsen, J. Kirz, H. Rarback, F. Cinotti, W. Thomlinson, R. Rosser, and G. Schidlovsky. Absorption microanalysis with a scanning soft x-ray microscope: mapping the distribution of calcium in bone. *Journal of Microscopy*, **138**, pp. 321–328, (1985).

[Kenney 1989] J. M. Kenney, G. R. Morrison, M. T. Browne, C. J. Buckley, R. E. Burge, R. C. Cave, P. S. Charalambous, P. D. Duke, A. R. Hare, C. P. B. Hills, A. G. Michette, K. Ogawa, and A. M. Rogoyski. Evaluation of a scanning transmission x-ray microscope using undulator radiation at the SERC Daresbury Laboratory. *Journal of Physics*, **E 22**, pp. 234–238, (1989).

[Kern 1984] D. Kern, P. Coane, R. Acosta, T. H. P. Chang, R. Feder, P. Houzego, W. Molzen, J. Powers, A. Speth, R. Viswanathan, J. Kirz, H. Rarback, and J. Kenney. Electron beam fabrication and characterization of Fresnel zone plates for soft x-ray microscopy. In F. J. Himpsel and R. W. Klaffky, editors, *Science with Soft X-Rays*, volume 447, pp. 204–213, Bellingham, Washington, (1984). Society of Photo-Optical Instrumentation Engineers (SPIE).

[Kinjo 1994] Y. Kinjo, K. Shinohara, A. Ito, H. Nakano, M. Watanabe, Y. Horiike, Y. Kikuchi, M. C. Richardson, and K. A. Tanaka. Direct imaging in a water layer of human chromosome fibres composed of nucleosomes and their higher order structures by laser plasma x-ray contact microscopy. *Journal of Microscopy*, **176**, pp. 63–74, (1994).

[Kinoshita 1992] K. Kinoshita, T. Matsumura, Y. Inagaki, N. Hirai, M. Sugiyama, H. Kihara, N. Watanabe, Y. Shimanuki, and A. Yagashita. The electronic zooming TV readout system for an x-ray microscope. In Michette et al. [Michette 1992], pp. 335–337.

[Kirkpatrick 1948] P. Kirkpatrick and A. V. Baez. Formation of optical images by x-rays. *Journal of the Optical Society of America*, **38**, pp. 766–774, (1948).

[Kirkpatrick 1949] P. Kirkpatrick. The x-ray microscope. *Scientific American*, **180**, pp. 44–47, (Mar. 1949).

[Kirtley 1992] S. M. Kirtley, O. C. Mullins, J. Chen, J. van Elp, S. J. George, C. T. Chen, T. O'Halloran, and S. P. Cramer. Nitrogen chemical structure in DNA and related molecules by x-ray absorption spectroscopy. *Biochimica et Biophysica Acta*, **1132**, pp. 249–254, (1992).

[Kirz 1974] J. Kirz. Phase zone plates for X rays and the extreme UV. *Journal of the Optical Society of America*, **64**, pp. 301–309, (1974).

[Kirz 1980] J. Kirz and D. Sayre. Soft x-ray microscopy of biological specimens. In H. Winick and S. Doniach, editors, *Synchrotron Radiation Research*, pp. 277–322, New York, (1980). Plenum Press.

[Kirz 1985] J. Kirz and H. Rarback. Soft x-ray microscopes. *Review of Scientific Instruments*, **56**, pp. 1–13, (1985).

[Kondratenko 1977] A. M. Kondratenko and A. N. Skrinsky. Use of radiation of electron storage rings in x-ray holography of objects. *Optics and Spectroscopy*, **42**, pp. 189–192, (1977).

[Koster 1993] A. J. Koster, M. B. Braunfeld, J. C. Fung, C. K. Abbey, K. F. Han, W. Liu, H. Chen, J. W. Sedat, and D. A. Agard. Towards automatic three dimensional imaging of large biological structures using intermediate voltage electron microscopy. *Microscopy Society of America Bulletin*, **23**(2), pp. 176–188, (1993).

[Kozhevnikov 1994] I. V. Kozhevnikov, A. I. Fedorenko, V. V. Kondratenko, Y. Pershin, S. A. Yulin, E. N. Zubarev, H. A. Padmore, K. C. Cheung, G. E. van Dorssen, M. Roper, L. L. Balakireva, R. V. Serov, and A. V. Vinogradov. Synthesis and measurement of normal incidence x-ray multilayer mirrors optimized for a photon energy of 390 eV. *Nuclear Instruments and Methods in Physics Research*, **A 345**, pp. 594–603, (1994).

[Krasnoperova 1993] A. A. Krasnoperova, J. Xiao, F. Cerrina, E. Di Fabrizio, L. Luciani, M. Figliomeni, M. Gentili, W. Yun, B. Lai, and E. Gluskin. Fabrication of hard x-ray phase zone plate by x-ray lithography. *Journal of Vacuum Science and Technology*, **B 11**, pp. 2588–2591, (1993).

[Krause 1979] M. O. Krause. Atomic radiative and radiationless yields for K and L shells. *Journal of Physical and Chemical Reference Data*, **8**, pp. 307–327, (1979).

[Krinsky 1983] S. Krinsky. Undulators as sources of synchrotron radiation. *IEEE Transactions: Nuclear Science*, **NS-30**, pp. 3078–3082, (1983).

[Ladd 1956] W. A. Ladd, W. M. Hess, and M. W. Ladd. High-resolution microradiography. *Science*, **123**, pp. 370–371, (1956).

[Lai 1992] B. Lai, W. B. Yun, D. Legnini, Y. Xiao, J. Chrzas, P. J. Viccaro, V. White, S. Bajikar, D. Denton, F. Cerrina, E. DiFabrizio, M. Gentili, L. Grella, and M. Baciocchi. Hard x-ray phase zone plate fabricated by lithigraphic techniques. *Applied Physics Letters*, **61**, pp. 1877–1879, (1992).

[Lamvik 1991] M. K. Lamvik. Radiation damage in dry and frozen hydrated organic material. *Journal of Microscopy*, **161**, pp. 171–181, (1991).

[Langmore 1992] J. P. Langmore and M. F. Smith. Quantitatitve energy-filtered electron microscopy of biological molecules in ice. *Ultramicroscopy*, **46**, pp. 349–373, (1992).

[Lei 1992] X. Lei, Y. Zhao, M. Wang, and X. Xie. Scanning x-ray microscope project at Hefei. In Jacobsen and Trebes [Jacobsen 1992d], pp. 104–111.

[Lin 1992] T. H. Lin, G. Wang, and P. C. Cheng. A multiple cone-beam projection algorithm for x-ray microtomography. In Michette et al. [Michette 1992], pp. 296–300.

[Lindaas 1992] S. Lindaas, C. J. Jacobsen, M. R. Howells, and K. Frank. Development of a linear scanning-force microscope for x-ray Gabor hologram readout. In Jacobsen and Trebes [Jacobsen 1992d], pp. 213–222.

[Lindaas 1994] S. A. Lindaas. **X-ray Gabor holography using a scanning force microscope**. PhD thesis, Department of Physics, State University of New York at Stony Brook, (1994).

[Lipson 1958] H. Lipson and C. A. Taylor. **Fourier Transforms and X-Ray Diffraction**. G. Bell and Sons, London, (1958).

[London 1989] R. A. London, M. D. Rosen, and J. E. Trebes. Wavelength choice for soft x-ray laser holography of biological samples. *Applied Optics*, **28**, pp. 3397–3404, (1989).

[London 1992a] R. London, D. Matthews, and S. Suckewer, editors. **Applications of X-ray Lasers**, number NTIS CONF-9206170, Washington, D.C., (1992). National Technical Information Service.

[London 1992b] R. A. London, J. E. Trebes, and C. Jacobsen. Role of x-ray induced damage in biological microimaging. In Jacobsen and Trebes [Jacobsen 1992d], pp. 333–340.

[Lonsdale 1962] K. Lonsdale, editor. **International Tables for X-ray Crystallography**, Birmingham, (1962). International Union of Crystallography.

[Loo 1992a] B. W. Loo, Jr., S. Williams, W. T. Lin, W. H. Love, S. Meizel, and S. S. Rothman. High resolution x-ray stereomicroscopy: true three-dimensional imaging of biological samples. In Jacobsen and Trebes [Jacobsen 1992d], pp. 392–396.

[Loo 1992b] B. W. Loo, Jr., S. Williams, S. Meizel, and S. S. Rothman. X-ray stereomicroscopy: high resolution 3-d imaging of human spermatozoa in aqueous suspension with natural contrast. *Journal of Microscopy*, **166**, pp. RP5–RP6, (1992).

[Maser 1992] J. Maser and G. Schmahl. Coupled wave description of the diffraction by zone plates with high aspect ratios. *Optics Communications*, **89**, pp. 355–362, (1992).

[Maser 1994] J. Maser. Theoretical description of the diffraction properties of zone plates with small outermost zone width. In Erko and Aristov [Erko 1994].

[Matsumura 1994] T. Matsumura, K. Kinoshita, Y. Shimanuki, and H. Kihara. Experimental evaluation of the semitransparent soft x-ray photocathodes and observation of various samples with the x-ray zooming tube using the photocathodes. In Erko and Aristov [Erko 1994].

[Matthews 1985] D. L. Matthews, P. L. Hagelstein, M. D. Rosen, M. J. Eckart, N. M. Ceglio, A. U. Hazi, H. Medecki, B. J. MacGowan, J. E. Trebes, B. L. Whitten, E. M. Campbell, C. W. Hatcher, A. M. Hawryluck, R. L. Kauffman, L. D. Pleasance, G. Rambach, J. H. Scofield, G. Stone, and T. A. Weaver. Demonstration of a soft x-ray amplifier. *Physical Review Letters*, **54**, pp. 110–113, (1985).

[McNulty 1992a] I. McNulty, J. Kirz, C. Jacobsen, E. Anderson, D. Kern, and M. Howells. High-resolution imaging by Fourier transform x-ray holography. *Science*, **256**, pp. 1009–1012, (1992).

[McNulty 1992b] I. McNulty, J. E. Trebes, J. M. Brase, T. J. Yorkey, R. Levesque, H. Szoke, E. H. Anderson, C. Jacobsen, and D. Kern. Experimental demonstration of high resolution three-dimensional x-ray holography. In Jacobsen and Trebes [Jacobsen 1992d], pp. 78–84.

[McNulty 1994] I. McNulty, J. E. Trebes, E. H. Anderson, J. M. Brase, W. S. Haddad, D. P. Kern, R. Levesque, and H. Szoke. Three-dimensional soft x-ray Fourier transform holography: experimental results. In Erko and Aristov [Erko 1994].

[Medenwaldt 1994a] R. Medenwaldt. **Development of x-ray microscopy in Aarhus and ultra thin foil production to speed up high resolution x-ray optics**. PhD thesis, Aarhus University, (1994).

[Medenwaldt 1994b] R. Medenwaldt, C. David, N. Hertel, and E. Uggerhøj. The Aarhus x-ray microscope. In Erko and Aristov [Erko 1994].

[Meyer-Ilse 1992] W. Meyer-Ilse, M. Koike, H. R. Beguiristain, J. Maser, and D. T. Attwood. X-ray microscopy resource center at the Advanced Light Source. In Jacobsen and Trebes [Jacobsen 1992d], pp. 112–115.

[Meyer-Ilse 1993] W. Meyer-Ilse, T. Wilhein, and P. Guttmann. Thinned back-illuminated CCD for x-ray microscopy. In M. M. Blouke, editor, *Charge-Coupled Devices and Solid State Optical Sensors III*, volume 1900. Society of Photo-Optical Instrumentation Engineers (SPIE), (1993).

[Meyer-Ilse 1994a] W. Meyer-Ilse, D. Attwood, and M. Koike. The x-ray microscopy resource center at the Advanced Light Source. In Chance et al. [Chance 1994], pp. 624–636.

[Meyer-Ilse 1994b] W. Meyer-Ilse, M. Moronne, C. Magowan, H. Medecki, J. Hearst, and D. Attwood. Techniques and applications of x-ray microscopy. In Erko and Aristov [Erko 1994].

[Michette 1986] A. G. Michette. **Optical Systems for Soft X Rays**. Plenum, New York, (1986).

[Michette 1988a] A. G. Michette. X-ray microscopy. *Reports on Progress in Physics*, **51**, pp. 1525–1606, (1988).

[Michette 1988b] A. G. Michette, R. E. Burge, P. Charalambous, C. P. B. Hills, and A. M. Rogoyski. The potential of laser-plasma sources in scanning x-ray microscopy. In Sayre et al. [Sayre 1988a].

[Michette 1992] A. G. Michette, G. R. Morrison, and C. J. Buckley, editors. **X-ray Microscopy III (Springer Series in Optical Sciences, Vol. 67)**, Berlin, (1992). Springer-Verlag.

[Michette 1993] A. G. Michette, I. C. E. Turcu, M. S. Schulz, M. T. Browne, G. R. Morrison, P. Fluck, C. J. Buckley, and G. F. Foster. Scanning x-ray microscopy using a laser-plasma source. *Reviews of Scientific Instruments*, **64**, pp. 1478–1482, (1993).

[Michette 1994] A. Michette. Laser plasma microscope. In Erko and Aristov [Erko 1994].

[Mochimaru 1994] S. Mochimaru, Y. Horikawa, S. Masui, H. Yamada, and H. Kihara. The Schwarzschild soft x-ray microscope using the compact SR-ring 'Aurora'. In Erko and Aristov [Erko 1994].

[Moewes 1994] A. Moewes, H. Zhang, C. Kunz, M. Pretorius, H. Sievers, I. Storjohann, and J. Voss. Scanning luminescence microscopy at HASYLAB/DESY. In Erko and Aristov [Erko 1994].

[Moronne 1994] M. Moronne, C. Larabell, P. Selvin, and A. I. von Brenndorff. Development of fluroescent probes for x-ray microscopy. In Bailey and Garratt-Reed [Bailey 1994], pp. 48–49.

[Morrison 1989] G. R. Morrison. Some aspects of quantitative x-ray microscopy. In Benattar [Benattar 1989], pp. 41–49.

[Morrison 1992a] G. R. Morrison. Phase contrast and darkfield imaging in x-ray microscopy. In Jacobsen and Trebes [Jacobsen 1992d], pp. 186–193.

[Morrison 1992b] G. R. Morrison and M. T. Browne. Darkfield imaging with the scanning transmission x-ray microscope. *Reviews of Scientific Instruments*, **63**, pp. 611–614, (1992).

[Morrison 1992c] G. R. Morrison, M. T. Browne, T. P. M. Beelen, and H. F. van Garderen. X-ray imaging of aggregation in silica and zeolitic precursors. In Jacobsen and Trebes [Jacobsen 1992d], pp. 312–315.

[Morrison 1992d] G. R. Morrison, M. T. Browne, C. J. Buckley, R. E. Burge, P. S. Charalambous, G. F. Foster, A. G. Michette, D. Morris, J. R. Palmer, , and G. E. Slark. Recent progress with the King's College scanning transmission x-ray microscope. In Michette et al. [Michette 1992], pp. 139–142.

[Morrison 1994a] G. R. Morrison. X-ray imaging with a configured detector. In Erko and Aristov [Erko 1994].

[Morrison 1994b] G. R. Morrison, M. T. Browne, T. P. M. Beelen, H. F. van Garderen, and P. A. F. Anastasi. Transmission x-ray imaging of hydrated silica gels. In Erko and Aristov [Erko 1994].

[Mott 1949] N. F. Mott and H. S. W. Massey. **The Theory of Atomic Collisions**. Oxford University Press, Oxford, second edition, (1949).

[Murakami 1992] K. Murakami, T. Oshino, H. Nakamura, M. Ohtani, and H. Nagata. Normal-incidence x-ray microscope with Carbon Kα radiation with 0.5 μm resolution. *Japanese Journal of Applied Physics*, **31**, pp. L1500–L1502, (1992).

[Myers 1951] O. E. Myers, Jr. Studies of transmission zone plates. *American Journal of Physics*, **19**, pp. 359–365, (1951).

[NASA 1993] NASA. NASA inventor of the year: Richard B. Hoover. *NASA Tech Briefs*, **17**(3), pp. 14–15, (Mar. 1993).

[Neff 1988] W. J. Neff, R. Lebert, and F. Richter. Plasmafocus as radiation source for soft x-rays. In Sayre et al. [Sayre 1988a], pp. 22–29.

[Newberry 1956] S. P. Newberry and S. E. Summers. The General Electric shadow x-ray microscope. In *Proceedings of the International Conference on Electron Microscopy (1954)*, pp. 305–307, London, (1956). Royal Microscopical Society.

[Newberry 1987a] S. P. Newberry. History of x-ray microscopy. In Cheng and Jan [Cheng 1987b], pp. 346–360.

[Newberry 1987b] S. P. Newberry. The shadow projection type of x-ray microscope. In Cheng and Jan [Cheng 1987b], pp. 126–141.

[Newberry 1992] S. P. Newberry. Time lapse x-ray microscopy by shadow projection microscopy. In Michette et al. [Michette 1992], pp. 367–369.

[Ng 1992] W. Ng, A. K. Ray-Choudhury, S. H. Liang, J. Welnak, J. P. Wallace, S. Singh, C. Capasso, F. Cerrina, G. Margaritondo, J. H. Underwood, J. B. Kortright, and R. C. C. Perera. New results from MAXIMUM: an x-ray scanning photoemission microscope. In Jacobsen and Trebes [Jacobsen 1992d], pp. 296–305.

[Niemann 1974] B. Niemann, D. Rudolph, and G. Schmahl. Soft x-ray imaging zone plates with large zone numbers for microscopic and spectroscopic applications. *Optics Communications*, **12**, pp. 160–163, (1974).

[Niemann 1976] B. Niemann, D. Rudolph, and G. Schmahl. X-ray microscopy with synchrotron radiation. *Applied Optics*, **15**, pp. 1883–1884, (1976).

[Niemann 1983] B. Niemann, D. Rudolph, and G. Schmahl. The Göttingen x-ray microscopes. *Nuclear Instruments and Methods in Physics Research*, **208**, pp. 367–372, (1983).

[Niemann 1987] B. Niemann. The Göttingen scanning x-ray microscope. In E.-E. Koch and G. Schmahl, editors, *Soft x-ray optics and technology*, volume 733, pp. 422–427, Bellingham, Washington, (1987). Society of Photo-Optical Instrumentation Engineers (SPIE).

[Niemann 1988] B. Niemann, P. Guttmann, R. Hilkenbach, J. Thieme, and W. Meyer-Ilse. The Göttingen scanning x-ray microscope. In Sayre et al. [Sayre 1988a], pp. 209–215.

[Niemann 1990] B. Niemann, D. Rudolph, G. Schmahl, M. Diehl, J. Thieme, W. Meyer-Ilse, W. Neff, R. Holz, R. Lebert, F. Richter, and G. Herziger. An x-ray microscope with a plasma x-ray source. *Optik*, **84**, pp. 35–36, (1990).

[Niemann 1992] B. Niemann. X-ray microscopy with the Göttingen scanning x-ray microscope at 2.4 nm. In Michette et al. [Michette 1992], pp. 143–146.

[Niemann 1994] B. Niemann, G. Schneider, P. Guttmann, D. Rudolph, and G. Schmahl. The new Göttingen x-ray microscope with object holder in air for wet specimens. In Erko and Aristov [Erko 1994].

[Niemeyer 1994] J. Niemeyer, J. Thieme, and P. Guttmann. Colloidal systems in the soil investigated by x-ray microscopy. In Erko and Aristov [Erko 1994].

[Nixon 1955] W. C. Nixon. High resolution x-ray projection microscopy. *Proceedings of the Royal Society*, **A 232**, pp. 475–485, (1955).

[Oehler 1994] V. Oehler, J. Fu, C. Jacobsen, W. Mangel, W. McGrath, S. Williams, and X. Zhang. Short-term radiation effects on cultured cells studied using x-ray microscopy. *(in preparation)*, (1994).

[Okada 1970] S. Okada. Cells. In K. I. Altman, G. B. Gerber, and S. Okada, editors, *Radiation Biochemistry*, volume I. Academic Press, New York, (1970).

[Palmer 1992a] J. R. Palmer and G. R. Morrison. Differential phase contrast imaging in x-ray microscopy. In Michette et al. [Michette 1992], pp. 278–280.

[Palmer 1992b] J. R. Palmer and G. R. Morrison. The use of avalanche photodiodes for the detection of soft x-rays. *Review of Scientific Instruments*, **63**, pp. 828–831, (1992).

[Parsons 1974] D. F. Parsons and V. R. Matricardi. Environmental wet cells. In P. R. Swann, C. J. Humphreys, and M. J. Goringe, editors, *High voltage electron microscopy: proceedings of the third international conference*, pp. 396–402, London, (1974). Academic Press.

[Parsons 1980] D. F. Parsons, editor. **Ultrasoft X-ray Microscopy: Its Application to Biological and Physical Sciences (Annals of the New York Academy of Sciences)**, volume 342, New York, (1980).

[Pattee 1963] H. H. Pattee, Jr., V. E. Cosslett, and A. Engström, editors. **X-ray Optics and X-ray Microanalysis**, New York, (1963). Academic Press. Stanford, 1962.

[Paulson 1977] J. R. Paulson and U. K. Laemmli. The structure of histone-depleted metaphase chromosomes. *Cell*, **12**, pp. 817–828, (1977).

[Pellegrini 1993] C. Pellegrini, J. Rosenzweig, H.-D. Nuhn, P. Pianetta, R. Tatchyn, H. Winick, K. Bane, P. Morton, T. Raubenheimer, J. Seeman, K. Halbach, K.-J. Kim, and J. Kirz. A 2–4 nm high power FEL on the SLAC linac. *Nuclear Instruments and Methods in Physics Research*, **A 331**, pp. 223–227, (1993).

[Pianetta 1989] P. Pianetta, I. Lindau, P. L. King, M. Keenlyside, G. Knapp, and R. Browning. Core-level photoelectron microscopy with synchrotron radiation. *Reviews of Scientific Instruments*, **60**, pp. 1686–1689, (1989).

[Pine 1992] J. Pine and J. Gilbert. Live cell specimens for x-ray microscopy. In Michette et al. [Michette 1992], pp. 384–387.

[Polack 1981] F. Polack and S. Lowenthal. Photoelectron microscope for x-ray microscopy and microanalysis. *Reviews of Scientific Instruments*, **52**, pp. 207–212, (1981).

[Polack 1988] F. Polack, S. Lowenthal, D. Phalippou, and P. Fournet. First images with the soft x-ray image converting microscope at LURE. In Sayre et al. [Sayre 1988a], pp. 220–227.

[Polack 1994] F. Polack and D. Joyeux. Soft x-ray interferential scanning microscopy: a feasability assessment. In Erko and Aristov [Erko 1994].

[Popov 1994] A. V. Popov, Y. V. Kopylov, and A. V. Vinogradov. Numerical simulation of imaging processes in x-ray microscopy. In Erko and Aristov [Erko 1994].

[Pouvelle 1991] B. Pouvelle, R. Spiegel, L. Hsiao, R. J. Howard, R. L. Morris, A. P. Thomas, and T. F. Taraschi. Direct access to serum by intraerythrocytic malaria parasites. *Nature*, **353**, pp. 73–75, (1991).

[Raju 1987] M. R. Raju, S. G. Carpenter, J. J. Chmielewski, M. E. Schillaci, M. E. Wilder, J. P. Freyer, N. F. Johnson, P. L. Schor, R. J. Sebring, and D. T. Goodhead. Radiobiology of ultrasoft X rays. *Radiation Research*, **110**, pp. 396–412, (1987).

[Ranwez 1896] F. Ranwez. Application de la photographie par les rayons Röentgen au recherche analytiques des matieres vegetales. *Comptes Rendue de l'Academie des Sciences, Paris*, **122**, pp. 841–842, (1896).

[Rarback 1983] H. M. Rarback. **The development of a scanning soft x-ray microscope**. PhD thesis, Department of Physics, State University of New York at Stony Brook, (1983).

[Rarback 1984] H. Rarback, J. M. Kenney, J. Kirz, M. R. Howells, P. Chang, P. J. Coane, R. Feder, P. J. Houzego, D. P. Kern, and D. Sayre. Recent results from the Stony Brook scanning microscope. In Schmahl and Rudolph [Schmahl 1984a], pp. 203–215.

[Rarback 1990] H. Rarback, C. Buckley, H. Ade, F. Camilo, R. DiGennaro, S. Hellman, M. Howells, N. Iskander, C. Jacobsen, J. Kirz, S. Krinsky, S. Lindaas, I. McNulty, M. Oversluizen, S. Rothman, D. Sayre, M. Sharnoff, and D. Shu. Coherent radiation for x-ray imaging—the soft x-ray undulator and the X1A beamline at the NSLS. *Journal of X-ray Science and Technology*, **2**, pp. 274–296, (1990).

[Reimer 1993] L. Reimer. **Transmission electron microscopy: physics of image formation and microanalysis**. Springer-Verlag, Berlin, third edition, (1993). Springer Series in Optical Sciences **36**.

[Rodenburg 1992] J. M. Rodenburg and R. H. T. Bates. The theory of super-resolution electron microscopy via Wigner-distribution deconvolution. *Philosophical Transactions of the Royal Society of (London)*, **A 339**, pp. 521–553, (1992).

[Rodenburg 1993] J. M. Rodenburg, B. C. McCallum, and P. D. Nellist. Experimental tests on double-resolution coherent imaging via STEM. *Ultramicroscopy*, **48**, pp. 304–314, (1993).

[Röntgen 1895] W. C. Röntgen. Über eine neue art von Strahlen. I Mitteilung. *Sitzungsber. Phys.-Med. Ges. Würzburg*, **137**, p. 41, (1895).

[Rose 1948] A. Rose. Television pickup tubes and the problem of vision. In L. Marton, editor, *Advances in Electronics*, volume 1, pp. 131–166. Academic Press, New York, (1948).

[Rosenbluth 1983] A. Rosenbluth. **Reflecting properties of x-ray multilayer devices**. PhD thesis, University of Rochester, (1983).

[Rosser 1985] R. J. Rosser, K. G. Baldwin, R. Feder, D. Bassett, A. Coles, and R. W. Eason. Soft x-ray contact microscopy with nanosecond exposure times. *Journal of Microscopy*, **138**, pp. 311–320, (1985).

[Rothweiler 1994] D. Rothweiler, K. Eidmann, G. Winhart, R. Lebert, and W. Neff. Laser- and pinch plasma x-ray sources for imaging microscopy. In Erko and Aristov [Erko 1994].

[Rudolph 1976] D. Rudolph, G. Schmahl, and B. Niemann. Applications of holographic structures as optical elements—x-ray microscopy. In *Proceedings of the International Conference on Applications of Holography and Optical Data Processing*, pp. 499–506, London, (1976). Pergamon Press.

[Rudolph 1980] D. Rudolph and G. Schmahl. High power zone plates for soft x-rays. In Parsons [Parsons 1980], pp. 94–104.

[Rudolph 1982] D. Rudolph, B. Niemann, and G. Schmahl. Status of sputtered sliced zone plates for x-ray microscopy. In E. Spiller, editor, *High resolution soft x-ray optics*, volume 316, pp. 103–105, Bellingham, Washington, (1982). Society of Photo-Optical Instrumentation Engineers (SPIE).

[Rudolph 1984] D. Rudolph, B. Niemann, G. Schmahl, and O. Christ. The Göttingen x-ray microscope and x-ray microscopy experiments at the BESSY storage ring. In Schmahl and Rudolph [Schmahl 1984a], pp. 192–202.

[Rudolph 1990] D. Rudolph, G. Schmahl, and B. Niemann. Amplitude and phase contrast in x-ray microscopy. In P. J. Duke and A. G. Michette, editors, *Modern Microscopies*, pp. 59–67. Plenum, New York, (1990).

[Rymell 1993] L. Rymell and H. M. Hertz. Droplet target for low-debris laser-plasma soft x-ray generation. *Optics Communications*, **103**, pp. 105–110, (1993).

[Rymell 1994] L. Rymell, H. M. Hertz, and L. Engström. Very-low-debris laser-plasma soft x-ray source for microscopy. In Erko and Aristov [Erko 1994].

[Sayre 1972] D. Sayre. Proposal for the utilization of electron beam technology in the fabrication of an image forming device for the soft x-ray region. Technical Report RC 3974 (#17965), IBM T. J. Watson Research Laboratory, Yorktown Heights, New York, (1972).

[Sayre 1977a] D. Sayre, J. Kirz, R. Feder, D. M. Kim, and E. Spiller. Potential operating region for ultrasoft x-ray microscopy of biological specimens. *Science*, **196**, pp. 1339–1340, (1977).

[Sayre 1977b] D. Sayre, J. Kirz, R. Feder, D. M. Kim, and E. Spiller. Transmission microscopy of unmodified biological materials: Comparative radiation dosages with electrons and ultrasoft x-ray photons. *Ultramicroscopy*, **2**, pp. 337–341, (1977).

[Sayre 1979] D. Sayre and R. Feder. Exposure and development of x-ray resist in microscopy. Technical Report RC-7498, IBM, (1979).

[Sayre 1980] D. Sayre. Prospects for long-wavelength x-ray microscopy and diffraction. In M. Schlenker, editor, *Imaging Processes and Coherence in Physics*, pp. 229–235. Springer-Verlag, Berlin, (1980).

[Sayre 1984] D. Sayre, R. P. Haelbich, J. Kirz, and W. Yun. On the possibility of imaging microstructures by soft x-ray diffraction pattern analysis. In Schmahl and Rudolph [Schmahl 1984a], pp. 314–316.

[Sayre 1987] D. Sayre. Diffraction-imaging possibilities with soft x-rays. In Cheng and Jan [Cheng 1987b], pp. 213–223.

[Sayre 1988a] D. Sayre, M. R. Howells, J. Kirz, and H. Rarback, editors. **X-ray Microscopy II (Springer Series in Optical Sciences, Vol. 56)**, Berlin, (1988). Springer-Verlag.

[Sayre 1988b] D. Sayre, W. Yun, and J. Kirz. Experimental observation of diffraction patterns from microspecimens. In Sayre et al. [Sayre 1988a], pp. 272–275.

[Sayre 1991] D. Sayre. Note on "superlarge" structures and their phase problem. In H. Schenk, editor, *Direct Methods of Solving Crystal Structures*, pp. 353–356. Plenum, New York, (1991).

[Sayre 1995] D. Sayre and H. N. Chapman. X-ray microscopy. *Acta Crystallographica*, **A51**, (1995).

[Schattenburg 1991] M. L. Schattenburg, K. Li, R. T. Shin, J. A. Kong, D. B. Olster, and H. I. Smith. Electromagnetic calculation of soft x-ray diffraction from 0.1-μm scale gold structures. *Journal of Vacuum Science and Technology*, **B 9**, pp. 3232–3236, (1991).

[Schmahl 1969] G. Schmahl and D. Rudolph. Lichtstarke Zonenplatten als abbildende Systeme für weiche Röntgenstrahlung (High power zone plates as image forming systems for soft x-rays). *Optik*, **29**, pp. 577–585, (1969).

[Schmahl 1974] G. Schmahl. Holographic structures for applications in the vacuum ultraviolet and soft x-ray region. In E.-E. Koch, R. Haensel, and C. Kunz, editors, *Vacuum Ultraviolet Radiation Physics*, pp. 667–681, London, (1974). Pergamon/Vieweg.

[Schmahl 1980] G. Schmahl, D. Rudolph, B. Niemann, and O. Christ. Zone-plate x-ray microscopy. *Quarterly Reviews of Biophysics*, **13**, pp. 297–315, (1980).

[Schmahl 1984a] G. Schmahl and D. Rudolph, editors. **X-ray Microscopy (Springer Series in Optical Sciences, Vol. 43)**, Berlin, (1984). Springer-Verlag.

[Schmahl 1984b] G. Schmahl, D. Rudolph, P. Guttmann, and O. Christ. Zone plate lenses for x-ray microscopy. In Schmahl and Rudolph [Schmahl 1984a], pp. 63–74.

[Schmahl 1987] G. Schmahl and D. Rudolph. Proposal for a phase contrast x-ray microscope. In Cheng and Jan [Cheng 1987b], pp. 231–238.

[Schmahl 1991] G. Schmahl and P.-C. Cheng. X-ray microscopy. In S. Ebashi, M. Koch, and E. Rubenstein, editors, *Handbook on Synchrotron Radiation*, volume 4, pp. 483–536. Elsevier, Amsterdam, (1991).

[Schmahl 1994a] G. Schmahl, P. Guttmann, G. Schneider, B. Niemann, C. David, T. Wilhein, J. Thieme, and D. Rudolph. Phase contrast studies of hydrated specimens with the x-ray microscope at BESSY. In Erko and Aristov [Erko 1994].

[Schmahl 1994b] G. Schmahl, D. Rudolph, P. Guttmann, G. Schneider, J. Thieme, B. Niemann, and T. Wilhein. Phase contrast x-ray microscopy. *Synchrotron Radiation News*, **7**(4), pp. 19–22, (July 1994).

[Schneider 1992a] G. Schneider. **Röntgenmikroskopie mit Synchrotronstrahlung an wäßrigen biologischen Systemen—experimentelle und theoretische Untersuchungen**. PhD thesis, Universität Göttingen, (1992).

[Schneider 1992b] G. Schneider and B. Niemann. Environmental chamber for x-ray imaging of wet biological specimens. In Michette et al. [Michette 1992], pp. 350–354.

[Schneider 1994a] G. Schneider. Investigations of soft x-radiation induced structural changes in wet biological objects. In Erko and Aristov [Erko 1994].

[Schneider 1994b] G. Schneider and B. Niemann. Cryo x-ray microscopy: first images of specimens at low temperatures. *X-ray Science*, **2**, pp. 8–9, (1994). Summer 1994 newsletter, Centre for X-ray Science, King's College, London.

[Schröder 1990] R. R. Schröder, W. Hofmann, and J.-F. Ménétret. Zero-loss energy filtering as improved imaging mode in cryoelectronmicroscopy of frozen-hydrated specimens. *Journal of Structural Biology*, **105**, pp. 28–34, (1990).

[Seely 1993] J. F. Seely, G. Gutman, J. Wood, G. S. Herman, M. P. Kowalski, J. C. Rife, and W. R. Hunter. Normal-incidence reflectance of W/B_4C multilayer mirrors in the 34–50-Å wavelength region. *Applied Optics*, **32**, pp. 3541–3543, (1993).

[Shealy 1992] D. L. Shealy, C. Wang, W. Jiang, L. Jin, and R. B. Hoover. Design and analysis of a fast, two-mirror soft-x-ray microscope. In Jacobsen and Trebes [Jacobsen 1992d], pp. 20–31.

[Sheppard 1986] C. J. R. Sheppard and T. Wilson. On the equivalence of scanning and conventional microscopes. *Optik*, **73**, pp. 39–43, (1986).

[Shi 1994] W. D. Shi, G. R. Morrison, M. T. Browne, T. P. M. Beelen, H. F. van Garderen, and E. Pantos. Microstructural investigation of aggregates formed from aged silica sol by STXM. *Nuclear Instruments and Methods in Physics Research*, **B (accepted)**, (1994).

[Shinohara 1986] K. Shinohara, S. Aoki, M. Yanagihara, A. Yagishita, Y. Iguchi, and A. Tanaka. A new approach to the observation of the resist in x-ray contact microscopy. *Photochem. Photobiol.*, **44**, pp. 401–403, (1986).

[Shinohara 1990a] K. Shinohara, H. Nakano, Y. Kinjo, and M. Watanabe. Fine structure of unstained human chromosome fibers dried with no fixative as observed by x-ray contact microscopy. *Journal of Microscopy*, **158**, pp. 335–342, (1990).

[Shinohara 1990b] K. Shinohara, K. Yada, H. Kihara, and T. Saito, editors. **X-ray Microscopy in Biology and Medicine**, Berlin, (1990). Springer-Verlag. Also Japan Scientific Societies Press, Tokyo.

[Shinohara 1991] K. Shinohara and A. Ito. Radiation damage in soft x-ray microscopy of live mammalian cells. *J. Microscopy*, **161**, pp. 463–472, (1991).

[Shinohara 1992] K. Shinohara, Y. Kinjo, M. C. Richardson, A. Ito, N. Morimoto, Y. Horiike, M. Watanabe, K. Yada, and K. A. Tanaka. Observation of human chromosome fibers in a water layer by laser-plasma x-ray contact microscopy. In Jacobsen and Trebes [Jacobsen 1992d], pp. 386–392.

[Shinozaki 1988] D. M. Shinozaki. High resolution image storage in polymers. In Sayre et al. [Sayre 1988a], pp. 118–123.

[Shinozaki 1992] D. M. Shinozaki, P. C. Cheng, and T. H. Lin. Statistical noise in soft x-ray images stored in PMMA resist. In Michette et al. [Michette 1992], pp. 329–334.

[Shu 1992] D. Shu, W. Wang, M. Wang, J. Liu, W. He, Y. Zhang, H. Zheng, Y. Zhang, and Q. Xie. The x-ray scanning microscope beam branch line and its scanning system design at BEPC. In Michette et al. [Michette 1992], pp. 154–156.

[Simpson 1983] M. J. Simpson and A. G. Michette. The effects of manufacturing inaccuracies on the imaging properties of Fresnel zone plates. *Optica Acta*, **30**, pp. 1455–1462, (1983). (now *Journal of Modern Optics*).

[Skinner 1990] C. H. Skinner, D. S. DiCicco, D. Kim, R. J. Rosser, S. Suckewer, A. P. Gupta, and J. G. Hirschberg. Contact microscopy with a soft x-ray laser. *Journal of Microscopy*, **159**, pp. 51–60, (1990).

[Solem 1982] J. C. Solem and G. C. Baldwin. Microholography of living organisms. *Science*, **218**, pp. 229–235, (1982).

[Solem 1986] J. C. Solem. Imaging biological specimens with high-intensity soft x rays. *Journal of the Optical Society of America*, **B 3**, pp. 1551–1565, (1986).

[Spears 1972a] D. L. Spears and H. I. Smith. High-resolution pattern replication using soft x rays. *Electronics Letters*, **8**, pp. 102–104, (1972).

[Spears 1972b] D. L. Spears and H. I. Smith. X-ray lithography—a new high-resolution replication process. *Solid State Technology*, **15**(7), pp. 21–26, (July 1972).

[Spiller 1972] E. Spiller. Low-loss reflection coatings using absorbing materials. *Applied Physics Letters*, **20**, pp. 365–367, (1972).

[Spiller 1976] E. Spiller, R. Feder, J. Topalian, D. Eastman, W. Gudat, and D. Sayre. X-ray microscopy of biological objects with Carbon Kα and with synchrotron radiation. *Science*, **191**, pp. 1172–1174, (1976).

[Spiller 1977] E. Spiller and R. Feder. X-ray lithography. In H.-J. Queisser, editor, *X-ray Optics (Topics in Applied Physics* **22***)*, pp. 35–92. Springer-Verlag, Berlin, (1977).

[Spiller 1978] E. Spiller. A zone plate monochromator for synchrotron radiation. Technical report, Stanford Synchrotron Radiation Laboratory, Stanford, California, (1978).

[Spiller 1993] E. Spiller. Early history of x-ray lithography at IBM. *IBM Journal of Research and Development*, **37**(3), pp. 291–297, (May 1993).

[Spiller 1994] E. Spiller. **Soft X-ray Optics**. Society of Photo-Instrumentation Engineers (SPIE), Bellingham, Washington, (1994).

[Stead 1987] A. D. Stead, T. W. Ford, W. J. Myring, and D. T. Clarke. A comparison of soft x-ray contact microscopy with light and electron microscopy for the study of algal cell ultrastructure. *Journal of Microscopy*, **149**, pp. 207–216, (1987).

[Stead 1989] A. D. Stead and T. W. Ford. A structural study of the floral epidermal hairs of *Digitalis purpurea* using light, electron and x-ray microscopy. *Annals of Botany*, **64**, pp. 713–719, (1989).

[Stead 1992] A. D. Stead, R. A. Cotton, A. M. Page, M. D. Dooley, and T. W. Ford. Visualization of the effects of electron microscopy fixatives on the structure of hydrated epidermal hairs of tomato (*Lycopersicum peruvianum*) as revealed by soft x-ray contact microscopy. In Jacobsen and Trebes [Jacobsen 1992d], pp. 351–362.

[Stead 1994a] A. D. Stead, R. A. Cotton, A. M. Page, J. A. Goode, J. G. Duckett, and T. W. Ford. The use of soft x-ray contact microscopy using laser-plasmas to study the ultrastructure of moss protonemal cells. In Erko and Aristov [Erko 1994].

[Stead 1994b] A. D. Stead, R. A. Cotton, A. M. Page, C. G. Steele, R. Bagby, and T. W. Ford. High resolution images of hydrated biological specimens by soft x-ray contact microscopy using TA4. Technical report, Rutherford Appleton Laboratory, (1994). Annual report to the Laser Facility Committee.

[Stöhr 1993] J. Stöhr, Y. Wu, B. D. Hermsmeier, M. G. Samant, G. R. Harp, S. Koranda, D. Dunham, and B. P. Tonner. Element-specific magnetic microscopy with circularly polarized x-rays. *Science*, **259**, pp. 658–661, (1993).

[Suckewer 1985] S. Suckewer, C. H. Skinner, H. Milchberg, C. Keane, and D. Voorhees. Amplification of stimulated soft-x-ray emission in a confined plasma column. *Physical Review Letters*, **55**, pp. 1753–1756, (1985).

[Talmon 1987] Y. Talmon. Electron beam radiation damage to organic and biological cryospecimens. In R. A. Steinbrecht and K. Zierold, editors, *Cryotechniques in Biological Electron Microscopy*, pp. 64–84, Berlin, (1987). Springer-Verlag.

[Taraschi 1994] T. F. Taraschi and B. Pouvelle. There is no ducking the duct. *Parasitology Today*, **10**, pp. 212–213, (1994).

[Tatchyn 1984] R. Tatchyn, P. L. Csonka, and I. Lindau. The constant-thickness zone plate as a variational problem. *Optica Acta*, **31**, pp. 729–733, (1984).

[Tennant 1991] D. M. Tennant, J. E. Gregus, C. Jacobsen, and E. L. Raab. Construction and test of phase zone plates for x-ray microscopy. *Optics Letters*, **16**, pp. 621–623, (1991).

[Thieme 1988] J. Thieme. Theoretical investigations of imaging properties of zone plates and zone plate systems using diffraction theory. In Sayre et al. [Sayre 1988a], pp. 70–79.

[Thieme 1992] J. Thieme, P. Guttmann, J. Niemeyer, G. Schneider, C. David, B. Niemann, D. Rudolph, and G. Schmahl. Röntgenmikroskopie zur untersuchung von waessrigen biologischen und kolloidchemischen systemen. *Nachr. Chem. Tech. Lab.*, **40**, pp. 562–563, (1992).

[Thieme 1994a] J. Thieme, C. David, N. Fay, B. Kaulich, R. Medenwaldt, M. Hettwer, P. Guttmann, U. Kögler, J. Maser, G. Schneider, D. Rudolph, and G. Schmahl. Zone plates for high resolution x-ray microscopy. In Erko and Aristov [Erko 1994].

[Thieme 1994b] J. Thieme, T. Wilhein, P. Guttmann, J. Niemeyer, K.-H. Jacob, and S. Dietrich. Direct visualization of iron and manganese accumulating microorganisms by x-ray microscopy. In Erko and Aristov [Erko 1994].

[Thomas 1992] X. Thomas, J. Cazaux, D. Erre, D. Mouze, and P. Collard. X-ray projection microscopy and microtomography in a scanning electron microscope. In Michette et al. [Michette 1992], pp. 190–194.

[Tomie 1991] T. Tomie, H. Shimizu, T. Majima, M. Yamada, T. Kanayama, H. Kondo, M. Yano, and M. Ono. Three-dimensional readout of flash x-ray images of living sperm in water by atomic-force microscopy. *Science*, **252**, pp. 691–693, (1991).

[Tomie 1992] T. Tomie, H. Shimizu, T. Majima, T. Kanayama, M. Yamada, and E. Miura. Flash contact x-ray microscopy of biological specimen in water. In Jacobsen and Trebes [Jacobsen 1992d], pp. 118–128.

[Tonner 1988] B. Tonner and G. R. Harp. Photoelectron microscopy with synchrotron radiation. *Review of Scientific Instruments*, **59**, pp. 853–858, (1988).

[Trail 1989] J. A. Trail and R. L. Byer. Compact scanning soft-x-ray microscope using a laser-produced plasma source and normal-incidence multilayer mirrors. *Optics Letters*, **14**, pp. 539–541, (1989).

[Trebes 1987] J. E. Trebes, S. B. Brown, E. M. Campbell, D. L. Matthews, D. G. Nilson, G. F. Stone, and D. A. Whelan. Demonstration of x-ray holography with an x-ray laser. *Science*, **238**, pp. 517–519, (1987).

[Trebes 1994] J. Trebes. X-ray imaging and x-ray source development at LLNL. In Erko and Aristov [Erko 1994].

[Tregear 1977] R. T. Tregear, editor. **Insect Flight Muscle**, Amsterdam, (1977). North Holland.

[Underwood 1994] J. Underwood, J. B. Kortright, R. C. C. Perera, F. Cerrina, C. Capasso, A. K. Ray-Chaudhury, W. Ng, J. Welnak, J. Wallace, S. Liang, and G. Margaritondo. X-ray microscopy with multilayer mirrors: the MAXIMUM photoelectron microscope. In Chance et al. [Chance 1994], pp. 601–609.

[von Brenndorff 1994] A. I. von Brenndorff, M. M. Moronne, C. Larabell, P. Selvin, and W. Meyer-Ilse. Soft x-ray stimulated high resolution luminescence microscopy. In Erko and Aristov [Erko 1994].

[Voss 1992] J. Voss, H. Dadras, C. Kunz, A. Moewes, G. Roy, H. Sievers, I. Storjohann, and H. Wongel. A scanning soft x-ray microscope with an ellipsoidal focusing mirror. *Journal of X-ray Science and Technology*, **3**, pp. 85–108, (1992).

[Voss 1994] J. Voss, I. Storjohann, C. Kunz, A. Moewes, M. Pretorius, A. Ranck, H. Sievers, V. Wedemeier, M. Wochnowski, and H. Zhang. Soft x-ray microscopy at HASYLAB/DESY. In Erko and Aristov [Erko 1994].

[Wang 1994] Y. Wang and C. Jacobsen. Modelling of dissolution and resolution in contact x-ray microscopy. In Bailey and Garratt-Reed [Bailey 1994], pp. 62–63.

[Wang 1995] S. Wang and C. Jacobsen. Contact microscopy modelling. *in preparation*, (1995).

[Watanabe 1994] N. Watanabe, S. Aoki, Y. Shimanuki, K. Kawasaki, M. Taniguchi, E. Anderson, D. Attwood, D. Kern, S. Shimizu, H. Nagata, and H. Kihara. Soft x-ray imaging microscope with sub-optical resolution at UVSOR. In Erko and Aristov [Erko 1994].

[Wijnen 1991] P. W. J. G. Wijnen, T. P. M. Beelen, H. C. P. L. Saejis, and R. A. van Santen. Silica gel from waterglass: a SAXS study of the formation and aging of fractal aggregates. *J. Appl. Cryst.*, **24**, pp. 759–764, (1991).

[Wilhein 1994] T. Wilhein, D. Rothweiler, A. Tusche, F. Scholze, and W. Meyer-Ilse. Thinned, back illuminated CCDs for x-ray microscopy. In Erko and Aristov [Erko 1994].

[Williams 1993] S. Williams, X. Zhang, C. Jacobsen, J. Kirz, S. Lindaas, J. V. Hof, and S. S. Lamm. Measurements of wet metaphase chromosomes in the scanning transmission x-ray microscope. *Journal of Microscopy*, **170**, pp. 155–165, (1993).

[Williams 1994a] S. Williams, C. Jacobsen, J. Kirz, S. S. Lamm, V. Oehler, J. van't Hof, S. Wirick, and X. Zhang. Metaphase chromosome DNA mass fraction is a constant, independent of species. *Chromosoma*, **(submitted)**, (1994).

[Williams 1994b] S. Williams, C. Jacobsen, J. Kirz, S. S. Lamm, J. van't Hof, and X. Zhang. Metaphase chromosome DNA mass fraction is independent of species. In Bailey and Garratt-Reed [Bailey 1994], pp. 46–47.

[Witt 1994] P. Witt. Preparation and thinning of sputtered sliced zone plates. In Erko and Aristov [Erko 1994].

[Wolf 1969] E. Wolf. Three-dimensional structure determination of semi-transparent objects from holographic data. *Optics Communications*, **1**, pp. 153–156, (1969).

[Wolter 1952] H. Wolter. Spiegelsysteme streifenden Einfalls als abbildende Optiken für Röntgenstrahlen. *Ann. Phys.*, **10**, pp. 94–114, 286, (1952).

[Wooten 1972] F. Wooten. **Optical Properties of Solids**. Academic Press, New York, (1972).

[Yada 1990] K. Yada and S. Takahashi. Projection x-ray microscope observation of biological samples. In Shinohara et al. [Shinohara 1990b], pp. 193–202. Also Japan Scientific Societies Press, Tokyo.

[Yada 1992] K. Yada and S. Takahashi. The recent development of projection x-ray microscopy for biological applications. In Michette et al. [Michette 1992], pp. 195–198.

[Yun 1987] W. B. Yun, J. Kirz, and D. Sayre. Observation of the soft X-ray diffraction pattern of a single diatom. *Acta Cryst.*, **A 43**, p. 131, (1987).

[Yun 1992] W.-B. Yun, P. J. Viccaro, J. Chrzas, and B. Lai. Coherent hard x-ray focussing optics and applications. *Review of Scientific Instruments*, **63**, pp. 582–585, (1992).

[Yun 1995] W. Yun, B. Lai, A. A. Krasnoperova, F. Cerrina, E. Di Fabrizio, L. Luciani, M. Figliomeni, and M. Gentili. X-ray zone plates and their applications. *Reviews of Scientific Instruments*, **66**, p. to be published, (1995).

[Zeitler 1970] E. Zeitler and M. G. R. Thomson. Scanning transmission electron microscopy. *Optik*, **31**, pp. 258–280, 359–366, (1970).

[Zhang 1992] X. Zhang, C. Jacobsen, and S. Williams. Image enhancement through deconvolution. In Jacobsen and Trebes [Jacobsen 1992d], pp. 251–259.

[Zhang 1994a] X. Zhang, H. Ade, C. Jacobsen, J. Kirz, S. Lindaas, S. Williams, and S. Wirick. Micro-XANES: chemical contrast in the scanning transmission x-ray microscope. *Nuclear Instruments and Methods in Physics Research*, **A 347**, pp. 431–435, (1994).

[Zhang 1994b] X. Zhang, R. Balhorn, C. Jacobsen, J. Kirz, and S. Williams. Mapping DNA and protein in biological samples using the scanning transmission x-ray microscope. In Bailey and Garratt-Reed [Bailey 1994], pp. 50–51.

[Zhang 1994c] X. Zhang, C. Jacobsen, S. Lindaas, and S. Williams. Exposure strategies for PMMA from *in situ* XANES spectroscopy. *(submitted to J. Vac. Sci. Tech. B)*, (1994).

[Zolfghari 1994] A. Zolfghari and P. Trebbia. 3D reconstructions in conical geometry from data obtained with an x-ray microtomograph. In Erko and Aristov [Erko 1994].

LAWRENCE BERKELEY LABORATORY
UNIVERSITY OF CALIFORNIA
TECHNICAL AND ELECTRONIC
INFORMATION DEPARTMENT
BERKELEY, CALIFORNIA 94720